Fundamental Sources of Error and Spectral Broadening in Doppler Ultrasound Signals

Steven A. Jones

Department of Biomedical Engineering
The Johns Hopkins University School of Medicine
Baltimore, Maryland

Published in: Crc Critical Reviews in Biomedical Engineering, **21**:399-483, 1993.

List of Symbols

$a(\mathbf{r},t)$	Spatial dependence of the particle concentration
B	Bandwidth
C_τ	Cross correlation function
C_{kl}	Cross-correlation coefficient
c	Speed of sound
$e_s(t)$	Transmitted signal pulse
$e(t)$	Envelope of a transmitted signal pulse
$\overline{f}$	Centroid frequency of the Doppler spectrum
f_0	Carrier frequency
f_d	Doppler shift frequency
$f_{\max}$	Maximum frequency of the Doppler spectrum
$f_{\mathrm{mod}\,e}$	Mode frequency of the Doppler spectrum
f_p	Pulse repetition frequency $(1/\tau_p)$
$G(r)$	Probe beam intensity
$G_r(r)$	Radial dependence of the probe beam intensity
$G_r(r \mid z)$	Radial dependence of the probe beam intensity at a given z
$g_r(t)$	Receiver gate
$\vec{k}$	wavenumber propagation vector of the transmitted sound wave
$P(f)$	Doppler power spectral density
P_x	Power spectral density of the transmitted signal
R_τ	Autocorrelation function.
$s_r(z,t)$	Quadrature signal as a function of particle position and time
s_{rf}	rf signal returned from the environment
$v(\vec{r},t)$	fluid velocity vector
v	Magnitude of the flow velocity
v_p	Component of velocity along the probe axis
W	Beam Width
α	$2v/c$
$\hat{\alpha}$	$\left(1+\frac{v}{c}\cos\theta_1\right)/\left(1-\frac{v}{c}\cos\theta_2\right)$
γ	Attenuation constant
ϕ	Phase of the Doppler signal
ψ	Instantaneous frequency
τ_b	Duration of the transmission gate
τ_d	Delay time between the start of the transmission gate and the start of the receiving gate
τ_g	Duration of the receiving gate

τ_p	Pulse repetition time
τ_s	Two-way sound-travel time between the probe and the particle
θ	Doppler angle when $\theta_1 = \theta_2$
θ_1	Angle between the transmitter probe-axis and the target velocity
θ_2	Angle between the receiver probe-axis and the target velocity
$\overline{\omega}$	Centroid frequency ($2\pi \overline{f}$)
ω_0	Carrier frequency ($2\pi f_0$)
ω_p	Pulse repetition frequency ($2\pi f_p$)
ω_d	Doppler shift frequency ($2\pi f d$)
z	Axial distance from the transducer face

Table of Contents

Fundamental Sources of Error and Spectral Broadening in Doppler Ultrasound Signals

Steven A. Jones

Abstract

Analysis of the signals, spectra and error bounds for Doppler ultrasound signals is challenging and involves numerous concepts in signal analysis, probability, acoustics and fluid mechanics. Nonetheless, the results of this analysis must be accessible to both engineers and clinicians who work with ultrasound technology. The engineer who designs, builds or maintains equipment must know whether specific artifacts are fundamental or can be eliminated. The clinician must be able to interpret whether specific signal features accurately represent the flow field or result from limitations of Doppler ultrasound. This article reviews recent advances in both conceptual and numerical models of the Doppler ultrasound process, and relates these advances to practical aspects such as spectral broadening, velocity estimation error and data analysis error. It then reviews recent innovations in system implementation and signal analysis which are indicative of the future potential of Doppler ultrasound instrumentation.

I. INTRODUCTION

A. Background

Doppler ultrasound velocimeters were introduced in 1959 by Satomura[1], and continued to evolve through the 1960's[2,3]. However, rigorous analysis of their properties did not begin until the mid 1970's. The analyses were motivated by a desire to extract specific physiologically relevant information with the devices. Measurements of interest included (1) flow rate[4-6], (2) velocity profiles[7-10] (3) coherent structures[11-14], (4) turbulent energy and turbulent spectra[7, 15-19] (5) velocity gradients (shear rate) [9, 17, 20-23] and (6) pressure drops[24-28]. Inaccuracies in all of these measurements result from fundamental limitations in the Doppler ultrasound method itself. The instruments measure neither true flow nor point velocity. They do, however, provide a measure of the velocity distribution throughout the interrogated volume, and this unique aspect has suggested to researchers that the spectral content of the quadrature signals could be correlated to the severity of flow pathologies such as arterial stenosis and aneurism.

Although the Doppler measurement cannot be precisely described in terms of flow rate or velocity profiles, the following simple model of the relationship between the blood (target) velocity and the Doppler spectrum is conceptually useful. If a target moves at a constant velocity through the measurement region, then the downmixed output (see section II-B) of the ultrasound device is approximately a sinusoid with frequency proportional to the target velocity. If multiple targets move with different velocities through the measurement region, the output will contain multiple sinusoids with frequencies propor-

tional to the velocities. In the Doppler spectrum,* the frequency axis corresponds to velocity. The power density, $P(\omega)$, describes the scattered power associated with each velocity. The exact relationship between the power density and the flow velocity distribution will be clarified in section III-A.

The ideal Doppler instrument would allow a precise, uniform measurement volume to be specified, and would yield a power spectrum whose frequency axis is directly proportional to velocity and whose power axis provides the velocity volume-density of fluid associated with each velocity. True Doppler instruments do this only approximately for reasons which will be closely examined in this review.

In terms of this ideal instrument, spectral broadening can be divided into two categories. The first is the increased range of frequencies in the spectrum which result from an increased range of velocities in the sample volume. This is the broadening component that is considered to have diagnostic potential because it is directly related to the blood velocity. The second category involves smearing or distortion of this ideal spectrum. This category is less directly related to the velocity field, and it is usually considered to be a source of error and artifact.

The degree to which artifact must be understood depends directly on the extent to which it prevents accurate results in a given application. Therefore the following section reviews some of the areas in which Doppler ultrasound has been applied and the degree to which it has proved useful in these areas. This will help to introduce some of the associated engineering problems and to motivate the remainder of this paper.

B. Common Uses of Doppler Ultrasound

Doppler ultrasound is commonly used in cardiology, obstetrics, neonatology and in the diagnosis of peripheral vascular stenosis. However, it has been applied to other vascular areas as well, and has been used in some non-medical applications.

1. Physiological Parameters

The objective of Doppler ultrasound in diagnosis is to obtain measurements of flow velocity and interpret them in terms of physiologically significant variables. In general, these variables are not measured directly by ultrasound, but must be derived from the velocity measurements, supplemental measurements, and assumptions.

The most fundamental quantity of interest is flow rate because this indicates how well an organ or region is perfused by blood. This can be obtained from multiple measurements of the velocity over the cross-section of a vessel which are then integrated over space and averaged over time. It can also be measured, in principle, by the "uniform insonification method" (see section III-A and subsection V-B-2-b), in which the spatially aver-

* Velocity volume-density ($V(v_p)$) is defined here such that $V(v_p)dv_p$ is the total volume within the sample volume in which the velocity component toward the probe is between v_p and $v_p + dv_p$, where dv_p is infinitessimally small.

aged velocity is obtained from a single measurement with a wide ultrasound beam and multiplied by the cross-sectional area. Cross-sectional area can be deduced from from Doppler imagers[29], from the locations at which velocity becomes zero [30], or from the power of the backscattered signal[31].

Pressure is a second quantity of interest. If pressure changes abruptly with position along a vessel, it indicates a restriction to blood flow. Pressure drop is calculated indirectly through the Bernoulli equation[25, 26, 32, 33], which relates changes in velocity to changes in pressure.

The blood flow waveform is a function of flow resistance, and vessel capacitance[34]. For example, a stenosis will decrease the pulsatility of the downstream flow waveform and increase the pulsatility of the upstream waveform. The pulsatility index introduced by Gosling et al.[35] is used to quantify this effect. This is commonly defined as $(v_{\max} - v_{\min})/v_{mean}$, where $v_{\max}$ is the maximum flow velocity, $v_{\min}$ is the minimum flow velocity, and v_{mean} is the time-averaged flow velocity over a cardiac cycle.

The spectral broadening index (see, for example, Kassam et al.[36]) is a ratio of the bandwidth of the Doppler spectrum to the Doppler frequency. Clinically this index is associated with phenomena which increase the range of velocities within the sample volume, such as high shear rate, turbulence, and rapid acceleration. However, it is also affected by other phenomena, described throughout this review, which affect the bandwidth of the Doppler spectrum.

2. Diagnostic Applications

Flows within, into, and out of the heart chambers are of primary interest to the cardiologist. Doppler ultrasound has been used to measure regurgitant blood volume for valvular insufficiency[24, 37-44], residual area and pressure drop for valvular stenosis[45], and overall cardiac output[46-54]. The numerous assumptions required to convert Doppler measurements to more canonical physiological variables have prompted some investigators to abandon some of these variables. For example, McLennan et al.[53] have investigated the use of “linear cardiac output” in lieu of volumetric cardiac output. They compute linear stroke distance, which is the the integral over time of the maximum velocity present in the Doppler sample volume. This corresponds to the distance traveled by the fastest fluid elements in one heart cycle.

Ventricular septal defects can be diagnosed either by the direct detection of flow from the left ventricle to the right ventricle, by the measurement of jet size[29, 55], or by measurement of the ratio of pulmonary to aortic flow[56]. The quantitative objective is to determine the size of the defect, as measured through the volume of blood flow through the defect.

Doppler ultrasound has been applied to the detection of coronary stenosis[57, 58] and the measurement of coronary blood flow rate [59-66]. The depth and small size of the coronary arteries, combined with the motion of the heart complicate velocity measurements in these vessels and preclude the use of external ultrasound probes. A number of ultra-

sound catheters and guidewires have been developed which can be directed into the coronary arteries from the femoral or brachial arteries. Although this type of measurement is certainly invasive, it is only moderately so in comparison with procedures in which the chest cavity must be opened. The body of literature on intracoronary Doppler catheter measurements is large and has been reviewed by Hartley[67]. It is still not possible to directly measure flow rate in this way, and much work has been done to measure coronary flow reserve instead[68-70]. This index is the ratio of flow rate when the distal circulation is maximally dilated to flow rate under resting conditions, and is known to decrease as a stenosis becomes more severe.

Applications of Doppler ultrasound to neonatology have been reviewed by Drayton and Skidmore[55]. Pathologies such as periventricular haemorrhage and hydrocephalus have been correlated with the pulsatility index in the anterior cerebral arteries. Patent ductus arteriosus has also been diagnosed through waveform analysis and is associated with increased pulsatility index and strong reverse flow in the abdominal aorta[71] and the common carotid artery[72].

Several authors have reviewed the use of Doppler ultrasound in obstetrics[73-75]. Increased placental resistance has been correlated with increased pulsatility[76, 77] and other waveform changes[78] in the umbilical artery. The relationship between resistance and pulsatility in this artery has been examined *in vivo* in sheep [79] and through mathematical modeling[80]. Vessels of the fetus such as the aorta[81, 82] and the cerebral arteries[83] have been studied *in-utero*. Fetal heart rate has also been monitored by Doppler ultrasound[84, 85].

In adults, the use of Doppler ultrasound on the cerebral arteries is complicated by the large acoustic impedance mismatch between the skull and intracranial tissue. This mismatch causes much of the transmitted power to be reflected, which results in low signal to noise ratios. Low carrier frequencies are used for transcranial measurements to reduce the attenuation of the sound by the tissue (see subsection III-B-1). The resulting power spectra tend to be broad for two reasons: 1) the low frequencies result in long wavelengths, which increase the transit time effects (see subsection III-C-2), and 2) velocity gradient broadening (see section III-A) is increased because the sample volumes are necessarily larger and include a wider range of velocities. Nonetheless, transcranial Doppler ultrasound provides useful diagnostic data[86-92].

Doppler ultrasound has also been applied to numerous other vessels. It has been used to study velocity waveforms in renal arteries [93-95]. It has been used to examine the relationship between flow velocity in the digital arteries and vibration white finger disease[96]. It has also been applied to the evaluation of tumors[97-103], and to the measurement of velocity in the microcirculation[104-106].

The application most commonly associated with the spectral characteristics of the Doppler ultrasound signals is diagnosis of vascular stenosis. Most of the numerous flow phenomena generated by vascular stenoses have been exploited for this purpose. The maximum frequency in the Doppler power spectrum has been used to determine the in-

crease in velocity that results from conservation of mass as fluid enters the stenosis[107-109]. The sharp velocity gradients between the jet and the recirculation region have been related to depressions in the power spectrum[23]. Coherent structures (see below) have been related, qualitatively[13] and quantitatively[11] to Doppler ultrasound velocity signals. Turbulence[15, 16, 110], strong velocity gradients[20], and rapid acceleration[111] have all been correlated with spectral broadening.

The spectral broadening index has been used by several authors to quantify the degree of stenosis[107, 108, 112, 113]. In one study it was shown to have diagnostic value in that it could distinguish severe stenoses from low grade stenoses with a specificity of 93% and a sensitivity of 74%[114]. However, it is not sensitive enough to detect low and moderate levels of disease[108], and is not as sensitive as the maximum peak systolic frequency[107]. Although overall accuracy of the diagnosis is improved when several indices are combined, the scatter in the data is great, and an accurate estimate of the stenosis diameter cannot be obtained[112]. In part the insufficiency of the spectral broadening index results because multiple factors contribute to the breadth of the spectrum. These include fluid mechanics, the stochastic nature of the scattering configuration, and acoustic limitations.

Often the term “turbulence” is used to describe the fluid mechanical sources of broadening[115-118]. It is known [119-121] that in the case of severe stenosis turbulent flow can occur. It is also known[15, 16, 110] that turbulence leads to spectral broadening. However, strong gradients in velocity are also sources of broadening[20] and are probably the more dominant sources in the post-stenotic flow field[122].

The flow downstream of a stenosis provides strong motivation for improvements in temporal and spatial resolution of non-invasive velocity measurements. Severe stenoses cause coherent structures and turbulence[12, 14, 123, 124], and the spectral content of both of these has been quantitatively correlated to stenosis severity[121, 125]. Figure 1 shows hot film anemometry measurements of centerline velocity downstream of a stenosis *in vitro*. Coherent structures (sinusoidal oscillations) at a frequency of 600 Hz (upper curve) are seen just downstream of the stenosis. Further downstream, these break up into turbulence (lower curve). Similar data exist from *in vivo* measurements[119, 126]. The frequency content of both signals is much too high to be accurately deduced from current Doppler ultrasound technology. Consider, for example, a pulsed Doppler instrument which receives samples at the realistic rate of 64,000 Hz. Initially, this seems more than adequate to capture structures at 600 Hz since, by the Nyquist (Shannon) sampling theorem[127] frequencies up to half the sample rate can be resolved. However, several ultrasound samples must be averaged together to obtain a stable velocity estimate. The typical number of samples is on the order of 100, which reduces the effective data rate to 640 Hz. Furthermore, even with this substantial averaging, coherent structures near the 320 Hz Nyquist rate would be difficult to resolve because the velocity signal can be masked by ambiguity noise (section III-C below) and spatial averaging (section III-A below).

Figure 1: Hot film anemometry data from flow downstream of a constriction. The upper curve is taken 0.84 diameters downstream of the stenosis and illustrates the sinusoidal characteristics of coherent structures. The lower curve is taken 2.9 diameters downstream of the stenosis and illustrates breakdown to turbulence. The high frequency fluctuations cannot be captured with conventional Doppler ultrasound.

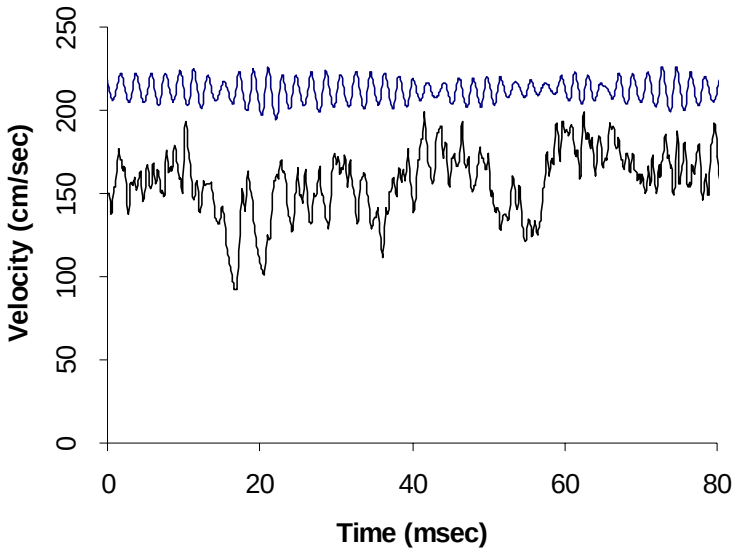

3. Other Applications

The above applications have been primarily diagnostic in nature. However, ultrasound has also been used in evaluation of flow patterns in prosthetic devices such as anastomoses[128] and cardiac assist devices[17, 129]. It has been used in *in vivo* animal models to determine flow patterns at bifurcations and to relate these to the buildup of atherosclerosis and intimal hyperplasia[59]. In diagnosis, it is sometimes sufficient to identify signal characteristics that are associated with a given pathology without concern for the underlying fluid mechanics. However, in an investigation of hemodynamic effects it is the specific fluid mechanical properties, such as shear stress, flow reversal, and turbulence, that are of interest. In this case, the ability to make accurate, high resolution measurements and to correctly interpret Doppler spectral characteristics in terms of the flow field becomes critical.

The applications and difficulties outlined above serve as motivation for a clearer understanding of the physics of Doppler ultrasound, and have led investigators to employ numerous innovations in hardware, data analysis methods and diagnostic techniques.

C. Objectives and Structure of this Review

This review examines current models for the physical processes which lead to the Doppler spectra encountered in practice. Part II describes some basic concepts which will be needed in later sections. Most of these concepts are explained in more detail in the numerous textbooks on Doppler ultrasound[130-136]. Part III discusses Doppler spectra, and is divided into three sections. Section III-A describes the base spectrum which results from the weighting of the velocity field with the probe beam intensity. Section III-B describes phenomena which distort this process through changes in the transmitted signal and beam pattern. Section III-C describes the measurement-related broadening processes which fundamentally limit the temporal and spatial resolution of the velocity measurement. These processes are variously known as ambiguity, transit time broadening, and geometric broadening. In part IV, a number of mathematical models for Doppler signals are presented. Then, in part V, innovations which have been recently

proposed or implemented are described. Emphasis is placed on innovations which result from the need to circumvent the ambiguity and broadening problems discussed in section III-C.

II. FUNDAMENTAL CONCEPTS

A. The Doppler Effect

The Doppler effect was first described by Christian Doppler in 1842[137]. Accounts of Doppler research in these early years is interesting from a historical perspective and can be found in articles by White[138], Jonkman[139] and Pasquale and Paulshock[140]. The basic Doppler equation for ultrasound is a composite of two phenomena[141]. First, sound at frequency f_0 is sent from a stationary transmitter to a target. The frequency f_t at the target is:

$$f_t = f_0\left(1+\frac{v}{c}\cos(\theta_1)\right). \qquad \text{Eq. 1}$$

Here, c is the speed of sound in the medium, v is the speed of the target, and θ_1 is the angle between the sound propagation direction and the target velocity direction. The sound at the receiver then has a frequency f_r is defined by

$$f_r = f_t/\left(1-\frac{v}{c}\cos\theta_2\right), \qquad \text{Eq. 2}$$

where θ_2 is the angle between the target velocity direction and the line between the target and the receiver. The frequency f_t is shifted from f_0 by $f_0 v\cos\theta_1/c$. To obtain the shift for Equation 2, the right hand side must be expanded in a Taylor series about $v=0$ and it must be assumed that $v<<c$. The result is:

$$f_r = f_t + f_t\frac{v}{c}\cos\theta_2 + O\left(\left(\frac{v}{c}\right)^2\right). \qquad \text{Eq. 3}$$

If $v<<c$, f_r is shifted from f_t by $f_t v\cos\theta_2/c$. It is then shifted from f_0 by $(f_0\cos\theta_1/c + f_t\cos\theta_2)v/c$, which is approximately $(f_0 v/c)(\cos\theta_1+\cos\theta_2)$. If, as is common, the source and receiver are at the same position with respect to the target, then $\theta_1=\theta_2\equiv\theta$ and the classic Doppler shift equation is obtained.

$$f_d = 2f_0\frac{v}{c}\cos\theta \qquad \text{Eq. 4}$$

The above derivation shows that even the most basic Doppler relationship is an approximation. For blood measurement it is an excellent approximation because the ratio between blood speed and sound speed is typically on the order of 1/1000. A more subtle lesson from the above equations is that the initial frequency is not shifted by a con-

stant frequency, but by an amount that depends on the initial frequency. The phenomenon is more accurately described as a multiplication of the initial frequency by the factor $\alpha \equiv \left(1+\frac{v}{c}\cos\theta_1\right)/\left(1-\frac{v}{c}\cos\theta_2\right)$. Thus, if the transmitted signal has multiple components, each component is shifted by a different amount. Any signal of finite duration has finite bandwidth and is altered through the Doppler effect by a "stretch" along the frequency axis rather than a true shift.

Although f_d is the quantity of interest, the signal returned from a scatterer is a cosine with frequency $f_0 + f_d$. It is more convenient to work with a cosine whose frequency is just the Doppler frequency. This is obtained by a process known as downmixing.

B. The Doppler Instrument and Downmixing

1. Continuous Wave Doppler

A continuous wave instrument is illustrated in Figure 2, and in the following description it will be assumed that the target consists of a single scatterer which moves along the axis of and toward the transmitter. One transducer sends a signal of the form $A_t\cos(\omega_0 t)$, and another receives the scattered sound, which has the form $A_r\cos([\omega_0+\omega_d]t+\phi)$. This returned signal, which is often called the radio frequency (rf) signal, is first multiplied by the transmitted signal, and it can be shown from standard trigonometric identities that the result is:

$$s(t)=\frac{1}{2}A_tA_r\cos(\omega_d t+\phi)+\frac{1}{2}A_tA_r\cos([2\omega_0+w_d]t+\phi) \qquad \text{Eq. 5}$$

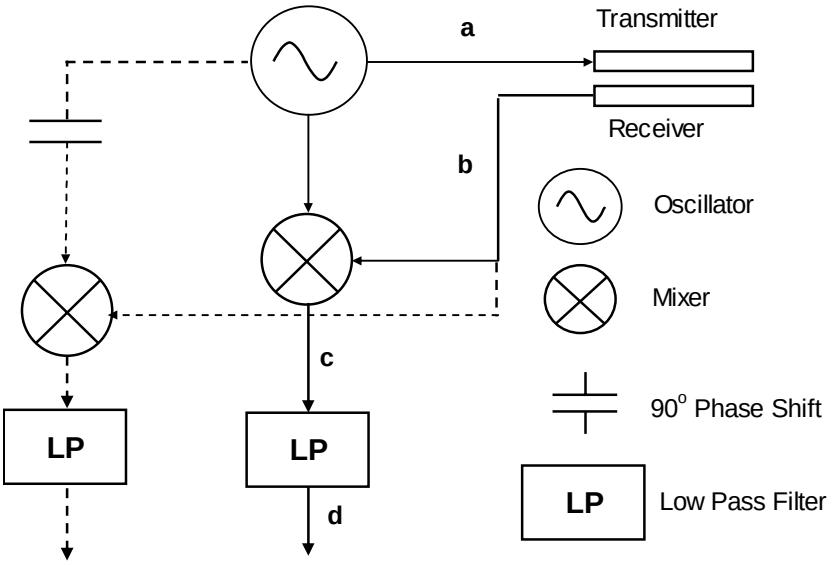

Figure 2: Schematic diagram of a continuous wave Doppler instrument. The signals associated with locations marked (a), (b), (c) and (d) are shown in Figure 3. The pathways represented by solid lines provide the in-phase signal, and the pathways represented by the dashed lines are needed to obtain the quadrature signal.

The high-frequency cosine term is eliminated by the low pass filter, and the target velocity is estimated from the frequency of the low-frequency term. Although the process of multiplication implies non-linearity, downmixing is a true linear operation in that if two signals are first added together and the result is downmixed, the result is the same as if the two signals were downmixed separately and then added. This means that if two particles travel through the sample volume with different velocities so that they have distinct Doppler frequencies, f_{d1} and f_{d2}, the downmixed signal will accurately exhibit both frequencies and will not exhibit frequencies such as $f_{d1} + f_{d2}$ or $f_{d1} - f_{d2}$. Thus, the frequency separation between the two downmixed signals will be the same as that for the original signals. Another feature of downmixing is that if the low pass filter does not change the phase of its input the phase in the downmixed signal is identical to the phase of the reflected signal. Thus, if two particles are $1/8$ of a wavelength apart so that their returned signals are 90° out of phase, the corresponding components of the downmixed signals will be 90° out of phase.

In most practical applications, two downmixed signals are used. The returned echo is mixed with the carrier signal for one of these and it is mixed with the carrier phase shifted by 90° for the other. The first downmixed signal is called the in-phase signal, and the second is called the quadrature signal. The two together are referred to as the quadrature signals because they are in quadrature with one another. The sign of the phase difference between the two signals indicates whether flow is toward or away from the ultrasound probe. When a single particle approaches along the axis of the probe, the signals and amplitude spectra* at the locations marked **a**, **b**, **c** and **d** in Figure 2 are as shown in Figure 3. Signal **a** is a cosine, and the corresponding spectrum consists of two delta functions at $\pm$ the carrier frequency. Signal **b** is the same as signal **a**, except that it is compressed in time by $\overline{\alpha}$. The corresponding spectrum is dilated by the same amount. Signal **c** exhibits the two frequencies, $2\omega_0 + \omega_d$ and ω_d, and if the upper curve is the real part of the signal and the lower curve is the imaginary part, the spectrum is identical to that of signal **b** except that it is shifted to the left by ω_0. Signal **d** is signal **c** with the high (negative) frequency component removed.

2. Pulsed Doppler and Range Gating

A schematic of a pulsed Doppler circuit is shown in Figure 4, and the signals and spectra at the marked locations are shown in Figures 5 and 6. A sinusoidal signal (signal **a**) is generated by an oscillator and multiplied by a gate function (signal **b**) such that a sinusoidal burst with envelope $e(t)$, oscillation $\cos(\omega_o t)$ and duration τ_b (signal **c**) is transmitted to the target every τ_p seconds. When the particle approaches along the axis of the probe, the returned signal is a delayed and dilated version of the transmitted signal (signal **d**). This is then multiplied by a second gate function (signal **e**) which is delayed by τ_d from the first gate. As a result of the compression of the returned signal,

* The power spectrum is the magnitude squared of the amplitude spectrum. Only the real part of the amplitude spectrum is shown.

the time between the returned bursts is not the same as the time between gate pulses, so the number of cycles at f_0 which pass through the gate changes with time (signal **f**).

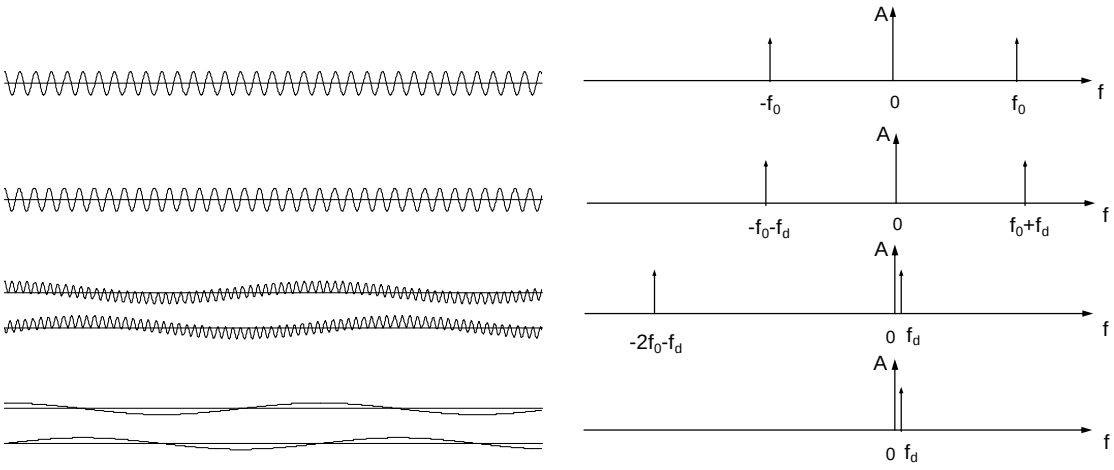

Figure 3: Signals (left hand side) and amplitude spectra (right hand side) for the marked locations on Figure 2. The returned signal (b) assumes a single target approaches the probe and neglects attenuation and beam spread. Location (a): the output of the oscillator ($\sin \omega_0 t$). The spectrum consists of two delta spikes at $\pm$ the carrier frequency. Location (b): the returned Doppler signal ($\sin((\omega_0 + \omega_d)t)$). The spectrum has been dilated in frequency. Location (c): the returned signal multiplied by the oscillator output. The spectrum has been shifted to the left by the carrier frequency. Location (d): the output of the low-pass filter. Only the Doppler shift component remains in the spectrum.

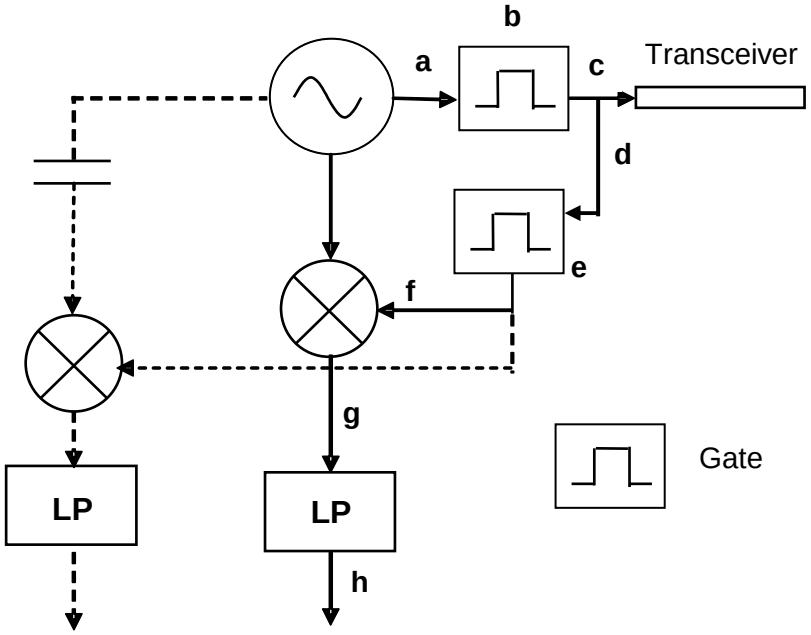

Figure 4: Schematic diagram of a pulsed Doppler instrument. Definitions for the schematic symbols are shown in Figure 2. The signals associated with locations marked **a**, **b**, **c**, **d**, **e**, **f**, **g** and **h** are shown in Figures 5 and 6. The pathways represented by solid lines provide the in-phase signal, and the pathways represented by the dashed lines are needed to obtain the quadrature signal.

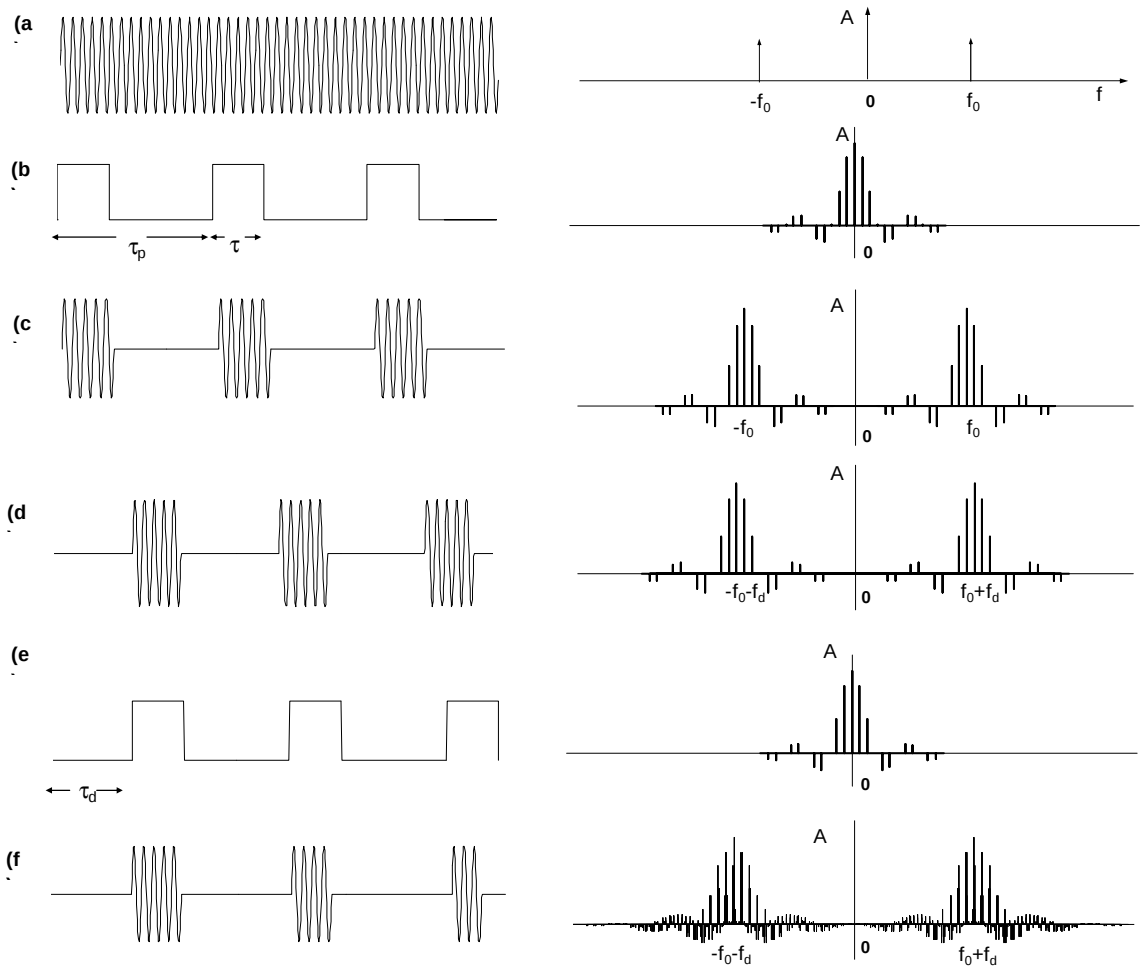

Figure 5: Signals (left hand side) and amplitude spectra (right hand side) for the marked locations on Figure 4. The returned signal **d** neglects attenuation, beam spread and the frequency response of the probe, and assumes a single target approaches the probe. Location (a): the output of the oscillator ($\sin(\omega_0 t)$). The spectrum is two delta functions at $\pm f_0$. Location (b): the gate $g_t(t)$ for the transmitted signal. The spectrum is a sinc function evaluated at frequencies separated by the pulse repitition frequency. Location (c): the gated oscillator signal. The spectrum is the convolution of spectrum (a) with spectrum (b). Location (d): the returned Doppler signal. The spectrum is a dilated version of spectrum (c). Location (e), the receiver gate $g_r(t)$. This is shifted in time by τ_d from the transmitter gate. Location (f): the returned signal after it has been multiplied by the receiver gate. The gating causes the pulse duration to change from pulse to pulse. The spectrum is the convolution of the spectrum in (d) with that in (e), and this causes the the individual spectral lines to spread in frequency.

As shown in Figure 6, the gated return is multiplied by the oscillator signal $\cos(\omega_0 t)$ to yield signal **g**, and the output of this is low pass filtered to obtain signal **h**. In the illustration, the low passed signal consists of samples which are time averages over τ_g of

the bursts in signal **g**. The objective of range gating is to localize the measurement volume to a region between $\frac{1}{2}c(\tau_d - \tau_b)$ and $\frac{1}{2}c(\tau_d + \tau_g)$. In practice, the measurement is localized to a series of sample volumes separated by $\frac{1}{2}c\tau_p$ (see aliasing below).

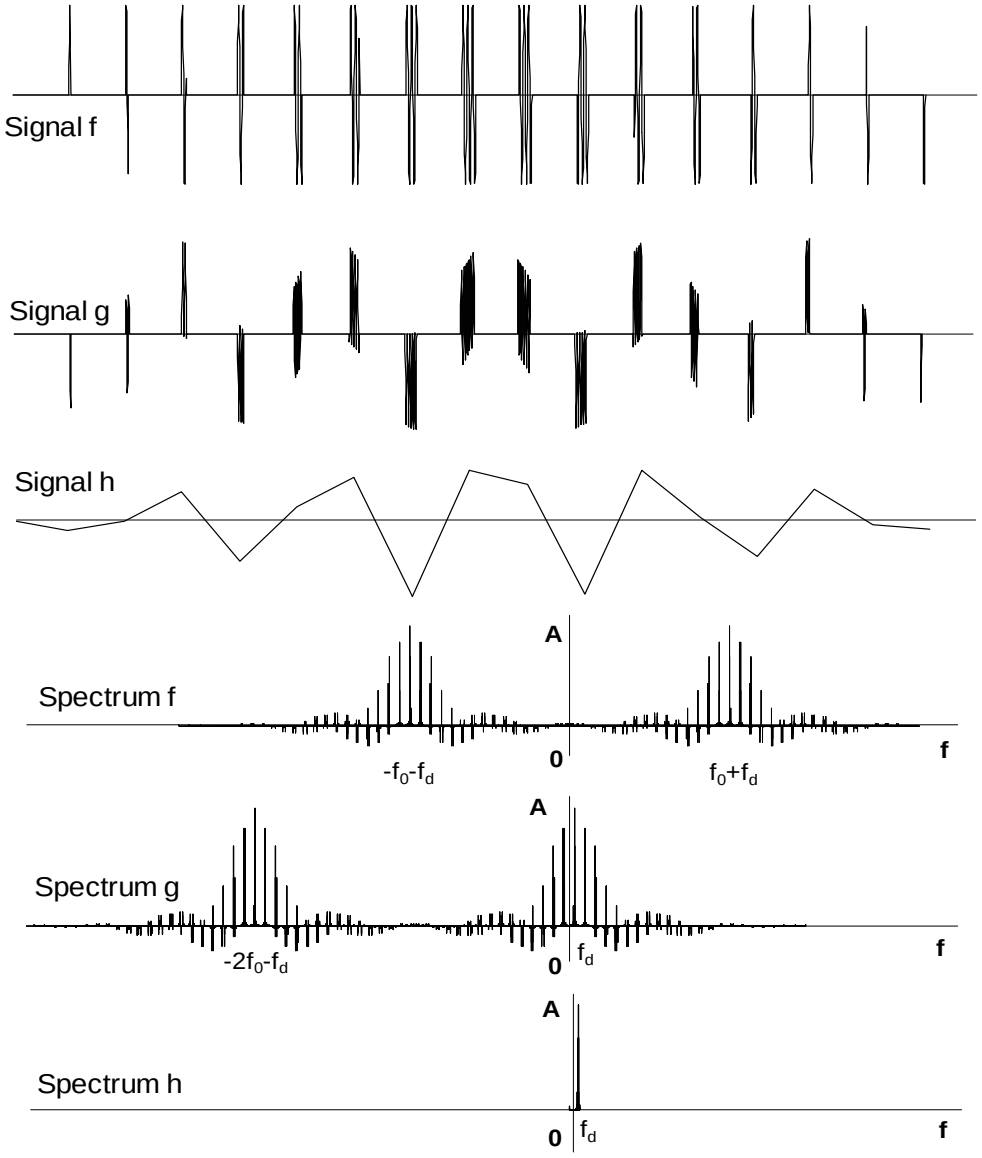

Figure 6: De-modulation of the pulsed instrument. Location (f): same is as in Figure 5 above, but more pulses are shown. Location (g): the returned signal has been multiplied by the oscillator signal, and the spectrum is that of (f) shifted by f_0. Location (h): the output of the low pass filter. Only a single broadened peak remains in the spectrum.

The gating dramatically changes the spectra of both the transmitted and downmixed signals. Spectrum **a** consists of two delta function spikes at $\pm f_0$. The spectrum of the gate has the shape of a **sinc** function, but since it is periodic, it contains components at discrete frequencies separated by the pulse repetition frequency, f_p. Since signal **c** is signal **a** multiplied by signal **b**, its spectrum is the convolution of spectrum **a** with spectrum **b**. Spectrum **d** is nearly identical to spectrum **c**, except that it is dilated in frequency by $\hat{\alpha}$. Spectrum **e** is again a sinc function evaluated at discrete frequencies separated by f_p. Spectrum **f** is the convolution of spectrum **d** with spectrum e. Since the separation between components in spectrum **d** is different from that in spectrum **e**, the convolution causes the frequency components to be broadened. This broadening impairs the ability to localize the precise Doppler shift and is a major source of ambiguity as discussed in section III-C.

The downmixing of the pulsed Doppler spectrum is similar to that of the continuous case. The range-gated spectrum (Figure 6, Spectrum **f**) is shifted to the left by the carrier frequency (Spectrum **g**), and a low pass filter is applied (spectrum **h**). However, the low pass filter must eliminate frequencies separated by f_p as well as the spectrum centered on $-2f_0 - f_d$. It must therefore have a much narrower bandpass.

In a more realistic measurement, where targets (red blood cells) are distributed in space, each pulse returns a signal similar to that shown in Figure 7, which is called an A-line. The time axis of this signal corresponds approximately to the depth in the vessel from which sound is scattered. The amplitude variations in this signal have a characteristic time scale of τ_b.

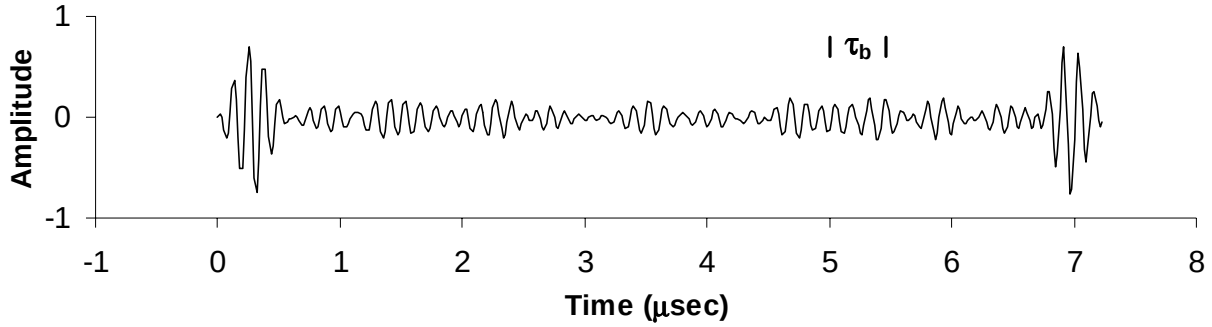

Figure 7: A simulation of an A-line from flow. The larger amplitude signals at $t = 0$ μsec and $t = 7$ μsec represent reflections from the vessel walls.

It will be important in part III to know how the signal from a given particle depends on the position of that particle within the sample volume. In the following discussion it is assumed that the ultrasound transducers do not filter the transmitted or received signals. Newhouse and Amir[142] examined pulsed Doppler instruments for which the duration of the receiver gate, τ_g, is much smaller than that of the echo signal. In this case, if a particle approaches the probe with constant velocity v, the downmixed signal is a rep-

lica of the echo from the particle, but is time-dilated by a factor of $\frac{c}{2v}$. If the particle is receding, the same theorem applies except that the signal is time-inverted. An alternative description of this, as shown in Figure 8, is that the envelope of the downmixed signal is directly related to the position of the particle within the sample volume. Consider $z_2 = \frac{1}{2}c(\tau_d + \tau_g)$ to be the far edge of the sample volume. Then if the distance from the particle to the probe is $z_2 - z_s$, the envelope of the downmixed signal is proportional to the envelope of the transmitted pulse evaluated at a time $t = 2z_s c$. This defines the sample volume shape to be identical to that of the transmitted signal, but inverted and constrained between z_2 and $z_1 \equiv (\tau_d - \tau_b)c/2$.

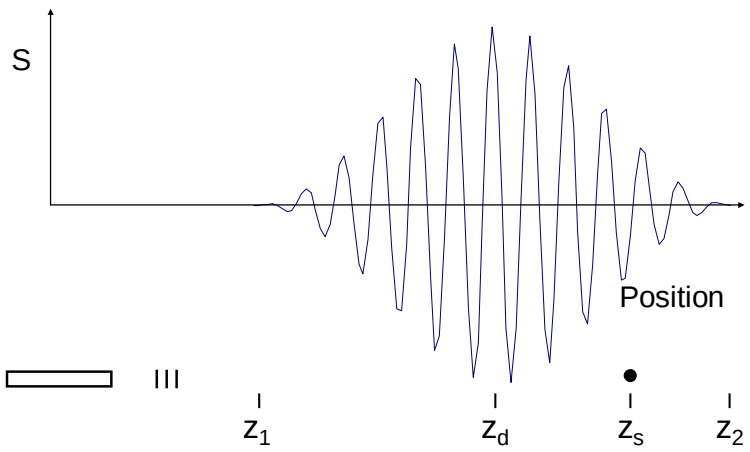

Figure 8: Illustration of how the pulsed Doppler signal depends on location within the sample volume. The signal (s) is the in-phase signal from the probe and has its peak value when the particle (p) is at the position $z_d = c\tau_d/2$. It is assumed that the particle velocity is high enough that the signal is not affected by the high pass filter in the Doppler instrument.

Forsberg and Jorgensen[143] have shown that when the range gate is vanishingly small, it is not necessary to mix the returned echo with the reference oscillator signal. The returned rf signal is sampled directly at the pulse repetition rate, and is therefore grossly undersampled. The spectral content of the signal is confined to a band between $\pm f_p/2$ through aliasing. The advantage to this is a reduction in hardware and hence in the amount of hardware related noise. However, their preliminary results did not show substantial improvements in overall signal quality.

In most pulsed Doppler instruments, the range gate duration is finite rather than infinitessimal. It can be shown that under these circumstances the axial dependence of the sample volume shape, defined here to be the envelope of the downmixed signal as a function of the particle position, is a convolution of the transmitted-signal envelope with the shape of the range gate. If the transmitted signal has the form $e_s(t) = e(t)\cos(\omega_0 t)$, and the receiving gate is $g_r(t)$, then the received signal is $g_r(t)e(t-2z/c)\cos(\omega_0 + \omega_d t + \phi)$, where z is the distance from the probe to the particle. It is assumed that v/c is small enough that the envelope is not significantly altered by the Doppler effect. The phase ϕ is $2\omega_0 z_0/c$ where z_0 is the particle position at time $t = 0$. When the returned signal is mixed with the carrier and integrated (low pass filtered) over a time Δt that is longer than the duration of $e(t)$ and long in comparison to $1/\omega_0$, but short in comparison to $1/\omega_d$, the result is:

$$s_r(z,t) = \tfrac{1}{2} \int_{-}^{t+t} g_r(\tilde{t})\, e(\tilde{t} - 2z/c) \cos(\omega_d \tilde{t} + \phi)\, d\tilde{t} + \tfrac{1}{2} \int_{-}^{t+t} g_\tau(\tilde{t})\, e(\tilde{t} - 2z/c) \cos((2\omega_0 + \omega_d)\tilde{t} + \phi)\, d\tilde{t}$$

Eq. 6

The argument of the second integral is a high frequency term and is filtered out by the integration. Furthermore, since Δt is short in comparison with $1/\omega_d$, the cosine in the first integral is essentially constant throughout the time of the integration and can be taken outside the integral. The result is:

$$s_r(z,t) = \tfrac{1}{2} \int_{-}^{t+\Delta t} g_r(\tilde{t})\, e(\tilde{t} - 2z/c)\, d\tilde{t}\ \cos(\omega_d t + \phi) \qquad \text{Eq. 7}$$

The integral in Equation 7, which is the amplitude of the returned echo, is the convolution of the transmitted signal envelope with the receiver gate. For example, if both the transmitted signal envelope and the receiving gate are rectangular, the downmixed signal from a particle that crosses the sample volume along the probe axis has a triangular envelope[144, 145]. The rectangular pulse shape is used here only as an idealized example. In practice, a rectangular pulse has significant sidebands outside the typical bandwidth of a Doppler transducer. This type of signal is thus, significantly altered upon transmission.

Equation 6 can be reconciled with the result of Newhouse and Amir[142]. For a short duration range gate, the gate in Equation 7 is a delta function at the delay time τ_d (i.e. $g_r(\tilde{t}) = \delta\tilde{t} - \tau_d$ and Equation 7 becomes $s_r(z,t) = \frac{1}{2} e(\tau_d - 2x/c)\cos(\omega_d + \phi)$. If velocity is constant and axial so that $z = vt$, the envelope of the signal is $e(\tau_d - 2vt/c)$, which is again a time-inverted and dilated version of the transmitted-signal envelope when the particle is receding from the probe.

3. Alternative Waveforms

In general it is not necessary for the transmitted signal to be a sinusoid since the Doppler effect dilates (or compresses) any signal which is scattered from a moving target. Some of the waveforms which have been used, such as narrowband noise, pseudorandom sequences, and frequency modulated sweeps are described by Newhouse[146], and will be discussed in section V-A.

C. Doppler Angle

One of the most difficult problems in Doppler ultrasound is the estimation of the angle θ between the target velocity and the probe axis. The Doppler shift is a strong function of this angle, particularly when θ is near 90°. The first order approximation is to assume that the flow velocity is in the direction of the vessel. Two problems arise from this assumption. First, some knowledge of anatomy is required if the vessel axis direction is to be approximated, and anatomy varies from individual to individual. Secondly, the velocity vector is not necessarily parallel to the vessel axis. It has even been asserted[147] that non-axial flows are more common than axial flows. Certainly at bifurcations, anasto-

moses and stenoses there is substantial secondary flow[148], and these are regions of high interest to vascular research.

Detection of the vessel axis orientation has become less of a problem since dual mode ultrasound devices have become more common (Barber et al.[149]). The vessel geometry is determined directly by ultrasonic imaging. However, this does not address the problem of flow velocity that is not paraxial. Some techniques which address the Doppler angle problem are described in subsections V-B-2 and V-B-3-b on multi-dimensional Doppler measurements.

D. Beam Patterns

Subsection II-B-2 above described how range gating localizes the Doppler sample volume axially. The radial extent of the sample volume is determined by the beam pattern of the ultrasound probe, $G(r,z,\theta)$, where, r, z and θ define a cylindrical coordinate system with z along the probe axis. Far from the probe (in the far-field), the transmitted intensity, for a circular transducer can be written as $G_r(r/z)G_z(z)$, where $G_r(r/z)$ is a self-similar radial component and $G_z(z)$ is an axial component. The wavefronts are nearly planar, so the Doppler angle is well defined. Often, however, measurements are made too close to the probe for the far-field approximations to hold[150], and in these cases the probe intensity is a complicated function of radial and axial position (see the intensity patterns shown by Wells[132]). This has important consequences to the spectral broadening effects described in subsection III-C.

By the well-known theorem of reciprocity[151], a transducer's receiver beam pattern is identical to its transmitter beam pattern. Usually, one transducer is used as both the transmitter and the receiver in pulsed Doppler ultrasound. In this case, the received power from a particle at a given point contributes to the received power (and hence to the power spectrum) in proportion to the square of the beam pattern intensity.

E. Aliasing

Pulsed Doppler measurements can be aliased in both space and frequency[152]. Frequency aliasing results from the Nyquist (Shannon) theorem for sampled signals; if a signal sampled at frequency f_s contains a frequency component f_a, outside the range $-f_s/2 \le f \le +f_s/2$, then its discrete Fourier transform will exhibit components at $f = -f_s/2 + (f_a - f_s/2) \bmod f_s$. This applies to conventional pulsed Doppler ultrasound because each pulse can be considered to provide a single sample of the downmixed signal. Thus, any frequencies in the downmixed signal which are outside the range $-f_p/2 \le f \le f_p/2$ are aliased. These frequencies correspond to velocity components along the probe axis from $-\frac{1}{4}cf_p/f_0$ to $\frac{1}{4}cf_p/f_0$. The presence of f_0 in the denominator of this range causes aliasing to be more of a problem for higher-frequency devices.

Spatial aliasing (range ambiguity) results because echoes from multiple pulses are received at any given time from secondary sample volumes separated by a distance of $c\tau_p/2$. The n^{th} gate receives an echo of the n^{th} pulse from a depth of $\frac{1}{2}c\tau_d$ and echos

of the $(n-l)^{th}$ pulse from a depth of $\frac{1}{2}c\tau_d + \frac{1}{2}cl\tau_p$. The signal from the earlier pulses are successively lower in amplitude as a result of the increase in signal attenuation with depth. A decrease in the pulse repetition frequency reduces the spatial aliasing problem because it separates the secondary sample volumes. However, it also increases the effect of frequency aliasing. Several methods have been proposed to compensate for frequency aliasing. The high frequency sampling methods of subsection V-B-3 do this through the use of information that is not considered in conventional pulsed-Doppler units. Other methods, described in subsection V-D-4 on time-domain signal analysis methods, use reasonable assumptions such as continuity in the Doppler shift, the Doppler spectrum, or the velocity profile.

F. Doppler Frequency Estimates

A number of methods are used to obtain the Doppler shift, and hence the velocity estimate, from the Doppler spectrum. The first moment or centroid frequency is defined as:

$$\overline{f} = \frac{\int_{-\infty}^{\infty} fP(f)df}{\int_{-\infty}^{\infty} P(f)df} \qquad \text{Eq. 8}$$

and is particularly important for its relation to the mean flow rate. The mode or peak frequency, f_{mode}, is the frequency which corresponds to the maximum power density in the spectrum. The maximum frequency, f_{max}, is the highest frequency for which $P(f)$ is non-zero. Since noise will almost always be present throughout all frequencies in the spectrum, the mode frequency is usually defined in practice as the highest frequency for which $P(f)$ is above some pre-selected threshold that depends on **a priori** knowledge of the background noise. This estimate is proportional to the highest velocity present in the sample volume.

III. DETERMINANTS OF DOPPLER SPECTRA

Numerous effects contribute to the ultimate shape of a Doppler ultrasound power spectrum. These are separated below into the following categories: 1) the relationship between the velocity field and the transducer beam pattern, 2) contributors to spectral distortion, such as reflection, refraction, scattering and attenuation, and 3) spectral broadening caused by ambiguity noise, which includes transit time and geometric broadening and the effects of multiple scatterers. An introduction to the composition of the Doppler spectrum is given in the review by Hoeks et al.[153]

A. Velocity Field and Beam Pattern

Velocity gradients, accelerations and turbulence cause broadened spectra for the same reasons; within the sample volume over the time of the measurement a range of velocities is present, and each velocity is associated with a frequency in the spectrum. Velocity gradients contribute because the measurement is taken over a finite sample volume. As that volume increases, the range of velocities increases. Accelerations contribute to spectral broadening because the measurement is taken over a finite period of time. If

the measurement begins when the velocity is 30 cm/sec and ends when the velocity is 40 cm/sec, the frequencies that correspond to that range of velocities will be present in the spectrum. Broadening associated with turbulence is caused by both spatial and temporal averaging because the turbulent velocity field is random in both time and space. Kikkawa et al.[111] have analyzed the effect of flow acceleration on the Doppler spectrum. They note that the acceleration portion of systole has a duration of about 20 msec, so that the mean frequency changes substantially for time records on the order of 10 msec. Fish[154] shows effects of similar magnitude for a common carotid waveform during the deceleration portion of systole. He states that a narrower spectrum can be obtained if the analysis window is shortened from 10 msec to 5 msec. Garbini at al.[15, 16] discuss velocity fluctuations caused by turbulence, and derive an expression for the shape and width of the consequent Doppler spectrum.

A number of authors have described how the interaction between the velocity field and the ultrasound sample volume shape determines the underlying Doppler power spectrum and the accuracy of the velocity measurement. Brody and Meindl[122] developed an analytical model that included these effects as well as transit time broadening effects. Brown et al.[155] used a computer model to simulate the effects of spatial averaging on spectra in small arteries, although they did not attempt to model the transducer beam pattern accurately. Cobbold et al.[156] generated a computer model that used the beam pattern and flow profile to generate the expected power spectrum. Experimental studies by Law et al.[157] on an 8.2 mm inner diameter tube demonstrated the effects of spatial averaging and other spectral broadening sources described below on the power spectra and derived indices. Jorgensen and Garbini[158] presented a method by which Doppler velocity measurements with severe spatial averaging could be corrected by a deconvolution process so that a more accurate velocity profile could be obtained. The contribution of flow velocity to the Doppler power spectrum can be described by Brody and Meindl's model for continuous wave Doppler ultrasound[122], which is simplified here to neglect transit time effects. For steady, deterministic flow, the equation is:

$$P(\omega) = \tfrac{1}{2}\rho\sigma_A^2 E_0 \iint G^2(\vec{r})\, a(\vec{r},t)\, e^{-j\left(\vec{k}\bullet\vec{v}(\vec{r},t)+\omega\right)t}\, dt\, d\vec{r} \qquad \text{Eq. 9}$$

The component of the spectrum at frequency ω is $P(\omega)$. The product outside the integral, and hence the overall magnitude of the power, depends on the average concentration of the scatterers, ρ, the scattering cross-section averaged over all scatterers, σ_A, and the amplitude of the transmitted signal, E_0. The integration is over time and the three dimensional spatial vector $\vec{r}$. The beam pattern function, $G(\vec{r})$ is the intensity of incident sound at position $\vec{r}$. The factor $a(\vec{r},t)$ is the spatial dependence of the particle concentration. The vector $\vec{k}$ defines the direction of propagation of the sound wave, and $\vec{v}(\vec{r},t)$ is the flow velocity vector as a function of position. The inner integral has the form of a Fourier transform with ω as the transform variable. Equation 9 can be further simplified when $a(\vec{r},t)$ and $v(\vec{r},t)$ do not depend on time and $\vec{k}\bullet\vec{v}(\vec{r},t)$ can be rewritten as $kv\cos\theta$. The scalars k and v are, respectively, $\left|\vec{k}\right|$ and $\left|\vec{v}\right|$, and θ is the angle between the $\vec{k}$ and $\vec{v}$ directions. This angle can, in general, be a function of $\vec{r}$. The

wavenumber $\vec{k}$ is $2\omega_0/c$, where ω_0 is the carrier frequency of the transmitted signal, and c is the speed of sound in the medium. With these considerations, Equation 9 can be integrated over t, and the result is:

$$P(\omega) = \tfrac{1}{2}\rho c \sigma_A^2 E_0 \int G^2(\vec{r}) a(\vec{r}) \delta\left(\frac{2\omega_0 v(\vec{r})}{c}\cos\theta(\vec{r}) + \omega\right) d\vec{r} \qquad \text{Eq. 10}$$

This equation, or an equivalent form, has been used by several authors to calculate spectra for specific flow velocities[122, 155, 159]. It states mathematically that each component, $P(\omega)$, in the Doppler spectrum arises from a weighted average over space of signals from all particles with velocity $v = c\omega/(2\omega_0 \cos\theta)$. The weighting function is the square of the local beam intensity, where the power of two results from the reciprocity of the transducer[151]. As will be shown later, the dependence on particle concentration $a(\vec{r},t)$ is an approximation that becomes invalid at high (i.e. physiological) hematocrits. Also, the power spectrum is strongly altered by transit time effects, as discussed in subsection III-C-2.

When $G(\vec{r})$ and $a(\vec{r})$ are uniform over the entire cross-section of a vessel, Equation 10 can be used to obtain the flow rate in the vessel[31]. To this end, the equation is multiplied by ω and integrated over ω. The result is:

$$\int \omega P(\omega) d\omega = \rho c \sigma_A^2 E_0 G^2 a \omega_0 \cos\theta \int v d\vec{r} \qquad \text{Eq. 11}$$

The integral on the right hand side is directly related to flow rate if it is assumed that the flow velocity is not a function of axial position and that the axial extent of the sample volume is constant throughout the vessel cross-section. This is the basis for the well known “uniform insonification” method for flow rate measurement [4, 31, 51, 160]. Problems associated with this method are discussed in subsection V-B-2-b below.

If the probe beam pattern is uniform over the sample volume, the above discussion leads to the model of the Doppler ultrasound spectrum described in Part I above; the frequency in the Doppler spectrum is proportional to velocity, and the total power between frequencies f_1 and f_2 is proportional to the volume occupied by particles with velocities in the corresponding range between v_1 and v_2. Some representative examples are shown in Figures 9 and 10. For blunt flow (**a**) only a single velocity is present, and the spectrum is a delta function at the corresponding frequency. For couette flow (**b**) $v(\vec{r})$ is Ky, where K is a constant and y is the distance from the wall, and the spectral density is constant up to the frequency that corresponds to the maximum flow velocity, and then drops to zero. For Poiseuille flow, (**c**), the same result holds because both the velocity gradient and the area of a band between r and $r + dr$ increase linearly with r and these cancel one another in the integral. For a blunter flow, such as entrance flow into a pipe, (**d**), the higher velocities are predominant, and the power spectrum exhibits a prominent high frequency peak. Downstream of a constriction, (Figure 10) a high frequency component is caused by the central jet region, a lower frequency peak is

caused by the forward-flow part of the recirculation zone, and a peak at negative frequency is caused by the reverse flow. In practical Doppler measurements, the spectral power approaches zero as the frequency approaches zero because a high pass filter is used to eliminate components from stationary boundaries, such as the vessel wall.

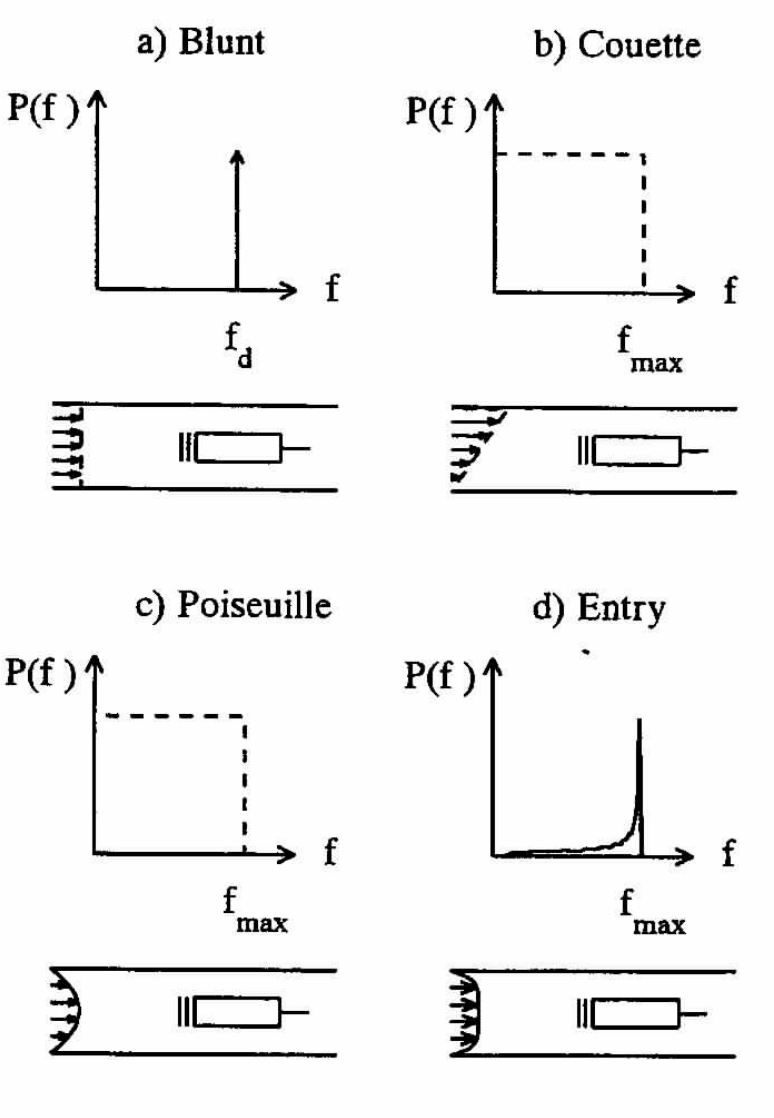

FIGURE 9. Theoretical spectra for several flow configurations with a uniform beam pattern. Couette and Poiseuille flow have identically shaped spectra. With a blunter entry flow, more power is concentrated near f_{max}.

Even under the most ideal measurement conditions, the probe beam pattern is non-uniform. Figure 11 shows the idealized Doppler spectrum downstream of a constriction for the case where the beam pattern shape is Gaussian. Since the beam power is much lower in the recirculation region, the reverse flow and forward recirculation parts of the spectrum are strongly attenuated. The beam pattern shape is primarily a function of the probe geometry and the transmitted signal. However, it can be distorted by refraction as a result of variations in acoustic impedance within the body. In addition, the returned power depends not only on the beam pattern, but on the scattering properties of blood and on the attenuation of sound in the intervening tissue. These phenomena are discussed in the following section.

B. Spectral Distortion

1. Scattering and Attenuation

The number and arrangement of scatterers directly affects the backscattered power. In the simplest model, backscattered power increases linearly with the number of scatterers. This assumes that the locations of the particles are independent of one another. The probability density for the returned signal then becomes Gaussian[161]. However, this

relationship holds only when the concentration of particles is small. For blood flow, where erythrocytes are the scatterers, the volume concentration of these cells is the hematocrit, which can be on the order of 50%, and the particles are not independently located because they cannot occupy the same space. Early studies of the relationship between intensity and hematocrit were undertaken by Shung et al.[162] and Borders et al.[163]. Shung et al.[162] found that intensity increased linearly with hematocrit for concentrations up to 8%, reached a peak at 25%, and then decreased as hematocrit increased. Borders et al.[163] found similar results, except that their curves were linear only up to 2% and did not decrease at the higher hematocrits. After subsequent attempts to correlate his results with theoretical models, Shung concluded that the decrease in backscattering at high hematocrits was correct, but that the peak near 25% hematocrit was valid only for turbulent flow[164]. Subsequent curves measured from laminar flow exhibited a peak at 13% hematocrit, which agreed quantitatively with theory[165] and qualitatively with one dimensional simulations by Routh et al.[166].

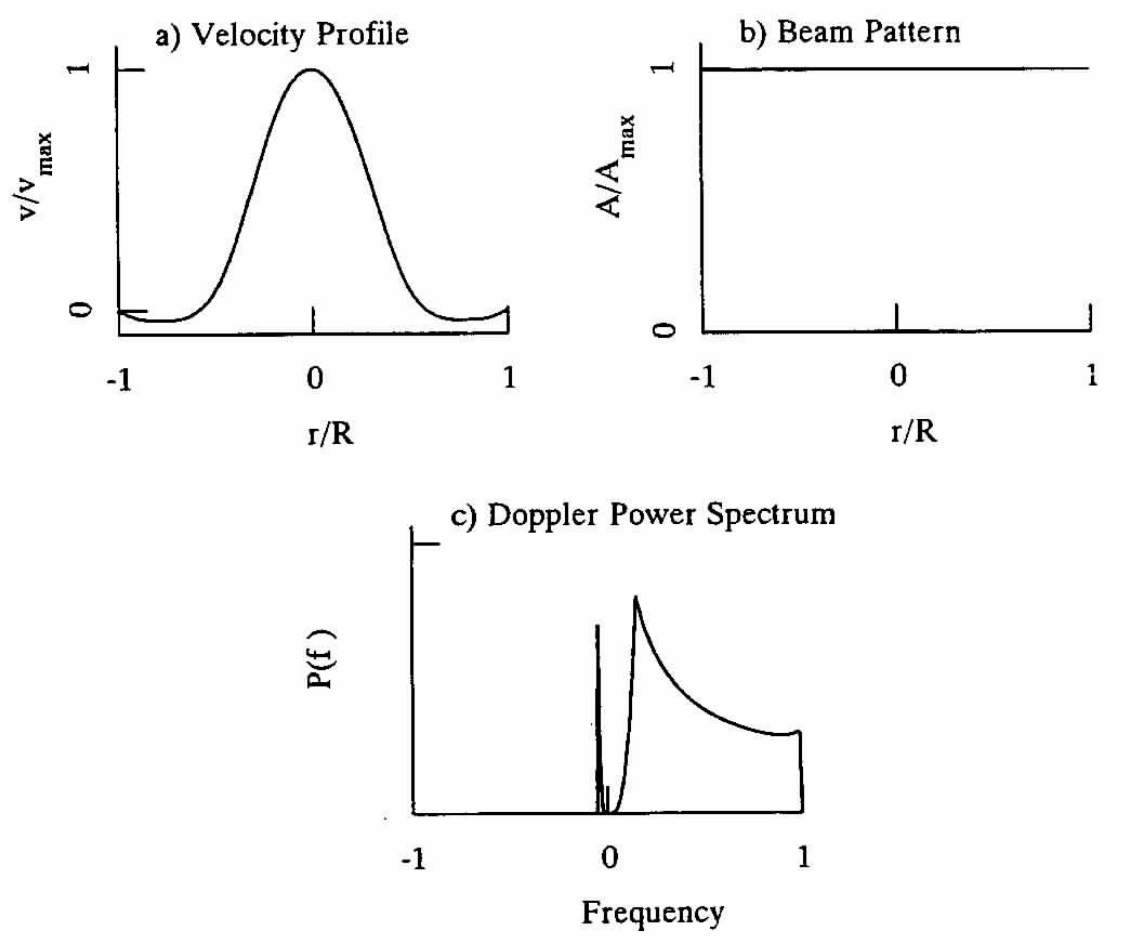

FIGURE 10. Theoretical spectrum for flow downstream of a stenosis when the beam pattern is uniform. The reverse flow causes the peak at negative frequency and the forward part of the recirculation region causes the high power at low positive frequencies. The reduction in power near zero frequency is caused by the high pass filter.

The decrease in scattered power at high hematocrits is a consequence of coherent scattering (see also subsection III-C-4). It is known that the pressure waves from uniformly and tightly packed particles interfere destructively, so that the ultrasound signals result from fluctuations in the particle concentration[161, 167, 168], rather than the particle concentration itself.

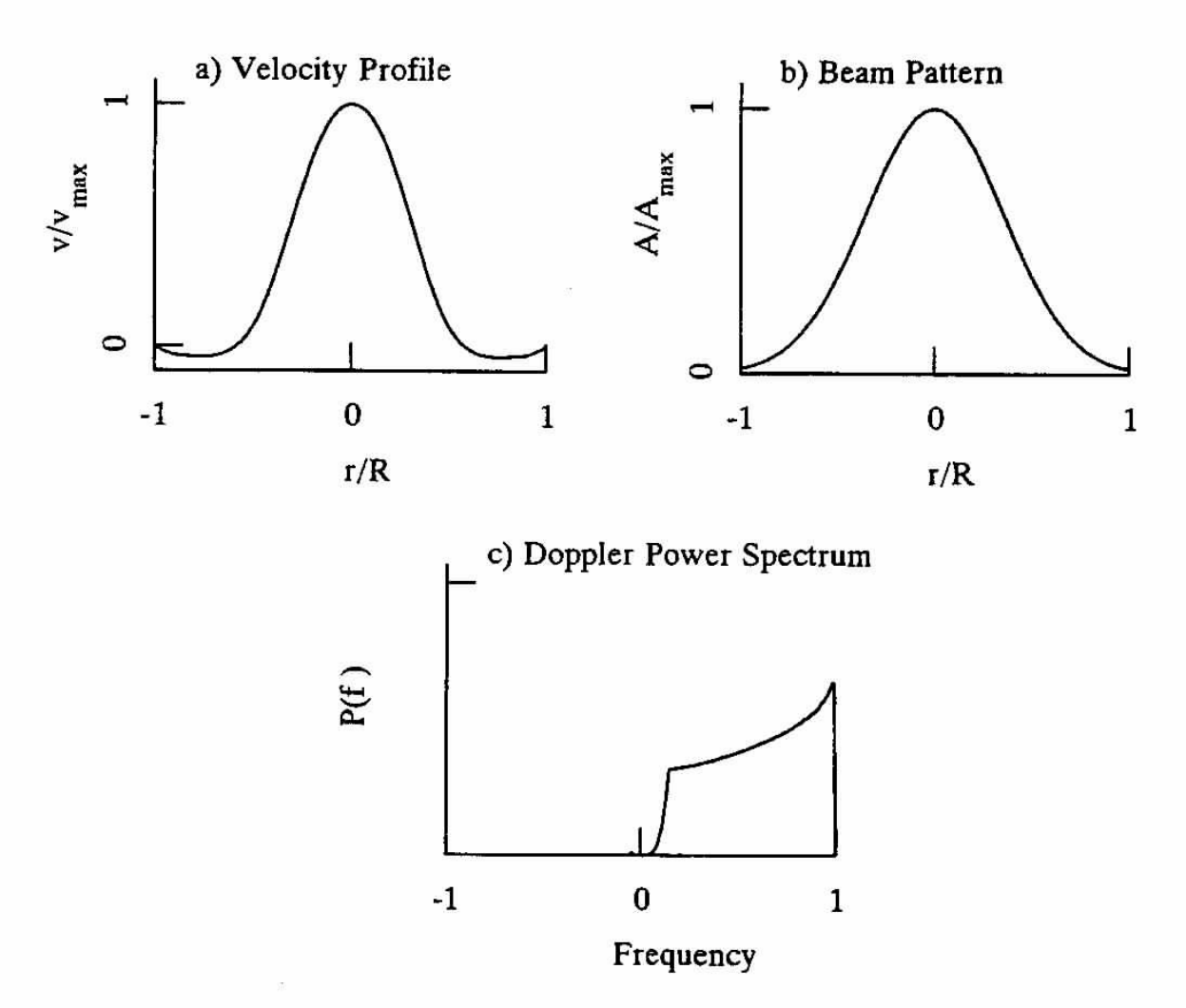

FIGURE 11. Theoretical spectrum for flow downstream of a stenosis when the beam pattern is Gaussian. The reverse flow and forward recirculation parts of the spectrum have been greatly reduced in power over the uniform beam case of Figure 10.

Since backscattering depends on the particle arrangement and the flow characteristics such as turbulence[164] and shear rate[169], it affects not only the magnitude of the Doppler signal, but also the shape of the power spectrum. This can be readily seen in the case of continuous wave Doppler, where the sample volume is large and can simultaneously include, for example, both laminar and turbulent flow downstream of a stenosis. In this case, the spectral components which correspond to the turbulent flow are weighted more heavily in the power spectrum as a consequence of the higher scattering coefficient.

Both attenuation and scattering increase with increased transmitted frequency. It is well accepted that attenuation in tissue causes a reduction in signal amplitude proportional to $e^{-\gamma\omega r}$, where γ is a constant and r is the distance traveled into the medium[170]. Scattering is generally accepted to increase in proportion to the square of the frequency[171]. This means that as the depth of the measurement increases, the amount of sound returned to the transducer decreases. Since attenuation is a stronger function of frequency than scattering is, the signal to noise ratio tends to decrease as the carrier frequency is increased. This is one reason why instruments with lower carrier frequencies are used for deeper measurements. The other reason is the direct tradeoff between pulse repetition frequency and carrier frequency which results from aliasing (section II-E). High carrier frequencies are otherwise desirable since they allow smaller sample volumes and reduce transit time effects (subsection III-C-2).

Attenuation and scattering have opposing effects on the mean frequency of the Doppler power spectrum. When the transmitted signal propagates through the tissue, the higher components of its spectrum are attenuated. However, the strength of the scattering from the higher components is stronger. Newhouse et al.[172] derived an expression for the net effect of these opposing processes on the spectrum. They showed that for a spectrum with Gaussian shape, the center frequency of the spectrum depended on the attenuation parameter $\varepsilon = D\gamma\omega_0$, where D is the depth of the measurement, and on the bandwidth ratio $b_r = \left(f_0 / B_0\right)^2$, where B_0 is the bandwidth of the transmitted signal. For example, when $\varepsilon < 1$, as is generally the case for ultrasound transmission through blood with a carrier frequency of 3.5 MHz, the center frequency tends to increase. For $\varepsilon > 1$, as in many measurements through muscle, the center frequency tends to decrease. Holland et al.[173] measured the affects of attenuation on spectra and showed qualitative agreement with the theory by Newhouse et al.[172] They suggested that the quantitative differences may be caused by an attenuation coefficient for their tissue phantom that was not linear with frequency. Similar results to those of Newhouse et al.[172] have been found by Gilson et al.[174], Round and Bates[171], and Embree and O'Brian[175]. The values cited for the shift in center frequency tend to be on the order of 100 KHz. This may be surprising at first, since it is much greater than the Doppler shift from the scatterers. However, the change in the center-frequency of the downmixed spectrum is equal to that of the rf spectrum multiplied by $2v/c$. The difference between the Doppler shift and the shift caused by attenuation and scattering can be seen from the spectrum of Figure 5c. For the Doppler shift, the discrete lines are shifted in frequency, whereas for attenuation and scattering the relative amplitude of each line is altered.

Frequency-dependent attenuation also results in frequency-dependent phase velocity for the ultrasound signal, as has been discussed by O'Donnell et al.[176] Fish and Cope[177] have shown that this has a small effect on the location and shape of the sample volume.

Changes in the backscattered spectra as a result of attenuation have been examined in applications to tissue characterization, since it may be possible to differentiate tissues from the slope of the attenuation-frequency curve[170]. It has also been noted that errors

in attenuation coefficients can occur when these are based merely on the peak values of incident and received waveforms, rather than on the complete spectra of the transmitted and received signals[178].

Attenuation and scattering effects greatly complicate the *in vitro* modeling of Doppler ultrasound blood flow measurements. Oates[179] has addressed a number of problems which must be solved if the blood analogue fluid is to strictly model *in vivo* conditions. The fluid must model the frequency dependent attenuation and scattering properties of blood. It must also exhibit the shear-dependent scattering described by Sigel et al.[169] and the turbulence-dependent scattering described by Shung et al.[164]. Hemodynamically, it must model the shear dependent viscosity of whole blood.

2. Reflection and Refraction

The standard acoustic phenomena of reflection and refraction also affect spectral shape. These alter the beam pattern of the probe and hence the spectral content of the returned signals. Thompson et al.[180] have modeled the effects of refraction and have shown that critical angle effects apply to ultrasound signals; when the angle between the acoustic wave vector, $\vec{k}$, and the interface between the blood vessel and the surrounding tissue is small, and when the acoustic impedance of the vessel is smaller than that of the surrounding tissue, there is total reflection over part of the beam.

A phenomenon known as mirroring[181] can lead to erroneous interpretations of the Doppler signals. This happens where large mismatches in acoustic impedance exist, such as at the lung interface. The large mismatch causes a sharp reflection of the ultrasound signal. Thus as the sample volume is marched past the vessel of interest, another vessel appears to be present.

There is evidence that partial reflections from the boundary between the blood and the arterial wall can alter the beam pattern of the ultrasound probe and strongly affect the shape of the Doppler power spectrum. This was noted in *in vitro* studies on an intracoronary Doppler guidewire[182]. Multiple spectral peaks were found when the acoustic impedance between the fluid and the model wall was not matched, and these disappeared when the impedance was matched. It was noted that spectral distortion was seen for impedance mismatches similar to those between blood and arterial walls.

A similar effect was noted by Poots et al.[183]. Their *in vitro* measurements from acrylic models indicated a reduction in transducer field strength near the model walls, which they attributed to refraction.

The spectral distortion discussed in this section results from the properties of the acoustic environment in which the measurements are made. However, the spectrum is further altered by effects which are present regardless of the environment. These have been called variously transit time broadening[122, 144, 184-186], geometric broadening [185, 187-189] and ambiguity[15, 16, 190] in the literature. Although the distinctions between these often seem clear from their descriptions, the true differences among them are not yet clearly defined.

C. Spectral Broadening and Ambiguity Noise

1. Ambiguity

In the literature, the term “ambiguity” seems to have several meanings. It can refer to the noise inherent in the velocity estimate, the multiple sample volumes present in pulsed Doppler ultrasound, or the velocity aliasing which results when the pulse repetition frequency is too low. In a strict sense, however, it is derived from the classic ambiguity function of Doppler radar, and generically refers to the inability to precisely measure both the location and velocity of a particle given a finite observation time. In general, an attempt to improve the accuracy of the velocity measurement results in a degradation of the position estimate. Thus, one cannot simply reduce the sample volume size and the time of observation in an attempt to obtain the high spatial and temporal resolution necessary for turbulent velocity measurement. The gain in spatial resolution achieved with a focused transducer, for example, is obtained at the expense of increased noise in the velocity estimate.

Different implementations of Doppler ultrasound, such as continuous, pulsed, or random have different ambiguity properties. If one is preferred over another for a given measurement it is because the ambiguity of that implementation is localized in time and space to a region that is deemed unimportant or for which *a priori* knowledge exists. For example, consider a single particle that moves along a transducer's axis. A continuous wave Doppler instrument can accurately measure the velocity of that particle, but cannot measure its location. A pulsed Doppler instrument can localize the particle to a series of regions separated by $\frac{1}{2}c/f_p$, where c is the sound speed and f_p is the pulse repetition frequency. As a consequence of the gain in localization, there is a loss in the accuracy of the Doppler shift estimate. Random Doppler can localize the particle to a single region, but the accuracy in the Doppler shift estimate is again reduced[191]. The choice of a given instrument depends on the relative importance of the velocity estimate and the distance measurement.

2. Transit Time Broadening

An analysis of transit time broadening has been described for Doppler radar by Altes[192]. It can be explained most simply from the perspective of Fourier analysis. The underlying signal for a conventional Doppler ultrasound device is a sine wave. The Fourier transform of a sine wave is a delta function, $\delta(\omega-\omega_0)$, at the frequency of the sine wave. However, if the sinewave is altered such that its amplitude changes in time, the Fourier transform is altered. For example, if the sine wave is turned on at time $t=0$ and then turned off at time $t=T$, the transform has the form $T\mathrm{sinc}[(\omega-\omega_0)t]$, which can be thought of as a broadened delta function[193]. As the duration T is decreased, the width of the sinc function is increased. The broader the width, the more difficult it is to locate the frequency of the absolute maximum of the spectrum. This is a fundamental and well understood concept in signal analysis[193], and it is intuitive that it should apply to Doppler ultrasound. The research in recent years related to this concept has examined the exact functional relationship between the transmitted signal, the transducer characteristics, the receiver electronics, and the downmixing process.

The term “transit time” is derived from the time required for a particle to cross the ultrasonic sample volume. For a continuous wave device, this sample volume is continuously insonified so that at any point in the beam the incident pressure is a true sinusoid. However, the intensity of the beam is a function of space, so that as a particle crosses the beam transversely, the scattered signal begins low in amplitude, then increases to a peak, and then decreases again. The half bandwidth is proportional to the reciprocal of the transit time of the particle across the beam, $B = \frac{v}{W}\sin\theta$, where v is the particle velocity, W is the width of the beam, and θ is the angle between the particle direction and the beam axis (see Wijn et al.[113]). Measurement accuracy is determined by the ratio of the half bandwidth to the Doppler shifted frequency, and this is:

$$\frac{B}{f_d} = \frac{Kc\tan\theta}{2 f_0 W} \qquad \text{Eq. 12}$$

The constant of proportionality, K, depends on the radial shape of the beam and the exact definition of bandwidth and beam width. If the beam is constant between $r = \pm W/2$ and zero elsewhere, so that the corresponding Fourier transform is a sinc function, and if the half-bandwidth is defined to be the frequency difference between the maximum and first zero of the spectrum, then $K = 1$. Consider a Doppler device with carrier frequency $f_0 = 10$ MHz and beam width $W = 2$ mm which is used to measure the velocity of a particle that moves at an angle of 60° from the probe axis at a velocity of 60 cm/sec. If the sound speed is 150,000 cm/sec, the Doppler shift is 4,000 Hz. The half bandwidth is then approximately 260 Hz, or 6.4% of the Doppler shift. This simple example emphasizes the trade off between spatial resolution and frequency resolution. As the beam width is decreased to improve spatial resolution, the broadening increases. Increased carrier frequency has no effect on the bandwidth, but it increases the Doppler shift so the percent broadening is reduced and the velocity estimate becomes more accurate. Equation 12 also shows that, for continuous wave Doppler, the percent transit time broadening increases with the Doppler angle and the sound speed in the medium. The dependence on sound speed arises because an increase in sound speed causes an increase in the wavelength of the sound.

A more rigorous treatment of transit time broadening in continuous wave ultrasound is given by Brody and Meindl[122]. They show that mathematically the effect changes the factor $G^2(\vec{r})$ in Equation 9 above to $G(\vec{r})G(\vec{r}+\vec{v}\tau)$. The same factor appears in the expression for the autocorrelation function. As τ increases, the product $G(\vec{r})G(\vec{r}+\vec{v}\tau)$ decreases, so the signal becomes less correlated with time, which means that it is no longer a pure sine wave, and thus a less accurate indicator of velocity. Note that, for continuous wave Doppler, if the particle moves along the probe axis, $G(\vec{r}+\vec{v}\tau)$ changes slowly with τ, and the decorrelation is not a problem.

For pulsed Doppler, transit time effects have essentially the same physical meaning. The amplitude of the signal from a particle in the sample volume depends on the position of the particle within the sample volume. The sample volume in this case is the axial dependence of sample volume shape, as described in section II-B-2 above.

The effect of the range cell on transit time broadening can also be described in terms of the spectrum of the transmitted signal, rather than the sample volume shape. Newhouse et al.[186] have derived the following expression where it is assumed that the returned echo is downmixed with a time delayed replica of the transmitted signal:

$$P(\omega) = A_0^2 \int_{-\infty}^{\infty} \frac{\rho(\alpha)}{|\alpha|} \left| P_x\left(\frac{\omega}{\alpha}\right) \right|^2 d\alpha \qquad \text{Eq. 13}$$

where the coefficient A_0 depends on the scattering cross-section of the particles and the tissue attenuation, α is $2v/c$, $\rho(\alpha)$ is the concentration of particles which travel with $v/c = \alpha$, and P_x is the time averaged power spectral density of the transmitted signal. The broadening arises because each velocity component, α, contributes a spectrum which has the shape of $|P_x(\omega/\alpha)|^2$. The magnitude of P_x is squared because P_x is both the transmitted signal and the signal with which the returned echo is mixed. Equation 13 is valid for both conventional pulsed Doppler and random Doppler instruments. However, in pulsed Doppler signals the returned echo is not, in general, downmixed with an exact replica of the transmitted signal since 1) the transducer frequency response alters the shape of the transmitted signal and 2) the duration of the receiving gate can differ from that of the transmitted signal. Another description of range gating effects is presented by Kim and Park[185].

3. Geometric Broadening

Geometric broadening was first described by Green[194]. In this description, the Doppler shift caused by a particle is given by Equation 4, but θ is the angle between the particle velocity and the distance-vector r_p from the transducer surface to the particle position. Since the direction of r_p changes as the particle crosses the sample volume, the Doppler shift also changes. The Doppler power spectrum is computed from the square of the incident sound intensity. This is equivalent to the spatial average, weighted by the square of the beam intensity, of all Doppler shifts from the sample volume.

Newhouse et al.[189] described geometric broadening more fully in terms of the angles between all differential elements of the transducer and all particles in the sound field. They showed that when measurements are taken in the near field of a transducer the spectral width is larger than that predicted by the transit time across the beam width, and that geometric broadening could account for the larger bandwidth. However, they later showed that transit time broadening was a consequence of the probe geometry and concluded that if the complicated beam pattern in the near field were used instead of simply the overall width of the beam, the bandwidths for geometric and transit time broadening would be identical[150]. They reference the surprising result of Edwards et al.[195] that transit time and geometric broadening are the same phenomenon.

A simple example illustrates why the equivalence of transit time and geometric broadening is initially difficult to understand. Consider a simple source, as shown in Figure 12a, which radiates sound uniformly in all directions, at cartesian coordinates $x = 0$, $y = 0$, and a particle which traverses through the sound field along a straight line $y = y_0$. The resulting signal is shown in Figure 12b. The Doppler angle between the particle and the source varies from 0° at $x = \infty$ to 180° at $x = -\infty$. This results in higher frequency oscillations at the tails of the Doppler signal than in the center, and causes components of the power spectrum (Figure 12c) to extend from $-f_d$ to $+f_d$. Furthermore, the sound intensity increases from 0 at $x = \infty$ to a maximum at $x = 0$. If the signal is represented as $A(t)e^{j\vec{k}(t)\bullet\vec{v}(t)}$, as in Equation 9, then $A(t)$ leads to what is intuitively thought of as transit time broadening, and the change in the angle between $\vec{k}$ and $\vec{v}$ leads to what is intuitively thought of as geometric broadening, and the two are not equivalent. The apparent conflict is easily resolved. The analysis of Edwards et al.[195] assumes that the angle between the field vector, $\vec{k}$ and the velocity vector $\vec{v}$ is independent of position within the sample volume. This is a reasonable assumption in many cases, but is not valid in all cases. Ata and Fish[196] discuss the effect of variations in the vector $\vec{k}$ on the Doppler ultrasound signal and provide further illustrative examples.

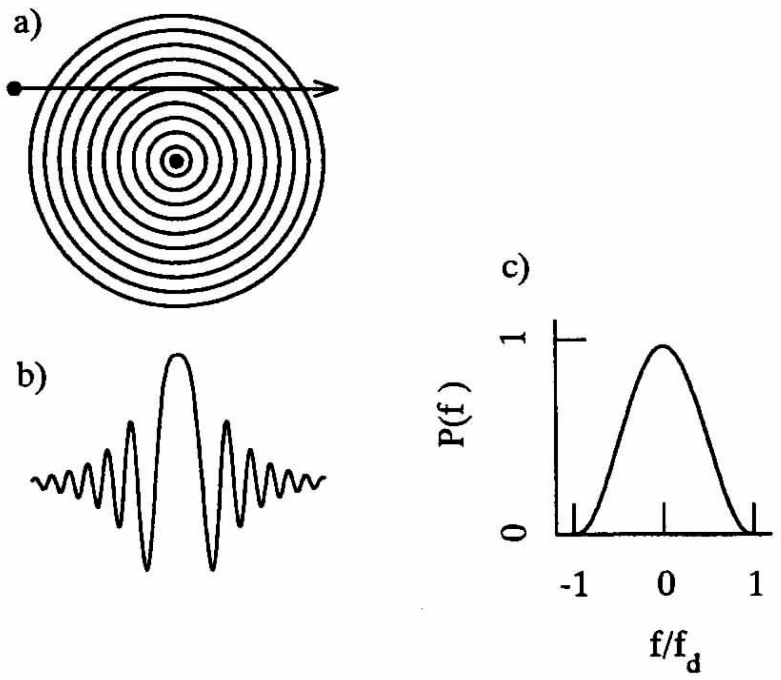

FIGURE 12. a) An illustration of a particle that crosses through the sound field of a simple source. b) The in-phase signal generated by a Doppler instrument signal which uses the simple sources as a transducer. The instantaneous frequency of this signal is high at first and then becomes lower as the angle between the particle velocity vector and the propagation direction of the wavefronts approaches 90°. c) The power spectrum of the signal in b). Broadening is caused by changes in both amplitude and instantaneous frequency.

The simple source example above implies that geometric broadening is defined by the change in angle of the wave propagation direction with spatial position, which is the product $\vec{k} \bullet \vec{v}$ in Equation (9). However, the historical definition of geometric broadening is in terms of the angles between positions on the transducer surface and positions within the sample volume region. These angles dictate both the beam pattern intensity and the wave propagation directions. Their effect on the beam pattern intensity is the amplitude modulation component of geometric broadening. If transit time broadening is defined to result from this

amplitude modulation component only, then it is not equal to geometric broadening, but is rather a subset of it. If, however, transit time broadening is defined, as by Newhouse, to be the variation in the signal caused by variations in the sound field, then geometric broadening and transit time broadening are equivalent.

Newhouse's group has given mathematical descriptions of geometric broadening[187, 189, 197, 198]. They note that since the bandwidth of the spectrum increases with increased velocity, it can, under some circumstances, be used as a measure of velocity[188] or to estimate the Doppler angle[150]. For these measurements it is necessary to know the theoretical Doppler spectrum that results from constant-velocity straight line flow through the ultrasound beam. This relationship changes if the particle path line is displaced laterally or axially since beam intensity is a function of position. However, Newhouse and Reid[199] have proven that the absolute bandwidth of the Doppler spectrum is independent of such lateral displacement in the far field of an unfocused transducer, or equivalently near the focal plane of a focused transducer. Their proof thus simplifies the extraction of information about Doppler angle or velocity. Although the proof holds strictly only in the far field or at the focal plane, experimental measurements[200] show that the theorem is reasonably accurate at other locations as well. The theorem seems to contradict a transit time model for spectral bandwidth since the width of the ultrasound beam increases with distance from the probe in the far field, which tends to cause a longer transit time and thus a narrower bandwidth. This shows that changes in the vector $\vec{k}$ of Equation (9) compensate for the longer transit time and that the full geometric broadening model must be used to obtain the correct bandwidth.

A summary of geometric broadening effects is shown in Figure 13. The sound field for this illustration is that for a cylinder in an infinite rigid wall[201]. The transmitted frequency is 5 MHz, and the transducer radius is 1 mm. The signals and spectra for four particle paths are shown. Paths 1-3 all pass through a point on the axis of the probe at a distance 9.075 mm from the transducer surface. Path 4 passes through the probe axis at a distance of 18.075 mm. For a sample volume of 2 mm in the axial dimension centered at 9 mm, three paths are shown. Path 1 shows the dependence of the signal on the gating as described in subsection II-B-2. Path 2 is at 60 degrees to the probe axis and the resulting signal is affected by both axial and lateral sample volume shape. The Doppler frequency in this case is half that for path 1. Path 3 is perpendicular to the probe axis. If the wavefronts of the sound field were planar, the signal would be positive valued everywhere. The wavefronts are circular, however, and this causes slight negative values as the particle crosses wavefronts. This effect is stronger for path 4. The spectrum for path 4 is generally narrower than that for path 3 because the beam pattern is wider at this further distance. However, the non-planar wavefronts cause the absolute spectral width to be identical for path 1 and path 2, as predicted by Newhouse and Reid[199].

4. Multiple Scatterers, Coherent and Incoherent Scattering

The above discussion does not completely explain why transit time/geometric effects lead to error in Doppler estimates of velocity. The spectrum of the signal is broadened, but if this spectrum is known, it is still possible to accurately determine the Doppler frequency as the absolute maximum of the spectrum.

It is the presence of multiple scatterers in the sample volume that aggravates the contribution of spectral broadening to frequency estimation error. This is illustrated by Figure 14. Figure 14a is an enveloped sinusoid which has the power spectrum shown in Figure 14b. Figure 14c shows a collection of such sinusoids which begin at different times. When these are summed, as in Figure 14d, a signal is generated which looks like a downmixed Doppler signal in that it exhibits amplitude modulation. The power spectrum of this summed signal is shown in Figure 14e. This spectrum is no longer smooth, and the peak of the spectrum does not coincide with the original frequency of the sinusoids. This does not contradict the linearity of the Fourier transform operation, which states that the Fourier transform of the sum of a set of signals is the sum of the Fourier transforms of the individual signals. The Fourier transform *is* a linear operation. However, since the power spectrum is the magnitude of the Fourier transform, which is a nonlinear operation, the sum of the power spectra is not the power spectrum of the sum.

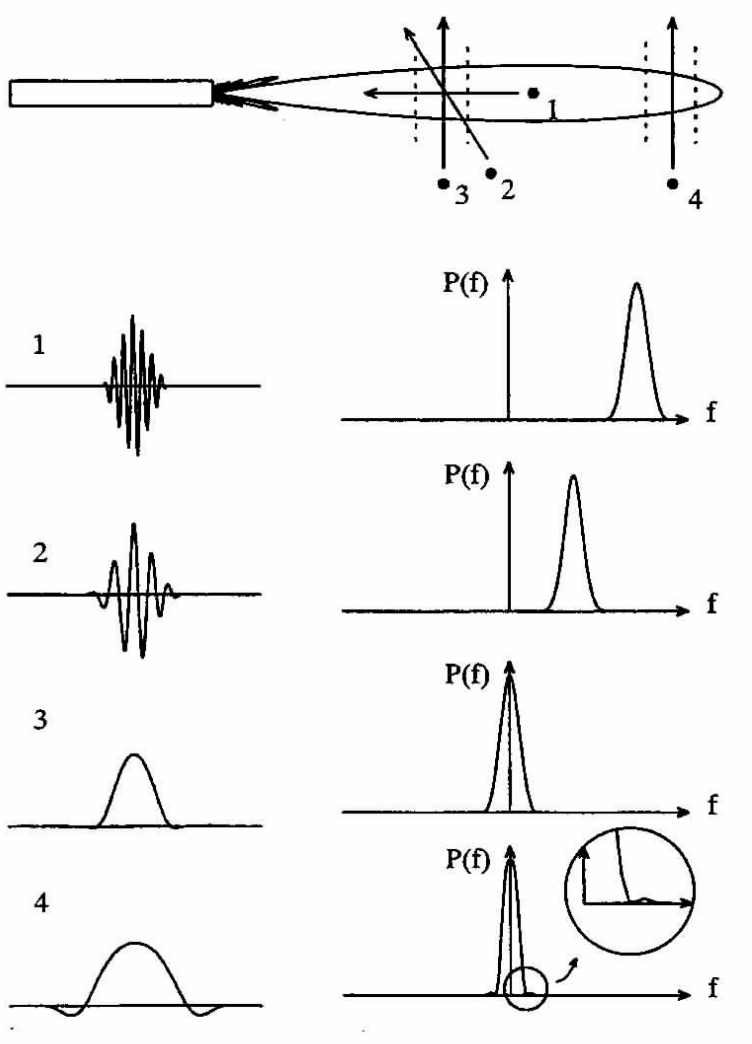

FIGURE 13. Signals and spectra generated by particles that traverse the sample volume. Two 2-mm long sample volumes are shown (dashed lines). One of these is centered 9 mm from the probe and the other is centered 19 mm from the probe. The beam pattern used is that for the far field of a circular piston in an infinite rigid wall. Particle path 1 crosses the near sample volume along the axial direction. Particle path 2 crosses the near sample volume at a flow-to-beam angle of 60°. Particle path 3 crosses perpendicularly through the near sample volume at a distance of 9.075 mm from the probe. Particle path 4 crosses perpendicularly through the far sample volume at a distance of 19.075 mm. The spectrum for particle 4 is generally narrower than that for particle 3 as a result of a longer transit time. However, as shown in the inset, energy in the spectrum for particle 4 extends to higher frequencies. The absolute bandwidth for particle 4 is thus as wide as that for particle 3, as predicted by Newhouse and Reid.[38]

The presence of multiple scatterers has been recognized as a determinant of the Doppler spectrum for ultrasound as well as radar[192, 202] and laser Doppler velocimetry[203]. For ultrasound, the effect was discussed mathematically by Censor and Newhouse[198]. The scattered sound waves from different particles can interfere with one another constructively and destructively, so the signal from the composite target depends on the relative

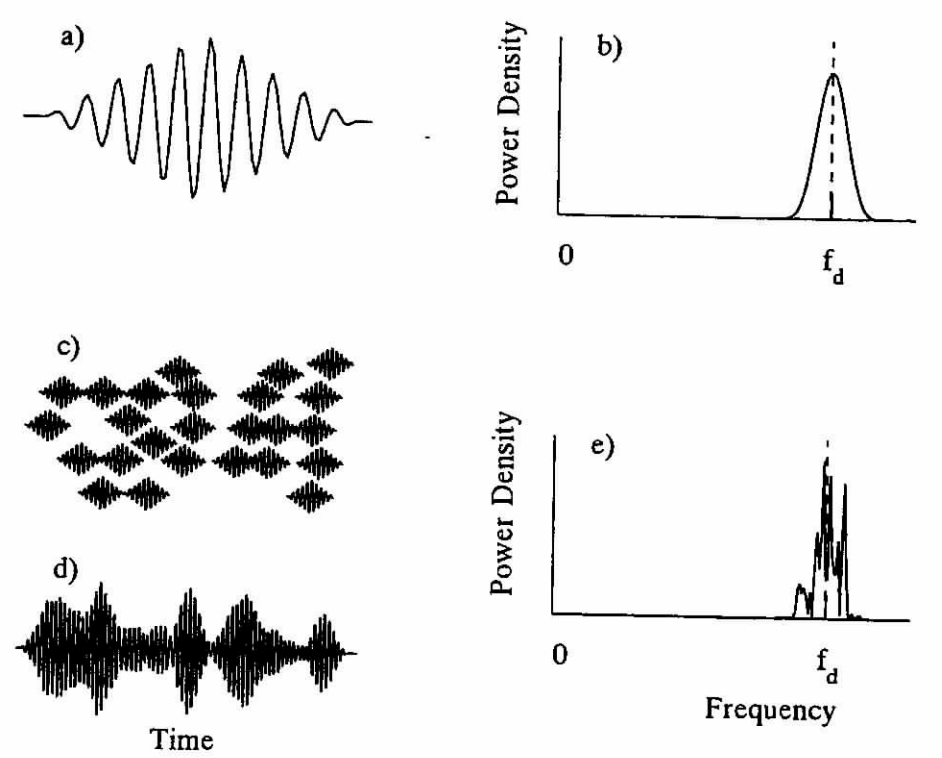

FIGURE 14. Effect of multiple scatterers on the estimated Doppler spectrum. The signal from a single particle (a) has a smooth spectrum (b) from which the Doppler shift (f_d) can be readily estimated. However, when signals from multiple particles (c) are summed (d), the result has a spectrum with sharp peaks, and the Doppler shift is difficult to locate (e).

positions of the individual scatterers and the locations of the transmitter and receiver. The phenomenon is described in terms of coherent and incoherent spectra. The coherent spectrum is the spectrum of the composite signal, which exhibits wave interference. The incoherent spectrum is the sum of the individual power spectra received from each scatterer. Wave interference effects are present regardless of the presence of a Doppler shift; Sigelmann and Reid[204] derived equations which show the characteristic amplitude and phase modulation effects for sound scattered from a stationary medium. Atkinson and Berry[205] have examined, theoretically and experimentally, two phenomena caused by coherent scattering from stationary (and non-stationary) media. The first is that returned A-lines exhibit amplitude modulation which has a characteristic time scale that is the duration of the transmitted pulse. This can be seen in Figure 7 as well as Figure 14d. The second is that two A-lines taken from laterally adjacent locations in space are correlated if the distance, between the two locations is short enough. The distance over which the correlation persists is proportional to the probe beam width. These phenomena appear as speckle patterns in B-mode and color Doppler images.

A distinction must be made between multiple scatterers and multiple scattering. The latter effect refers to sound that reflects from one target, then hits another target (or other targets) and returns to the receiver. This is a particularly difficult problem in acoustics, and is usually neglected; it is typically noted that the sound scattered from any given particle is low in comparison to the transmitted sound intensity, so when this reflects from a second particle, the result is of second order[161].

IV. MODELS OF DOPPLER ULTRASOUND SIGNALS

Mathematical models of Doppler ultrasound signals have several purposes. One of their most common uses is in the optimization of Doppler signal analysis methods. To this end, a time domain signal that is representative of either the Doppler quadrature signal or the rf signal is generated, and this is used as input to one or several frequency estimators. The design of the ultrasound instrument itself can also be improved through signal modeling. This, however, requires a sophisticated model which includes not only the statistics of the signal, but the relationship between signal characteristics and device parameters such as sample volume dimensions, carrier frequency and pulse repetition rate. Finally, the models can be used to interpret the signals from specific pathologies. The investigator may see, for example, a particular spectral pattern and wish to determine whether this results from a specific pathology or flow pattern. This places exceptional demands on the model. It becomes important to include a detailed description of the flow patterns, and it may be necessary to include effects of acoustic impedance mismatches and refraction.

The simplest model of a Doppler ultrasound signal is a sine wave. Typically, white noise is added to the sine wave. This is an idealized model which neglects transit time and geometric broadening effects. The added noise corresponds to noise introduced by the instrumentation only.

A signal that is more representative of Doppler ultrasound is filtered white noise[206, 207]. As in the true Doppler signal, this signal has finite bandwidth. The accuracy of this model depends on the shape of the filter.

The presence of finite bandwidth in the signal can also be modeled by Fourier transform methods. This was accomplished for Doppler radar by Sirmans and Bumgarner[208]. Several variations on this model have been published for ultrasound[209, 210]. The signal is presented by Mo et al.[209] as:

$$s(t) = \sum_{m=1}^{M} \sqrt{(2P(f_m)\Delta f y_m)} \cos(2\pi f_m t + \phi_m) . \qquad \text{Eq. 14}$$

The factors y_m are chi-squared distributed random numbers with two degrees of freedom. $P(f_m)$ is the power spectral density for an assumed input spectrum, evaluated at frequencies, f_m separated by Δf. The phases ϕ_m are uniformly distributed. The random variables are used to simulate the effect of coherent scattering, and the transit time effects are incorporated into $P(f_m)$. As written, $s(t)$ is a stationary process, and therefore represents steady flow. To extend the model to pulsatile flows, Mo et al.[211] have allowed $P(f_m)$ to be a function of time.

Models which use the sum of sinusoids can accurately represent the statistics of Doppler ultrasound signals. However, the useful duration of the signal is its period, T. This

period is $1/\Delta f$, so it can be made arbitrarily large if enough spectral components are used.

The models themselves do not directly relate the signal to instrument parameters, beam patterns and velocity profiles. However, these factors can be incorporated if they are used to establish the underlying input spectrum for the simulation.

Talhami and Kitney[212] have used a model that is based on the amplitude modulation inherent in Doppler ultrasound signals. In this model, the signal is modeled as,

$$s(t) = A(t)\cos \omega t \qquad \text{Eq. 15}$$

where $A(t)$ is a stochastic function of time. To generate this function, Gaussian white noise is convolved with a window function to impose a specific autocorrelation function on the signal. The signal does not exhibit the random phase modulation inherent in Doppler ultrasound signals, but does model the signal as fundamentally broadband rather than discrete.

Another time domain model was proposed by Jones and Giddens[144] for steady uniform flow and extended to pulsatile and nonuniform flow by Wendling et al.[145] This model does account for random phase shifts in the signal. For steady, uniform flow, it has the form:

$$s(t) = A(t)\cos \omega_d t + B(t)\sin \omega_d t \qquad \text{Eq. 16}$$

which can be rewritten as:

$$s(t) = C(t)\cos(\omega_d t + \phi(t)) \; . \qquad \text{Eq. 17}$$

The phase of the cosine is a function of time, so the instantaneous frequency of the signal is:

$$\omega_{inst} = \omega_d + \frac{d\phi(t)}{dt} \qquad \text{Eq. 18}$$

Statistically, the signal is the same as that of Mo et al.[209] if equivalent input parameters are used. However, the time domain approach provides additional insight into the effects of transit time broadening. In particular, it was shown that for a signal which includes only transit time noise and no additive noise, the instantaneous frequency of the signal, weighted by the instantaneous amplitude and averaged over a finite data record, corresponds almost exactly with the centroid frequency for that record. This implies that the centroid frequency is the best estimator of the true Doppler frequency as defined by Equation 18. Alternative spectral analysis and frequency estimation methods can reduce the noise in velocity waveforms, therefore, only when additional sources of noise are present.

A simulation was presented by D'Luna and Newhouse[11] to examine the character of signals from vortices as they passed by a probe perpendicular to the mean velocity vector. The goal of this work was to compare the simulation to *in vivo* Doppler ultrasound signals and identify features that might be observable from vortex shedding downstream of a stenosis. The simulation and experiment compared well, and the vortices were detectable in the Doppler spectra from both.

Perhaps the most direct simulation method models the returned echoes rather than the downmixed signals. This method uses the transducer beam pattern and the velocity profile directly, and can also include effects such as scattering, attenuation, reflection and refraction. Olinger and Siegel[213] used this method to study the usefulness of correlation receivers as Doppler signal processors. Bonnefous and Pesqué[214] used this method to generate input signals for the time-domain correlation velocity estimation algorithm (See subsection V-B-3-a). These signals correctly model transit time effects because the configuration of particles within the sample volume changes from pulse to pulse. A similar simulation was developed by Azimi and Kak[215], although in this version the scatterers were modeled as a continuum rather than as discrete particles. Kerr and Hunt[216, 217] have extended the simulation of Bonnefous and Pesquè to generate two-dimensional color Doppler images (See subsection V-B-1).

V. DOPPLER ULTRASOUND INNOVATIONS

Numerous innovations in Doppler ultrasound methods have been proposed and implemented since the early experiments of Satomura et al.[1] These have arisen from the need to circumvent some of the problems already discussed, such as Doppler ambiguity (section III-C), spatial and frequency aliasing for pulsed Doppler (section II-E), and lack of information about the Doppler angle. Some of these innovations have already been accepted in clinical diagnosis. Of those which have not, some have exhibited disadvantages which outweighed the advantages they offered, while others hold strong promise for the future.

A. Variations in the Transmitted Waveform

To circumvent the range ambiguity problem, several authors have proposed Doppler ultrasound instruments for which transmitted signals other than sinusoids are used. These are generally derived from similar radar systems. The three most common of these are random, pseudorandom, and frequency modulated, but numerous other waveforms can be used. The more common signals used are summarized in Figure 15.

Random signal Doppler radar has been described by McGillem et al.[218] Its use in ultrasound has been examined by Bendick and Newhouse[219] and by Jewtha et al.[220] A review is given by Newhouse et al.[221] The transmitted signal, $e_r(t)$, is white noise that has been passed through a narrow band filter (see Figure 15 c). The returned signal from a single scatterer is $Ae_r([1+\alpha]t-\tau_s)$, where $1+\alpha$ is the time dilation caused by the Doppler effect, α is $v(\cos\theta_1+\cos\theta_2)/c$, and τ_s is the time required for sound to propagate from the transmitter to the particle and then to the receiver at time $t=0$. The angles θ_1 and θ_2 are as defined in Equations 1 and 2. The return signal is processed in a man-

ner nearly identical to that of conventional Doppler. It is multiplied by a delayed version of the transmitted signal and then averaged over time (low pass filtered). The time delay, τ_d, dictates the range of the measurement. The output is the time average of $Ae_r[(1+\alpha)t-\tau_s]e_r[t-\tau_d]$, which is an estimate of $AR[\alpha t-(\tau_s-\tau_d)]$, where $R(\tau)$ is the autocorrelation function of the transmitted signal. The parameters τ_s and τ_d are fixed by the time reference and the instrument delay. Thus, the Doppler shift information is contained in the argument αt. The overall output of the instrument is a time signal which has the shape of the autocorrelation of the transmitted signal but is dilated in time by a factor of $1/\alpha$. The Doppler shift can be estimated from the Fourier transform of this signal.

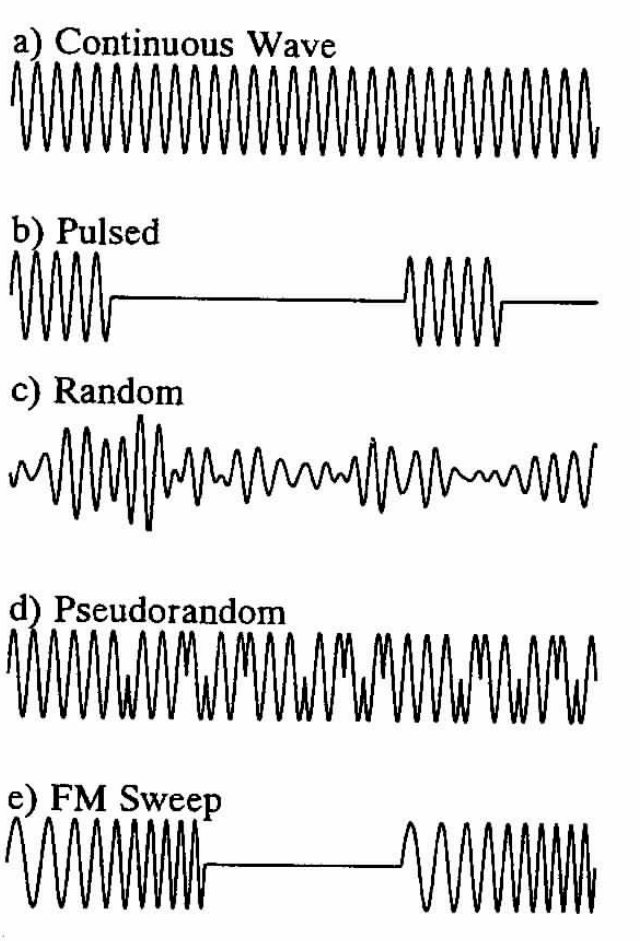

FIGURE 15. A summary of transmitted signals that have been commonly used in Doppler ultrasound.

The primary advantage of random Doppler is that it results in only a single range cell because the autocorrelation function of the signal tends to zero for large times and is significant only near $t=(\tau_s-\tau_d)/\alpha$. Hence, signals from undesired ranges are not detected and much higher velocities can be detected because the pulse repetition frequency can be increased. The transmitted signal can even be continuous, which means that there are no rapid changes in transmitted power as there are in pulsed Doppler. The reduction in range ambiguity is obtained at the cost of velocity resolution however. This is because echoes from outside the sample volume cannot be completely rejected in the correlator. The unrejected part of these signals is referred to as clutter, and hence the signal to clutter ratio is a measure of how well they have been rejected. A good estimate of the autocorrelation of a random signal requires statistical averaging, so the quality of the output autocorrelation function depends strongly on the integration time of the low pass filter. Jewtha et al.[220] compare output spectra from a random Doppler system to those from a conventional pulsed Doppler system which at first seem to imply that both spatial resolution and velocity resolution are improved. Their random spectra are much narrower than their pulsed spectra. However, the pulse width of their conventionaly device was 10 microseconds, which corresponds to a sample volume length of 1.5 cm. Although the size of the tubing used in this experiment was not quoted, it is likely that the broad spectra result from spatial averaging rather than poor velocity resolution.

As in random Doppler methods, the main advantage of pseudorandom Doppler methods is a reduction in the number of secondary sample volumes. Two implementations exist, the cross-correlation method described by Shiozaki et al.[222], and the autocorrelation method described by Cathignol et al.[223] Chen and Wan[224] have compared the two methods and their results indicate that the cross-correlation method provides a better signal-to-clutter ratio. Extensive descriptions of pseudorandom methods are given by Newhouse[146].

The technique will be described first in terms of a special case, where the transmitted signal consists of two sequences, and $s_2 = F_2(t)\cos(\omega_0 t)$. The functions $F_1(t)$ and $F_2(t)$ are called pseudorandom sequences. They alternate between $+1$ and -1 at unevely spaced times which are multiples of some time base τ_m. Each is selected such that its autocorrelation evaluated at multiples of τ_m other than zero is zero. An example pseudorandom sequence is shown in Figure 15 d. The two signals, s_1 and s_2, are repetitively transmitted with an interval of τ_p between them, so that the total transmitted signal is $s(t) = s_2(t) + s_2(t - \tau_p)$ repeated with period $2\tau_p$. The returned signal is multiplied by another signal, $c(t)$, which consists of sequences c_1 and c_2 separated by τ_p. Sequence c_1, has a high correlation with s_1 and a low correlation with s_2, and sequence c_2, has a high correlation with s_2 and a low correlation with s_1. The result of each multiplication is integrated over a time τ_p and combined to yield a Doppler signal which is sampled at a rate of τ_p. The result has the form of a sinusoid of frequency f_d from which the Doppler shift can be detected.

When echoes of s_2 return from a distance d_1, echoes from s_1 return from a distance $d_1 + c\tau_p/2$. The combination of these two signals is mixed with c_1 so that the signal from distance d_1 is rejected. At a time τ_p later, the locations of echoes from s_1 and s_2 are reversed, and the combined return is mixed with c_2. In this way the depth of measurement is always $d_2 + c\tau_p/2$. This enables the maximum depth of the measurement to be increased by a factor of two for a fixed pulse repetition rate, or, equivalently, it enables the pulse repetition rate, and thus the maximum measurable Doppler shifted frequency, to be increased by a factor of two for a fixed measurement distance. Greater extensions in measurement depth or maximum velocity can be obtained if more than two signals are used. For the implementation of Cathignol et al.[223], enough sequences are used to make the transmitted signal continuous in time.

The autocorrelation and cross-correlation methods differ in the signals c_1 and c_2 which are mixed with the received echoes. For the autocorrelation method, $c_1 = s_1$ and $c_2 = s_2$. For the cross-correlation method, c_1 and c_2 are constructed from other pseudorandom sequences besides those used for the transmitted signal.

A pseudorandom Doppler ultrasound system with two transmitted sequences can be thought of as a compromise between random Doppler, which has no secondary sample volumes and high clutter, and conventional Doppler, which has more secondary sample volumes and low clutter. One can consider the secondary sample volumes as spatial ambiguity in that the detector can not distinguish between these and the main sample volume. For random and pseudorandom Doppler, this ambiguity is not eliminated, but it is made more diffuse in space. The choice of method depends on the a priori knowledge of the system. If it is known, for example, that there are no moving scatterers at the locations of the secondary sample volumes, then conventional pulsed Doppler ultrasound is viable. If, however, the desired measurement location is farther than $c\tau_p/2$ from the probe and there are moving scatterers between the two, then either random or pseudorandom Doppler are needed. Cathignol[225] has mathematically related pseudorandom Doppler clutter to the vessel diameter. As the diameter increases, clutter increases because there are more moving scatterers to return partially-correlated echoes to the receiver.

Frequency modulated Doppler ultrasound uses a non-conventional but deterministic waveform, and has been described by Wilhjelm and Pedersen[226]. The transmitted waveform is a linearly frequency modulated sweep which begins at frequency f_1, increases to f_2 at a rate of S_0, and is repeated in time intervals of T_p (Figure 15e). The returned signal is multiplied by a time delayed version of the transmitted signal and then low pass filtered. The time delay is $2D/c$, so it is the time required for sound to reach a depth D in the medium and then return. The result is a frequency modulated sinusoid ($\cos\psi(t)$) with an instantaneous frequency $d\psi/dt$ that contains four terms.

$$\frac{d\psi}{dt} = \frac{2\dot{v}}{c} f_1 + \frac{2(D-d)}{c} S_0 + \frac{2Dv}{c^2} S_0 + \frac{4v}{c} S_0 t \qquad \text{Eq. 19}$$

This form is derived from Wilhjelm and Pedersen[227] with the assumption that $v << c$. They also discuss the use of a stationary echo canceler which, for simplicity, has been neglected here. The variable d is the distance from the probe to the scattering particle. The first term is the familiar Doppler shift on the initial frequency f_1. The second term is a shift in frequency that results because the onset of the returned signal occurs after (or before) the onset of the signal it is mixed with by a time $2(D-d)/c$. The third term can be thought of as a Doppler shift on the second term. It arises because the instantaneous depth of the particle changes with time. The last term is the Doppler shifted sweep rate.

In a practical implementation of this technique, the center frequency of the final signal indicates the depth of the measurement since the second term on the right hand side of Equation (19) is, in general, much greater than any of the other contributions to the instantaneous frequency[227]. The velocity is obtained from the sweep rate through the fourth term. For a single scatterer, this implementation is straightforward. For multiple scatterers, a more innovative approach has been suggested[228]. Short-record frequency spectra of the returned Doppler signal are computed for two consecutive returned

sweeps. These are then windowed around zero frequency and cross correlated to determine the shift in frequency between the first and the second sweep. This frequency shift, divided by the time between sweeps, is an estimate of the returned sweep rate, $4vS_0 / c$, and hence of the flow velocity.

A complete study of the ambiguity properties of frequency modulated Doppler ultrasound has not yet been reported, and the specific applications in which it would be superior to conventional methods have not yet been identified. As in the random and pseudorandom methods, however, the method decreases the power fluctuations in the transmitted signal.

The above methods have a common basis in that in general a signal is transmitted and the returned signal is first multiplied by the transmitted signal (or some other signal) and then low pass filtered. The technique can be applied to any signal, and the usefulness of the results will depend on the autocorrelation properties of the original signal. Holland and Orphanoudakis[229] have described a Doppler system which uses an arbitrary signal generator to allow flexibility in the choice of the transmitted signal. Zrinc[230] has examined the spectral moments of pulse pairs, where the two pulses are of different frequencies. Gilson and Orphanoudakis[231] have computed error bounds for a frequency modulated chirp with a Gaussian envelope.

The use of alternative Doppler ultrasound signals has led to several innovative approaches, such as those outlined above. The descriptions of the approaches can often lead one to believe that one method is universally better than the others. It must be emphasized that this is not the case and that the best method for a given application depends on what is known *a priori* about the velocity field and on what information is needed.

B. Use of Supplementary Information

Much information in Doppler ultrasound signals is either not acquired or not processed in conventional single channel pulsed Doppler systems, but can be exploited with the addition of hardware for data acquisition, signal processing, or signal transduction. Recent advances in electronics have made it practical to implement systems which use this information. Most systems do not attempt to circumvent the fundamental range-ambiguity conflict, but instead try to simultaneously obtain information from multiple locations, or to obtain more complete descriptions of the velocity vector.

1. Multiple Doppler Measurements from One Probe

A simple example of such a system is the multigate pulsed Doppler device (McLeod[232], McLeod and Anliker[233], Brandestini[10]). This device transmits a pulse in the same manner as a single gate device, but it divides each returned echo into several, possibly overlapping, segments which are evenly spaced in time. Each segment corresponds to a different measurement depth, so when all segments are processed in parallel, velocities from multiple depths are obtained simultaneously. There is no fundamental limit on the number of channels that can be implemented since the time interval between samples can be made arbitrarily small. However, it is of little practical value to take measurements with a spacing that is significantly finer than the spatial resolution of the

measurement. Casty and Giddens[234] describe a system which uses 26 channels, 25 of which are processed by a zero crossing method and 1 of which is processed by a fast Fourier transform method. Kajiya et al.[59] describe a similar system that uses 80 channels. A system with 128 channels has been described by Kim[235]. The systems are simple in concept, but it is challenging to implement data analysis hardware with sufficiently high data rates to process the multiple channels. This is why the majority of the devices use zero crossing technology rather than spectral analysis methods on the majority of the channels.

Multigate Doppler ultrasound systems can provide information about both velocity profiles and the motion of the arterial walls. A general review of these systems and their applications is provided by Reneman et al.[236]

Color Doppler ultrasound is an extension of multigate Doppler to two dimensions. As in multigate Doppler, velocities are measured at numerous sample volumes along a line of sight. The line of sight is then moved and another measurement is made. This is repeated until measurements from N lines of sight, which compose one frame, have been taken, so that velocities throughout an entire plane are measured. The change in the line of sight of the probe is accomplished electronically, either by phased array technology or by the use of multiple crystals which are excited sequentially. The velocity is color coded and displayed along with a B-mode image of the artery. Color schemes vary, but a typical encoding represents flow toward the transducer in red, and flow away from the transducer in blue[237]. Larger velocity is denoted by brighter colors. Usually the variance of each velocity estimate is computed, and to display this parameter the third primary color, green in this case, is added to the color derived from the velocity estimate.

Since N scan lines are interrogated, the time devoted to each each line is decreased by a factor of $1/N$, which means that either the frame rate or the number of pulses processed along each line of sight must be low. As was discussed earlier, the accuracy of a Doppler measurement depends on the time over which the measurement is taken, and usually numerous pulses must be processed if a good velocity estimate is to be obtained. Color Doppler systems must balance the need for accurate velocity measurements with the need for good temporal resolution. Some systems use as little as three pulses per velocity estimate (Mitchell[238]), so the ambiguity noise in each measurement is high.

The signal processing of color Doppler systems is complicated by the high data throughput. In general, analogue methods are used to circumvent the need for high speed digital processing. Many systems use an autocorrelation method, such as that described by Kasai et al.[115] or by Barber et al.[239] (See “Time Domain Methods”, subsection V-D-4). A frequency-domain processor has been described by Tortoli et al.[240] This processor uses an analogue frequency processor known as a surface acoustic wave (SAW) device.

Reviews of the limitations and artifacts of color Doppler are given by Mitchell[238] and by Goldman[241].

An alternative technique is based on x-ray tomography methods (see Cormack[242]). In x-ray tomography, an x-ray is transmitted through a line in the region of interest and its overall attenuation is measured. The line of the trajectory is then changed by rotation and/or translation, and another attenuation value is obtained. If the attenuation from each translation and rotation of the trajectory line is known, it is possible to reconstruct an image of the attenuation properties of the entire region by an inverse radon transform (See Beylkin[243]). The radon reconstruction method is generally computationally intensive, but it is necessitated because there is no range information in the x-ray method. By analogy, there is no range information in CW Doppler ultrasound, but an image can be constructed from values of backscattered power from multiple rotations and translations of the CW probe. Similarly, the power spectrum of the signals from each orientation can be computed, and the inverse radon reconstruction can be made on each frequency band to obtain a reconstruction of the total velocity distribution. Doppler tomography was introduced by Greenleaf and Ylitalo[244] as a tool for breast cancer diagnosis. It is particularly suited to this application because the breast lacks intervening structures, such as bone, which would otherwise refract or redirect the transmitted sound. The authors present data from an *in vitro* model in which a tube was inserted into an excised human breast. In these studies, only the locations of blood flow were mapped, but the method by which the entire velocity field could be mapped was also described. They also noted that the method can be used with a sinusoidal pulse as the transmitted signal to reduce clutter signals from stationary boundaries. This is not identical to pulsed Doppler ultrasound; the returned echo is not range gated, so a single signal is obtained for each orientation of the probe.

It is not yet known under what conditions this method would be advantageous to conventional pulsed Doppler ultrasound. However, it should be remembered that range gating contributes substantially to Doppler ambiguity, so it would be worthwhile to determine the ambiguity properties of the method. Certainly the need to obtain numerous lines of data is a disadvantage of the technique.

A form of tomography which uses range-gated Doppler ultrasound was described by Schmolke et al.[245] and Schmolke and Ermert[246]. This does not use the inverse radon transform technique since resolution along the axis of the transmitted beam is obtained through the range gating. However, it does use measurements from multiple angles. This enables two dimensional velocity vectors to be mapped within a plane. The system is a hybrid between tomography, as described above, and two-dimensional point velocity measurements to be described below.

2. Multi-Dimensional Velocity Measurements

The Doppler ultrasound methods as described in section I-B measure the component of flow velocity along the probe axis. This restricts the usefulness of the devices because velocity is inherently three dimensional. Without some assumption about the velocity vector direction, it is impossible to determine even the magnitude of the flow velocity. Several techniques which have been implemented to provide two or three dimensions of velocity information are described in this section.

a. Single Probe Measurements

One technique to address the problem of Doppler angle measurement is described by Guler[247]. In this method, one pulse is transmitted, the sample volume is then translated by some percentage of the sample volume and a second pulse is transmitted. The correlation coefficient between the returned echos from the first and second pulses indicates what percentage of particles have moved out of the sample volume between pulses. If the flow velocity is in the direction of the change in position of the sample volume, relatively few particles leave the sample volume, and the correlation is high. If the flow velocity is perpendicular to the direction of the position change, more particles leave the sample volume width and the correlation is lower. Based on this concept, Guler found a relationship between the correlation coefficient, velocity and Doppler angle. The accuracy of this method has not yet been tested. It is certain that the translation of the sample volume will alter the ambiguity properties of the signal. For example, whenever the correlation is reduced through the motion of the probe, the accuracy of the velocity measurement will decrease. Conversely, however, if the probe is moved in such a way that it follows the particle motion, the velocity estimate will be improved.

Newhouse et al.[248] have shown that geometric broadening can be used to estimate two velocity components transverse to the beam axis. They first consider a rectangular transducer with length W_x along the x axis and width W_y along the y axis. If the wavenumber magnitude is k_0 and the sound is focused by a lens with focal length F, then the bandwidth of the Doppler spectrum for uniform flow is

$$\frac{k_0}{F}\left(W_x v_x + W_y v_y\right) \qquad \text{Eq. 20}$$

where v_x and v_y are the x and y components of velocity. The bandwidth thus depends on the orientation of the probe surface with respect to v_x and v_y. To estimate both velocity components, Doppler bandwidth is estimated with the probe in one orientation, the probe is then rotated 90° about its axis, and the bandwidth is estimated from a second measurement. The results of the measurements can be used in Equation (20) to yield two simultaneous equations in the two unknowns v_x and v_y. The authors expand this idea to other transducer geometries. For example, if the transducer sensor consists of two parallel strips which are both parallel to the x axis, the Doppler spectrum has three peaks. The velocity component v_x can be estimated from the separation of the two outer peaks, and the component v_y can be obtained from the width of these two peaks. The center peak can partially or completely overlap the two outer peaks, and thus corrupt the frequency and bandwidth estimates. It can be suppressed, however, by simple techniques described by Newhouse et al.[248]

Geometric broadening can be used to estimate multiple velocity components only if the flow is relatively uniform so that the component of spectral broadening caused by flow effects is minimal. Also, the Doppler transit time for transverse flow must be much less than that for axial flow.

b. Multiple Probe Measurements

A more straightforward method to determine the Doppler angle is to measure the complete three dimensional velocity vector. This can be done with multiple ultrasonic transducers. One method has been described by Daigle et al.[249]. Fox and Gardiner[250] tested the method on a turntable device, an *in vivo* flow phantom, and a free jet and showed that good estimates of true velocity magnitude could be obtained. Three pulse-gated probes are used to measure three non-coplanar components of the velocity, and the velocity magnitude and direction are determined in closed form from straightforward geometric calculations (Fox[251]). In general, the measurements from each probe must be taken sequentially rather than simultaneously to prevent cross-clutter from one probe to another. Fox and Foster[252] present an application of this to the measurement of volume flow rate. The same technique was developed by Ashrafzadeh et al.[22] and used to measure turbulent blood flow[19]. The analysis of error caused by uncertainty in the angles between the probes was presented by Ashrafzadeh et al.[253] Cheung et al.[9] used this to correlate stenosis diameter to turbulent shear stresses. The method has been used in a color Doppler system by Tamura et al.[254]

Another method to determine the velocity vector from multiple probes was described by Furuhata et al.[255] They used one transmitter and two receivers to obtain the two-dimensional velocity vectors. The Doppler shift for one of the receiver probes is $(f_0 v/c)(\cos\theta_1 + \cos\theta_2)$, where θ_1 is the angle between the transmit probe and the flow velocity vector, and θ_2 is the angle between the receive probe and the flow velocity vector. Again, the true velocity vector is determined from straightforward geometrical calculations. This method can be readily extended to three dimensions. It has been described in depth more recently by Overbeck et al.[256] They show good accuracy in measurements of velocity magnitude for a string target system, and present limited measurements from the carotid artery.

In a method proposed by Dotti et al.[257], a Doppler probe is divided into two independent halves. The halves are pulsed simultaneously with the same signal, and the received echoes are processed separately. In contrast to the previous two methods, the beam patterns of the two probe sections are nearly collinear. Two quadrature signals, $S_1(t_i)$ and $S_2(t_i)$ are obtained from the two probe partitions. From these, four cross-correlations are computed:

$$C_{11} = \left\langle S_1(t_i) S_1^*\left(t_{(i+1)}\right)\right\rangle \qquad C_{12} = \left\langle S_1(t_i) S_2^*\left(t_{(i+1)}\right)\right\rangle \qquad \text{Eq. 21}$$

$$C_{21} = \left\langle S_2(t_i) S_1^*\left(t_{(i+1)}\right)\right\rangle \qquad C_{22} = \left\langle S_2(t_i) S_2^*\left(t_{(i+1)}\right)\right\rangle$$

where the angled brackets denote time average. The following relationships can be derived:

$$C_{11} + C_{22} = p(\xi,\eta) e^{2jk\xi} \qquad \text{Eq. 22}$$

$$C_{12} + C_{21} = q(\xi,\eta) e^{2jk\xi} \qquad \text{Eq. 23}$$

where p and q are measurable functions which depend on probe geometry, ξ is the longitudinal fluid displacement, and η is the lateral fluid displacement between times t_i and t_{i+1}. The sums $C_{11}+C_{22}$ and $C_{12}+C_{21}$ are calculated from the Doppler quadrature signals. Since the former sum is real, the phase of the exponent in Equation (22) can be computed, where it is assumed that the displacement in the direction of sound propagation is not larger than a wavelength. This gives longitudinal displacement. With this, both p and q can be computed and η can be deduced from these.

The uniform insonification method of Equation 11 is a technique by which flow rate can be measured without knowledge of the Doppler angle. The returned power from the signal indicates the cross-sectional area of the vessel and the normalized first moment of the Doppler power spectrum provides an estimate of the mean velocity. The angle independence arises because the first moment frequency decreases in proportion to $\cos\theta$ and the insonified cross-sectional area increases in proportion to $\cos\theta$. It is difficult to apply this method *in vivo*, however, because the attenuation of the signal is usually unknown *a priori*, so the relationship between returned power and cross-sectional area cannot be deduced. Hottinger and Meindl[258] suggested a solution to this problem, which is known as the attenuation-compensated method. This requires two beams, one with a sample volume smaller than the vessel lumen, and the other with a beam pattern that is uniform throughout the vessel lumen. The attenuation caused by the tissue is determined from the backscattered power of the first beam, and this is used to determine flow rate from the signal returned by the second beam.

Evans et al.[51] have designed a transducer which can transmit, alternatively, the required narrow and broad beam patterns. In their method, only a single wide-beam signal is transmitted. Narrow and wide sample volumes are achieved with receiving arrays that focus on a narrow and a wide region, respectively. Thus, there is no reduction in the effective pulse repetition frequency. The same group[31] showed good correlation ($r=0.96$) between volume flow rates measured with this method and with dye or thermal dilution techniques. They also found good correlation ($r=0.98$) between the Doppler estimated diameters and diameters estimated from ultrasonic imaging.

3. High Frequency Sampling of the RF Signal

As discussed in subsection II-B-2, in pulsed Doppler the amplitude spectrum of the transmitted waveform has a shape similar to that shown in Figure 5 c, where the peak of the spectrum is at the carrier frequency, and the other components are separated by the pulse repetition frequency. When the returned signal is downmixed, the Doppler shifted frequencies from the non-carrier components are generally removed by the low-pass filter. These frequencies contain additional information about the scattering process. Since this information comes from regions of the spectrum far from the narrow band carrier signal, it is referred to as “wide band”. Wide band information can be used if the returned rf signal is sampled directly with high speed analogue-to-digital converters. The associated signal processing can be performed either in the time domain (time-domain correlation and maximum likelihood) or the frequency domain (two-dimensional Fourier methods).

a. Time Domain Correlation

The principle of time domain correlation is illustrated in Figure 16 for two simulated A-lines from parabolic flow with a Doppler angle of 30°. The digitized rf signals (c and d) are first windowed into short segments separated by the pulse repetition time. This windowing is analogous to gating in conventional pulsed Doppler. The cross-correlation between a windowed segment of one A-line and the windowed segment from the next A-line is then computed. The component of flow velocity toward the probe is computed as:

$$v = \frac{c\tau_l}{2\tau_p}, \qquad \text{Eq. 24}$$

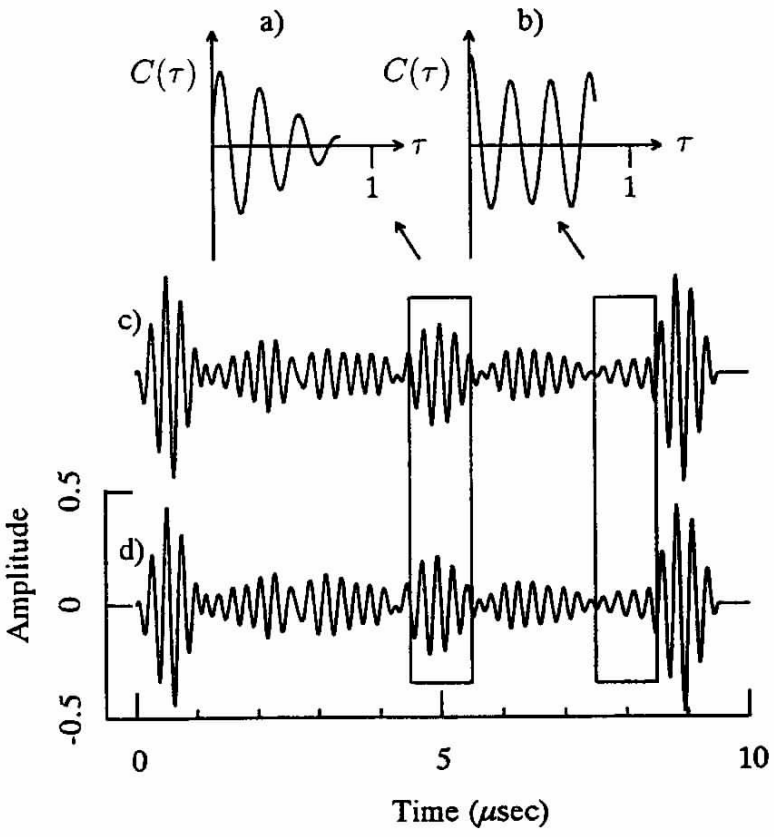

FIGURE 16. Illustration of the time domain correlation technique. a) and b) show the cross correlation functions between the two A-lines at times surrounded by the boxes. The two A-lines represent the return from two consecutive transmitted pulses scattered from Poiseuille flow with a beam-to-flow angle of 30°. The second return (lower A-line) is shifted to the left with respect to the first return (upper A-line). The shift is more noticeable near the center of the A-line since this represents signal returned from the centerline of the flow, where the velocity is higher. This is reflected in the value of τ at which the cross correlations are maximal.

where τ_l is the time lag at which the cross-correlation function is maximum. The interpretation of this relationship is simple. In a time τ_p, a particle in the sample volume moves toward the probe by an amount $d = v\tau_p$. The time required for sound to travel from the probe, to the particle and back is therefore reduced by $2d/c$. This change in round trip time is the time lag in the cross-correlation function. In essence, the method measures the velocity of the particles from the displacement of the particles between pulses divided by the time between pulses.

The left window shown Figure 16 corresponds to the center of the vessel, where velocity is highest, and the right window is near the wall, where velocity is near zero. The cross-correlation (Figure 16 a) for the centerline window has a maximum at a positive lag, whereas that for the near-wall window (16 b) has a

maximum closer to zero.

The technique was first described for Doppler ultrasound by Dotti et al.[259] and implemented by Bassini et al.[260] It was applied to *in vivo* measurements and *in vitro* measurements downstream of a stenosis by Bassini et al.[261] Bonnefous and Pesqué[214] further described the advantages of the technique. They developed a computer simulation tool which could be used to generate realistic Doppler echos which could then be processed by time domain correlation. Bonnefous et al.[262] described the application of the method to color Doppler ultrasound. To implement the method in real time, they used a single bit correlator, so that only the signs of the A-line data were used. Even with this simplification they showed improvements in their method over conventional pulsed Doppler methods.

One advantage of this method is that frequency aliasing is eliminated. In standard downmixing, only the phase difference between signals is detected, and thus the greatest time shift detectable between two pulses is a multiple of the carrier period. In time domain correlation, however, wide band information, such as the shape of the amplitude envelope, is also used, and this allows time shifts on the order of the entire width of the receiving window to be detected.

There is a connection between time-domain correlation and the frequency domain cross-correlation method described by Pedersen et al.[228] for frequency modulated Doppler. Both use cross-correlation, and both use wide band information. However, the former performs a cross-correlation in the time domain, whereas the latter does so in the frequency domain.

The most thorough error analysis of time domain correlation is given by Foster et al.[263] and experimental verification of the conclusions is presented by by Embree and O'Brian[264]. They divided the error into four sources: 1) windowing of the returned echo, 2) the presence of multiple scatterers in the range cells that move at different velocities, 3) increase in the sample volume size as a result of finite system impulse-response time, and 4) variation in beam intensity as a particle traverses the ultrasound beam. Of these four categories, 1) and 4) relate closely to classical Doppler ambiguity.

Error from the windowing of the returned echo increases in importance when the ratio of the correlation time lag to the total window length increases. This ratio is a function of 1) the velocity component of the flow parallel to the probe axis, 2) the sample volume size and 3) the pulse repetition rate. For example, if the velocity is high enough that all particles move out of the sample volume between pulses, then the correlation between consecutive A-lines is negligible and the velocity cannot be determined. In general, a larger velocity along the probe axis, a smaller sample volume, and a lower pulse repetition frequency reduce the accuracy in the estimated time lag. Nonetheless, Foster et al.[263] found that noise caused by windowing led to standard deviations in the estimated time shift of only about 0.5% for typical *in vivo* parameters. This implies that estimates

obtained from only two pulses with time domain correlation result in lower noise than than estimates from multiple pulses with conventional pulsed Doppler ultrasound.

In most Doppler ultrasound measurements, however, the velocity vector is not parallel to the axis of the probe. When the velocity has a component perpendicular to the probe axis, the variation in beam intensity with radial position causes substantial ambiguity noise. This is because the change in the configuration of the particles in the sample volume is manifested by a change in the shape of the entire A-line rather than merely a time shift. Simulation results of Foster et al. [263] yield a standard deviation of 3.7% for the centerline of a physiological Poiseuille flow. It must again be emphasized that this is without temporal averaging, and therefore suggests strong potential for decreased noise in the velocity estimates.

The presence of multiple scatterers at different velocities in the range cells also increases the variance in the velocity estimation. The mechanism is similar to that for transverse velocity components described above since the entire shape of the A-line is again altered from pulse to pulse. This is a spatial averaging effect, and is identical to spatial averaging in conventional pulsed Doppler. The effect of finite system impulse response time is also mainly a spatial averaging effect since it lengthens the device sample volume.

Time domain correlation also lacks the velocity bias that results from frequency dependent attenuation[262]. This is because the cross-correlation is between two signal segments which undergo identical attenuation.

The disadvantage of time domain correlation is the high cost of hardware needed to implement it. Some techniques have been used which avoid the need to compute a complete cross-correlation between sequential echos. Bonnefous et al.[262] show that good results can be obtained when only the sign of the received signals is used, and this speeds up calculations significantly. Another technique is described in the paper by Bassini et al.[260] First, the cross-correlation at times $\tau + \Delta$ and $\tau - \Delta$ are computed, where Δ is a small time increment. This indicates whether the this function increases or decreases with τ. The value of τ is then changed in the direction of increase and this is repeated until a local maximum is reached. The method decreases the number of cross-correlation values which must be calculated, but it converges to a local maximum rather than an absolute maximum. If the transmitted signal is a sinusoidal burst, aliasing remains a problem because the cross-correlation then has multiple local maxima (see Figures 16 a and 16 b).

The work of Embree and O'Brian[264], illustrates the demanding requirements when complete cross-correlation is implemented. They used a 50 MHz analogue to digital converter and a processor which could multiply two samples and add the result to the previous result in 1 μsec. This means two samples of 256 points each could be cross-correlated in 0.066 sec, or 15 correlations could be done per second, which is roughly 15 measurements per cardiac cycle. Although the number of required multiplies can be reduced by Fourier methods, widespread use of the system and exploitation of its full potential must nonetheless await advances in computer and data acquisition hardware.

The time domain correlation method does not eliminate ambiguity noise, but it does seem to reduce it significantly. It still suffers from the well-known tradeoff between temporal and spatial resolution. For example, the sample volume can be made smaller if the receiving window is shortened, but this in turn reduces the accuracy of the velocity estimate. To quantify the ambiguity, it is necessary to compare time-domain correlation directly to conventional pulsed Doppler with identical transducers and averaging times. If the method proves to be as accurate as is indicated by initial studies, it has strong potential for application to *in vivo* measurement with high spatial and temporal resolution.

b. **Speckle Tracking**

Trahey et al.[265] have proposed a method which uses the speckle pattern of B-mode images to track blood flow velocity. B-mode images are similar to color Doppler images in that signals are transmitted sequentially along multiple adjacent lines of sight to form a two-dimensional image. % todo 11a) Want to say that B-mode images are more wide band. As discussed in subsection III-C-4, the speckle pattern is caused by interference between echoes from numerous scatterers. If the relative distances between scatterers does not change, the speckle pattern remains relatively constant. For uniform flow, for example, the speckle pattern will appear to move at the velocity of the flow. Time domain correlation exploits this phenomenon in one dimension. However, if multiple A-lines are available along adjacent lines of sight, as in B-mode images, the two dimensional images can be processed to find the correlation in the speckle pattern between sequential images. In the method described by Trahey et al.[265], each B-mode image is divided into cells. Correlation coefficients, C_{kl}, are computed between the speckle pattern in cell k of frame i and that in cell l of frame $i+1$. The cell l for which C_{kl} is maximum is then matched with cell k, and the displacement between these two is the estimated displacement of cell k between the two frames.

The implementation described above differs from time domain correlation in that correlation coefficients between a finite number of cells are computed rather than the cross-correlation function. This reduces the necessary computation time, but causes the resolution of the possible displacement estimates to be limited to the cell size rather than the pixel size. The full cross-correlation function implementation is, however, theoretically possible, should the necessary high-speed hardware become available.

The two major advantages of speckle tracking over conventional color Doppler are 1) it generates two components of the velocity vectors, and 2) it does not exhibit spatial aliasing. Several problems can degrade the quality of speckle tracking results, however. One is that the speckle pattern does change somewhat with location within the scanned sector. It does so more rapidly for lateral target translations than for axial ones. Another problem is that the speckle pattern will change when the configuration of the target particles changes, such as when the fluid shear rate is non-zero.

c. Two-Dimensional Fourier Transform

A method related to time domain correlation and speckle tracking has been reported by Mayo and Embree[266] and by Wilson[184]. The returned A-lines from sequential pulses are

acquired and aligned with one another to form the two-dimensional function, $S(z,t)$ shown in Figure 17 a. The z-dimension approximately represents the depth of the measurement and the t-dimension represents time in multiples of the pulse repetition time, τ_p. A two-dimensional Fourier transform is computed on this data as:

$$F(g,h)=\frac{1}{N}\sum_{k=0}^{N-1}\int_{-\infty}^{\infty}S(z,t)e^{-2\pi igz}e^{-2\pi ihk\Delta t}dx\,, \qquad \text{Eq. 25}$$

where h is associated with a frequency and g is associated with a wavelength. The transform in time is written as discrete because the function $S(z,t)$ is inherently discrete in the time dimension. The method is most easily explained if all insonified particles move parallel to the probe axis with the same speed. In this case, each successive A-line is identical to the previous one except for a time shift. Thus, if values of $S(z,t)$ are plotted for a fixed value of z and successive values of t, the resulting time series will have the same shape as a discretized version of the A-line itself. If a single A-line is represented as $S_x(z)$, then the time series for a fixed z_0 is $S_x(vt)$, where v is the particle velocity. Any spectral component in the g dimension thus has a corresponding

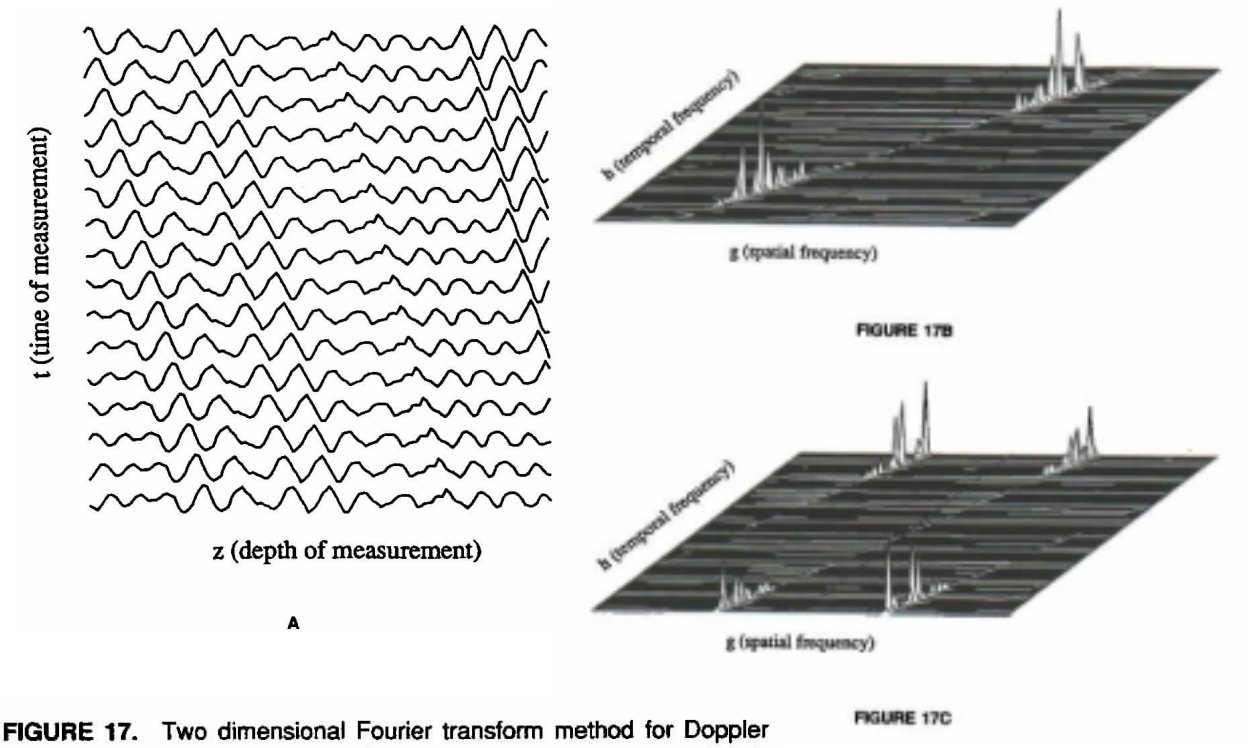

FIGURE 17. Two dimensional Fourier transform method for Doppler ultrasound signal processing. A): Consecutive A-lines are arranged such that the coordinate along the A-line represents (approximately) depth, and the coordinate from one A-line to the other represents time. B): The two-dimensional spectrum has components along the line $g = h/v$, where g represents the spatial part of the transform and h represents the temporal part. C): If aliasing occurs, some spectral components lie on lines which do not pass through the origin.

component in the h dimension along the line in $h-g$ space $h=gv$. The resulting spectrum thus has components only along the line $h=gv$. This is illustrated in Figure 17 b. In this figure, the transmitted signal is wide-band, and this causes a wide distribution of spectral power along $h=gv$. If the target contained multiple velocities, each velocity, v_i, would cause a separate ridge in the spectrum along a line $h=gv_i$. In the idealized case where the transmitted signal is a pure sine wave of frequency ω_0, the two-dimensional spectrum of the returned signal is a delta function at approximately $g=\omega_0/(2c)$ and $h=v\omega_0/(2c)$.

Wilson explains the relationship between the two-dimensional Fourier transform method and conventional pulsed Doppler. This is readily explained if the gating of the returned signal is neglected. In conventional pulsed Doppler, the returned signal is multiplied by a sinusoid at the carrier frequency $e^{-2\pi i f_0 t}$, then integrated (low pass filtered) over the length of the A-line to yield a new time series. This new time series is then commonly transformed into frequency space. In equation form, the processing is expressed as follows:

$$F_c(f)=\frac{1}{N}\sum_{k=0}^{N-1}\int_{-\infty}^{\infty}S(t,k\Delta t)e^{-2\pi i f_0 t}dt\,e^{-2\pi i f k\Delta t} \qquad \text{Eq. 26}$$

If f_0 is associated with cg, f with h, and t with z/c, Equation (26) is identical to Equation (25) evaluated at $g=f_0/(2c)$. Conventional pulsed Doppler thus evaluates the two dimensional Fourier space at only one value of g. In the idealized case, where the two dimensional spectrum is a delta function, no information is lost since that delta function occurs at $g=f_0/(2c)$. However, this idealized case never exists, and useful information can be gained from an examination of the entire two dimensional spectrum.

An example application described by Wilson[184] and patented by Mayo and Embree[266] concerns aliasing. If the transmitted signal is broadband, the spectral content is spread over a line $h=gv$. If the signal is aliased, usually as a result of a pulse repetition frequency that is too low, spectral power will be on a line that does not pass through the origin, as in Figure 17 c. Simple algorithms can be devised to detect this condition and correct for it.

Two effects cause the true Doppler spectrum to have components that are not on the line $h=gv$: 1) The finite signal length in the z and t directions, tends to broaden the spectrum. 2) Transverse velocity components cause geometric broadening. Nonetheless, the two-dimensional Fourier transform approach and the time-domain correlation method demonstrate that important information is present in the rf signals that is typically neglected and that could lead to improved spatial and temporal resolution for Doppler instrumentation.

d. Maximum Likelihood Estimation

Ferrara and Algazi[267, 268] have applied a wide band technique known as maximum likelihood estimation to Doppler ultrasound. This is another method that has been borrowed from Doppler radar. The method develops from the following probability question: If the signal $e_s(t)$ is sent into a given scattering environment, and the signal $s_{rf}(t)$ is received, what is the most likely velocity at which the scattering medium travels? It is possible to write the likelihood as a function of velocity as:

$$l(v) = \frac{1}{N_0} \int_{T_i}^{T_f} \int_{T_i}^{T_f} s_{rf}^{*}(t) h'(t,u;v) s'_{rf}(u) dt du \qquad \text{Eq. 27}$$

where s_{rf}' is the complex envelope of s_{rf}, N_0 is the power of the additive noise in the signal, T_i and T_f are the initial and final times over which the estimate is computed, and the superscript * denotes complex conjugate. The function $h'(t,u;v)$ depends on two time variables, t and u, with v as a parameter. It must be derived from a mathematical model of the scattering process. Conceptually, for each possible value of v, the returned signal and the function $h'(t,u;v)$ are used in the above integral, and $l(v)$ is evaluated. The velocity which yields the highest value for $l(v)$ (i.e. the most likely velocity) is taken as the velocity estimate.

Ferrara and Algazi[267] derive $h(t,u;v)$ for the case where a single scatterer is present and for the case where multiple scatterers are present. For both cases the use of this wide band technique significantly improved the accuracy of the velocity estimation over narrowband methods.

Maximum likelihood estimation has a distinct advantage over the other wide-band methods described here in that the rf signals can be downmixed before they are processed. This downmixing is different from the process that leads to quadrature signals, however. The signal is multiplied by the carrier frequency, but the bandwidth of the subsequent low pass filter is wider than that of the transmitted signal. The components of the rf signal which result from the harmonics shown in spectrum g of Figure 5 are kept. Thus, whereas Embree and O'Brian sampled their data at 50 MHz, Ferrara and Algazi[268] downmixed this same data and then applied a filter to it with a -3 dB bandwith of 3 MHz. This means that the signal could have been downmixed first and then digitized at a frequency slightly higher than 6 MHz, which is substantially more accessible than 50 MHz.

C. Solid Mechanical Applications

Doppler ultrasound is typically associated with the measurement of fluid velocities. However, two methods have recently been examined which relate to solid mechanical measurements.

The first of these methods has been called “Sonoelasticity,” and was described by Lee et al.[269] and Lerner et al.[97] In this method, a sound wave in the audio spectrum is introduced into the tissue of interest, and simultaneously color Doppler imaging is applied. The
audio wave excites motion in the tissue, and this is detected with the imager. Since the frequency of the audio wave is fixed, the velocity of the motion is directly proportional to the amplitude, and the imager displays vibration amplitude as a function of spatial coordinates. The authors note that stiffer tissues, such as hard tumors, show less vibration than the surrounding tissues, and are thus candidates for diagnosis by this technique.

The second solid mechanical method is not strictly a Doppler method. It has been described by Tristam et al.[270], and uses M-mode images. M-mode images are sequences of A-lines which are presented with depth along the vertical axis, time along the horizontal axis and echo strength encoded in gray scale. If a tissue boundary is in motion, the depth at which that boundary occurs changes in time, and this depth can be plotted as a function of time. The objective of the technique is to discern pathological from non-pathological organ motion. Although this at first seems to have little relation to Doppler ultrasound, it is, like Doppler, a motion detection technique, and it can be considered to be a low frequency analogue to time-domain correlation in which the velocity is deduced from a shift in the A-lines.

D. Doppler Signal Analysis

It has long been recognized that the quality of the velocity estimate in Doppler ultrasound depends on the method by which the returned signals are processed. Doppler signal analysis has evolved along with improvements in hardware and signal analysis algorithms, and each new method has resulted in important studies designed to determined whether that method truly improved the measurement of flow velocity and hence the diagnosis of disease. The sections on zero crossing detectors and Fourier transform methods below are intended for historical perspective only and are not intended as complete reviews. Of central concern in this section is the use of alternatives to the Fourier transform in the analysis of Doppler quadrature signals.

1. Zero Crossing Detectors

In the earliest Doppler ultrasound implementations, the echos were downmixed with the transmitted carrier and then processed by a zero crossing detector. This was the most expedient method at the time, but numerous authors suggested that other methods would be more appropriate.

Flax et al.[271] showed that the zero crossing frequency (f_Z) is related to the power spectrum ($P(f)$) of the signal by the rms calculation:

$$f_z = \sqrt{\frac{\int_0^\infty f^2 P(f) df}{\int_0^\infty P(f) df}} \qquad \text{Eq. 28}$$

The disadvantage of this is that it assigns more weight to high frequency components than to lower frequency components, and thus introduces a bias in the Doppler frequency.

Further analysis of the artifact caused by the zero crossing detector was given by Jorgensen et al.[272] They concluded that the results depend on the relationship between signal strength and the signal threshold used in the detector and called for improvements in frequency detection circuitry. A summary of other artifacts of the zero crossing detector with appropriate publications can be found in Reneman and Hoeks[273].

Some efforts have been undertaken to improve the performance of the zero crosser. A simple example is a dynamic gain on the quadrature signals, which keeps the amplitude above the trigger level and below the level at which clipping would occur[272]. Another example is the zero crosser interval histogram technique[95, 274], which uses the full histogram, rather than a simple mean, of the zero crossing intervals, and therefore approximates the Doppler power spectrum. A third technique is the offset detector (Burkhardt[275], and see also Gill[276]) in which the Doppler signal is first frequency shifted by an amount f' before zero crossing detection. Early comparisons of velocity waveforms derived from a zero crossing detector and those derived from analogue spectral analysis indicated that the latter could reduce numerous artifacts caused by signals that are below the zero crossing threshold and by other factors[277].

2. Fast Fourier Transform Methods

As computer technology advanced and digital signal processing methods became more affordable, real time fast Fourier transform-based Doppler instruments were developed (Blackshear et al.[278], Rittgers et al.[279]). Power spectral analysis had been used much earlier than this (see, for example, Sigel et al.[110]), but not in real time. Many authors presented studies which compared Fourier transform methods for Doppler frequency estimation, such as first moment, mode and maximum, to the zero crossing technique (Burkhardt[275], Goldberg et al.[280]). In many cases, the quantitative differences between velocity estimators computed from the fast Fourier transform and the zero crossing detector were not substantial. Voyles et al.[281] concluded that mode frequencies were comparable in accuracy to zero crossing frequencies, but were less affected by turbulence. They found that first moment frequencies often provided underestimates of flow velocity and suggested that this was a result of noise in the downmixed quadrature signals. The inaccuracies associated with the first moment calculation are consistent with results of Cote and Fox[282]. They found that for low signal to noise ratios, velocity waveforms estimated from the first moment method were not representative of expected waveforms and that a thresholded zero crossing method was superior. Thus, it was never shown that fast Fourier methods were universally better than zero crosser methods. Rather, it was shown that the benefits of Fourier methods depended on how the spectrum was post processed and the nature of the downmixed signals. Perhaps the greatest advantage of real time Fourier analysis was in the ability to visualize the complete Doppler spectrum rather than extract a single numerical parameter.

3. Alternative ("Modern") Spectral Analysis Methods

The fast Fourier transform is a highly convenient and efficient method for spectral analysis. However, in recent publications[283] it has been emphasized that all spectral analysis techniques are based on some underlying model of the time-domain signal and that all signals do not have the same underlying form. For example, if white noise is passed through a low pass single-pole filter, the power spectrum of the output has the form:

$$\left|H(j\omega)\right|^2 = \frac{1}{1-\left(\frac{\omega}{\omega_0}\right)^2}, \qquad \text{Eq. 29}$$

where ω_0 is the cutoff frequency of the filter. If a short segment of the output signal is examined, its energy spectrum is not identical to that of Equation (29) for two reasons:*

1) The signal is a random process, and thus exhibits spectral variation from segment to segment, and 2) The short segment is finite in length and therefore exhibits artifacts as a result of windowing. There is no question that a precise representation of the short segment energy spectrum can be obtained from the Fourier transform. Furthermore, if the signal is sampled and the sample rate is higher than twice the highest frequency contained in the finite signal, then the fast Fourier transform yields a nearly exact representation of the signal segment's energy spectrum. However, that representation may not accurately represent the underlying power spectrum of the filter output. If one knows the shape of the filter, a better estimate of the underlying spectrum may be obtained from a least squares fit of the filter shape to the energy spectrum of the finite segment. This approach could be used, for example, to find the cutoff frequency ω_0 if it were not known.

For Doppler ultrasound, one wishes to obtain an accurate representation of the underlying power spectrum, since this is related to the flow velocity more directly than the spectra from short segments. In an effort to determine which model is the most appropriate, a number of investigators have applied alternative spectral analysis techniques to digitized or simulated Doppler quadrature signals.

The modern spectral analysis methods include autoregression (or maximum entropy), moving average, and autoregressive moving average (ARMA). These are called rational transfer function models, and they have been reviewed, along with other methods, by Kay and Marple[283]. They have also been reviewed in the context of Doppler ultrasound by Vaitkus and Cobbold[284]. The first two methods are special cases of ARMA.

* Note the distinction between the term `power spectrum' for the stochastic signal and `energy spectrum' for the finite duration segment. Since the stochastic process is considered to be of infinite duration, it has infinite energy and its energy spectrum is not defined. Conversely the power in the finite segment, averaged over all time, is zero and hence its power spectrum is zero.

For ARMA, it is assumed that a discretized white noise signal, n_j is the input to a digital filter. The output signal, x_j, then depends on both the input noise signal and previous values of the output by:

$$x_j = -\sum_{k=1}^{p} a_k x_{j-k} + \sum_{k=1}^{q} c_k n_{j-k} + n_j \ . \qquad \text{Eq. 30}$$

The a_k are called the autoregressive coefficients because they reflect the dependence of the time sequence x_j on previous values of itself. The c_k are called the moving average coefficients because they are the weighting factors in a moving average of the noise sequence n_j. The magnitude of the power spectrum $P_{arma}(\omega)$ of x is:

$$P_{arma}(\omega) = \sigma^2 \Delta t \frac{\left|1 + \sum_{k=1}^{q} c_k e^{-i\omega k}\right|^2}{\left|1 + \sum_{k=1}^{p} a_k e^{-i\omega k}\right|^2} \qquad \text{Eq. 31}$$

where σ_2 is the power of n_j. If all the c_k coefficients are assumed to be zero, an autoregressive model results. If all the a_k coefficients are assumed to be zero, a moving average model results. The autoregressive method is the most computationally efficient of the three, since the autoregressive coefficients can be evaluated by linear algorithms. Numerous methods exist by which autoregressive spectra can be evaluated. Two of the more common methods are the Burg method[285] and the Marple least squares method[286, 287]. Other methods include the Yule-Walker method, the Box-Jenkins method, and the forward backward error method.

The number of autoregressive coefficients, p, and the number of moving average coefficients, q, are both variables in the spectral models, and are called model orders. In general, these are not known *a priori*, and their determination can be problematic.

As was the case with other technologies, alternative signal analysis techniques were applied to Doppler radar systems several years before they were used with Doppler ultrasound. Hsu and Giordano[288], for example, concluded that autoregressive methods could significantly improve frequency tracking. It was later shown by Kay[289] that the improvement depended on the tracking method and that for low signal to noise ratios Fourier and autoregressive results were virtually identical.

Thorvaldsen[290] has compared the Burg and Marple autoregressive methods on signals which consist of two equal-amplitude sine waves in white noise. He concluded that for this ideal case the Marple method was superior and that the Burg method was often inferior, in terms of bias in the peak locations, to conventional Fourier methods.

Shon and Mehrotra[291] compared six algorithms for autoregressive spectral analysis. They used true autoregressive processes as the input signals so that the estimated autoregressive coefficients, a_k, could be compared to known values. They concluded that the Marple method generally had the lowest root mean square error except when the processes were highly correlated. For best overall estimation of the coefficients, they recommended the Burg algorithm, but for best estimation of peak frequency they recommended the forward-backward method.

It is difficult to extrapolate these early studies to Doppler ultrasound signals which are neither sine waves in noise nor true autoregressive processes. Consequently, studies have been undertaken recently to determine if modern spectral analysis methods could provide better spectral and velocity estimates than Fourier transform methods.

Kitney and Giddens[13] applied autoregressive techniques to Doppler ultrasound signals from the flow downstream of a stenosis in a canine aorta. Their objective was to extract velocity waveforms that exhibited coherent structures. The ultrasound measurements were made simultaneously with hot film anemometry measurements so the two could be compared. For the signal analysis, the ultrasound signals were first bandpass filtered to eliminate baseline shifts associated with cardiac contraction. A homomorphic filter was then applied. The effect of this filter is to eliminate amplitude modulation in the signal. Autoregressive spectral analysis was then used to transform the signal into the frequency domain, and an estimate of the Doppler shift was obtained from the spectra. Finally, a nonlinear filter was applied to eliminate noise spikes in the traces of frequency as a function of time. From the results, it appeared that these techniques could extract features in the Doppler-estimated velocity signals which were similar to those of the hot film anemometry signals. However, the comparison between Doppler traces and hot film traces was qualitative, and no comparison was made between the autoregressive methods and Fourier methods.

Another study of autoregressive methods was reported by Kaluzynski[292]. Doppler signals were collected *in vitro* from steady parabolic flow and *in vivo* from a brachial artery for both small and large sample volumes, which gave, respectively, narrow band and wide band spectra. Unsmoothed and smoothed Fourier spectra were studied along with the autoregressive spectra. It was concluded that for the wide band spectra the smoothed Fourier spectra and the autoregressive spectra were equivalent. However, the autoregressive spectra varied less from record to record for the narrow band spectra, which indicated that they provided more stable spectral estimates. No attempt was made to compare the results to theoretical spectra for the given flow geometries.

Talhami and Kitney[212] used a simulated Doppler signal to study the potential of the maximum likelihood spectral estimator.[1] They showed that the mode frequency of the maximum likelihood spectrum followed rapid changes in input frequency of the simulated signal with significantly greater accuracy than the mode frequency of the Fourier

[1] Maximum likelihood in this context is substantially different from the method of Ferrara and Algazi in section V-B-3-d in that the quadrature signals, rather than the rf signal, are processed here.

spectrum. However, this simulation included only the amplitude modulation properties of the Doppler signals and not the inherent frequency modulation properties associated with Doppler ambiguity.

An in depth study of numerous spectral analysis techniques was undertaken by Vaitkus and Cobbold[284] and Vaitkus et al.[293] This was again a simulation study, which used the simulation of Mo and Cobbold[209]. The input spectrum was representative of spectra from a carotid artery at the peak of systole. It had a gradually increasing amplitude from 0 Hz to approximately 1.2 KHz followed by a more rapid increase to a peak at approximately 2.3 KHz. For spectral analysis, the authors used two Fourier based methods, one moving average method, three autoregressive methods, three ARMA methods and one maximum likelihood method. They concluded that ARMA by singular value decomposition and autoregression by the Yule-Walker method yielded the best results in terms of bias and variance in the spectra. They recommended the ARMA method because the inclusion of both poles and zeros in the model should allow greater flexibility.

The most substantial difference between the Fourier methods and the modern methods was in the variance of the spectra. The bias of the Fourier method was actually lower than that for all other methods except for the case of low signal to noise ratio (0 db) for which the ARMA singular value decomposition method yielded slightly lower bias. Most of the bias in the Fourier method resulted from the natural peakiness of this method, which is described in terms of low flatness by Vaitkus et al.[293] This raises the question as to whether the variance in the Fourier spectra could be adequately reduced by a simple smoothing algorithm as studied earlier by Kaluzynski[292].

It is also important to remember that the extensive work of Vaitkus et al.[284, 293] was applied to one spectral shape. It is not certain that the results are directly applicable to other shapes, particularly since the ability of a given parametric spectral analysis method to model a particular spectral shape depends directly on the model order or model orders. Some evidence that the results can be generalized is given by the *in vivo* data presented in part two of their study[293].

David et al.[294] applied autoregressive, maximum likelihood and Fourier analysis to *in vitro* and simulated signals and studied the effects of model order, signal to noise ratio and velocity gradient on both velocity estimates and spectral estimates. The most stable spectral estimates were obtained with the maximum likelihood method of Musicus[295]. For peak tracking at the centerline of Poiseuille flow, where the velocity within the sample volume was relatively uniform, the bias in the autoregressive and Fourier estimates was nearly identical (3.1%), and the bias in the maximum likelihood was slightly higher (4.4%). The variance in these estimates depended on both model order and signal to noise ratio. For moderate signal to noise ratios, there was a range of low model orders, usually centered around model order 5, for which the variance of the autoregressive methods was lower than that for the Fourier transform. For higher model orders, the variance was larger or equal to that of the Fourier transform estimates. However, for high signal to noise ratios, estimates of the Doppler frequency from the first moment of the Fourier transform had consistently lower bias than any of the estimates which used peak tracking. Furthermore, estimates based on the first moment of

any of the modern spectral analysis methods were virtually identical to estimates based on the Fourier spectrum. Thus, for narrow band signals free of additive noise, the Fourier method was preferred on the basis of lower computational complexity. Simulation studies corroborated these results and showed that the bias of the first moment estimate became significant for signal to noise ratios below about 20 db, but the bias in the peak tracker estimates remained low for signal to noise ratios as low as -9 db. Thus, as signal to noise ratio becomes low, peak tracking becomes the preferred method of analysis, and the modern signal analysis methods perform better.

For signals from a shear region, which have wide-band spectra, the first moment method again had the lowest variance, but had the highest bias. Of the modern methods, the maximum likelihood method had the lowest variance, mainly as a result of isolated anomalous frequency estimates in the autoregressive methods.

These results indicate the complicated nature of Doppler ultrasound signal analysis. The optimal processing method depends strongly on the nature of the signal itself. In particular, for narrow band signals, better Doppler frequency estimates can be obtained from the Fourier first moment if the signal to noise ratio is high, and with the maximum likelihood or autoregressive peak tracker if the signal to noise ratio is low. Studies by Jones and Giddens[296] show that not only the signal to noise ratio, but also the shape of the additive noise affect the model order at which peak tracking is optimal. For purely white additive noise, the best model order was model order 1. For additive noise with a higher power level in the low frequency range, model order 1 gave a variance comparable to the bias in the Fourier peak tracker, and the optimal model order was near 5. In some cases, however, the variance was anomalously high at some model order at or near 5. There was no single processing method that universally gave superior results. It is possible, however, that if foreknowledge of the bandwidth or signal to noise ratio of the Doppler signal is available, one of the alternative spectral analysis methods can be used to advantage.

One curiosity of autoregressive analysis was illustrated by Wendling et al.[145]. They showed simulated signals with no additive noise for which the variance in the autoregressive peak tracker frequency estimates was high (Figure 18 a). When additive noise was added to this same signal, the variance

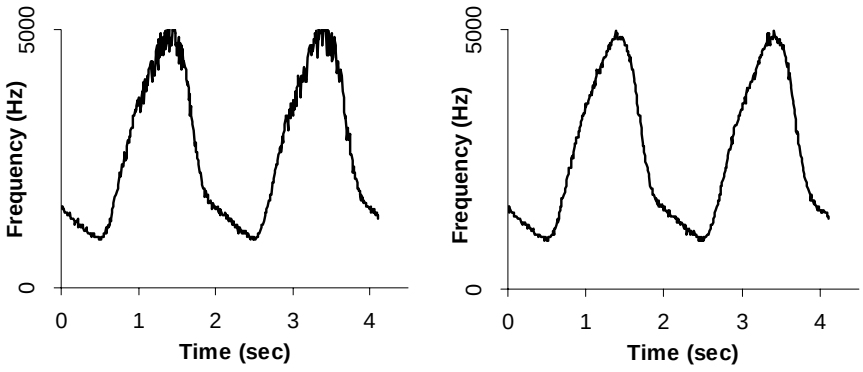

Figure 18: The *addition* of noise to the quadrature signal can *reduce* the variance in the estimates of Doppler frequency when an autoregressive routine is used for spectral analysis. (a) No added noise. (b) Signal to noise ratio 25 db.

in the peak tracker was dramatically reduced (Figure 18 b). This initially suggests that frequency estimates might be improved if Gaussian white noise is added to the Doppler ultrasound signals prior to autoregressive analysis. However, it must be remembered that the original signal had no additive noise and would therefore have been best analyzed via the first moment of the Fourier transform. A real time system for autoregressive signal analysis was implemented by Schlindwein and Evans[297] for application to Doppler ultrasound. This group later compared four of the more common methods for model order selection.[298] They examined five signals, which included both pulsed and continuous wave Doppler, from a variety of artery geometries. They found that the first zero crossing criterion yielded results that differed greatly from those of the final prediction error, Akaike's information criterion, and the criterion autoregressive transfer function (see Kay and Marple[283] for an explanation of these methods). They then used simulated autoregressive processes and found that none of the techniques yielded model orders that consistently agreed with the order of the simulated signal, although agreement improved with record length. They concluded that less error was introduced when the model order was overestimated than when it was underestimated, and that the most appropriate approach was to use a fixed model order of 10 or 12.

The selection of model order for autoregressive signals was also studied by Kaluzynski[299] with signals collected from the exposed carotid artery of an anaesthetized canine. He concluded that incorrect results were often obtained from the standard criteria for model order selection, and that the application of a single model order to all signals was also inadequate. In particular, he noted that signals obtained during systolic acceleration differed markedly from those obtained during systolic deceleration. Forsberg[300] has studied the application of singular value decomposition ARMA to Doppler ultrasound signals. He used a simulation model based on that of Hoeks[301]. This model uses filtered white noise, where the filter parameters are time variant, and where Gaussian white noise is added to vary the signal to noise ratio. Conclusions were similar to those of Kaluzynski[299] for autoregressive modeling. Improved spectra could be obtained through the ARMA method, but spectral shape was highly dependent on model order, and the correct model order could not be selected by any existing criterion.

The model order of 5 cited by David et al.[294] differs from the higher model orders cited by other investigators, such as 10 or 12 for Schlindwein and Evans[297] and for Vaitkus et al.[293] The probable reason for this is that the latter groups implemented real autoregressive algorithms, whereas the work of David et al.[294] used complex algorithms and operated on both the in-phase and quadrature signals. The factor of two difference in optimal model order is reasonable since the complex algorithm uses twice as many real coefficients for a given model order as the real algorithm.

Bharath and Kitney[302] used modern spectral estimation techniques in an attempt to determine Doppler angle from the bandwidth of the Doppler spectrum. They used the spectral shape obtained by Censor et al.[187] which accounts for geometric broadening effects in uniform flow, as the input to the simulation model of Mo and Cobbold[209] They found that the bandwidth of the spectrum was most consistently and accurately estimated by an ARMA model with 4 poles and 3 zeros. Although this does not address the

problem of model order selection which results from highly variable flow conditions, it demonstrates that, with foreknowledge that the flow is uniform, one can obtain good bandwidth estimates and hence good estimates of Doppler angle through an ARMA model.

The bias of several velocity estimators has been studied by Markou and Ku[21] in laminar and turbulent pipe flow. They found that zero crossing, and peak tracking by either Fourier, autoregressive or maximum likelihood methods performed equivalently when velocity gradients were low. For large velocity gradients, the peak tracking methods were superior, but there was no significant difference in the bias among the Fourier and the modern methods. This study did not address the variance in the spectral estimates.

Mohamed[303] has applied autoregressive modeling to Doppler diagnosis of cardiac pathologies. The method uses spectral features as well as the poles of the autoregressive model to classify the signals from normal patients and patients with aortic or mitral stenosis, aortic or mitral regurgitation, or pulmonary hypertension. This is a method which *requires* autoregressive techniques since the information derived from the poles of the autoregressive model could not be obtained from Fourier analysis. However the diagnostic value of this information has not yet been evaluated.

The use of modern spectral analysis techniques was originally motivated by the desire to find a spectral model that adequately represents the underlying Doppler process. However, in most cases the techniques are used without specific justification in terms of the underlying signal statistics. A more ideal approach is to base the signal analysis method directly on a mathematical model for the Doppler signal. This approach has been used in the work of Ferrara and Algazi[267, 268] for wide band processing. For analysis of the quadrature signals, the approach has only recently been taken in work by Destefano[304], which uses the simulation of Jones and Giddens[144] as the underlying model for the signal.

4. Time Domain Methods

A number of methods exist by which the Doppler shift can be obtained from time domain processing of the quadrature signals. The zero crossing detector is perhaps the simplest of these. Another group of estimators is based on the following relationship between the spectral centroid frequency, $\overline{\omega}$, and the autocorrelation, $R(\tau)$, of the complex Doppler signal (Angelsen[305]):

$$\overline{\omega} = -j\frac{\dot{R}(0)}{R(0)} \qquad \text{Eq. 32}$$

where the dot notation denotes the derivative with respect to τ. Different implementations are distinguished by the method used to estimate $\dot{R}(0)$. This in turn depends on the assumptions made about the signals. For example (see Kristoffersen and Angelsen[306]), if $p(t)$ and $q(t)$ represent the in-phase and quadrature components of the downmixed signal, respectively, then

$$\frac{\dot{R}(0)}{R(0)} = \frac{\dot{R}_{pq}(0) - \dot{R}_{qp}(0)}{R_{pp}(0) + R_{qq}(0)} \qquad \text{Eq. 33}$$

This is the double correlator proposed by Brody[307]. If the velocity field is stationary in time, however,

$$\dot{R}_{pq}(0) = -\dot{R}_{qp}(0), \quad R_{pp}(0) = R_{qq}(0), \text{ and } \frac{\dot{R}(0)}{R(0)} = \frac{\dot{R}_{pq}(0)}{R_{pp}(0)}, \qquad \text{Eq. 34}$$

which is the single correlator estimator of Arts and Roevros[308]. For an analysis of the properties of the double correlator, see Gerzberg and Meindl[309] and Angelsen[305]. For much more complete discussion of these time domain methods, see Kristoffersen and Angelsen [306].

Kasai et al.[115] use Equation (32) to show that the instantaneous frequency can be approximated as $\phi(\tau_p)/\tau_p$, where ϕ is the phase of the complex autocorrelation. They further derive an expression for the variance, σ, in the mean frequency as:

$$\sigma^2 = \frac{1}{\tau_p}\left\{1 - \frac{|R(\tau_p)|}{R(0)}\right\}. \qquad \text{Eq. 35}$$

This expression is often used to estimate flow variance in color Doppler systems.

The primary advantage of time domain methods is that they can be easily implemented in real time. Many of them also enable compensation for bias caused by low signal to noise ratios. An example was described by Gerzberg and Meindl[309] and further studied by Barber et al.[239] This is based on the following idea. If $\overline{\omega}_n$ is the mean frequency of the noise, $\overline{\omega}_s$ is the mean frequency of the signal with noise, P_n is the total power of the noise, and P_s is the total power of the signal plus noise, then the corrected Doppler centroid frequency is:

$$\omega_d = -\overline{\omega}_s\left(\frac{P_s}{P_s - P_n}\right) - \overline{\omega}_n\left(\frac{P_n}{P_s - P_n}\right) \qquad \text{Eq. 36}$$

Thus, the mean frequency and power of the noise are estimated, and these are used in Equation (36) to obtain the corrected centroid frequency. This assumes that the signal and noise are uncorrelated. Another example, the adaptive scheme of Angelsen and Kristoffersen[306, 310, 311], assumes that the noise spectrum is white. Here, the original Doppler signal is shifted in frequency by $-\omega_m$, where ω_m is the current estimate of the Doppler frequency. The result has a spectrum for which the mean frequency is approximately zero. This signal is the input to a mean frequency estimator and the output is averaged over time (low pass filtered) to yield a new estimate of ω_m. The output frequency, ω_m, changes over time with a rate that depends on the frequency response of

the low pass filter. White noise does not contribute significantly to bias in the estimate because its spectrum is symmetric around $\omega = 0$.

A second feature of the adaptive scheme is that it can track the Doppler shift beyond the Nyquist limit. This does not mean that the method uses information in the signal that is lost when the Fourier transform is used. Rather, the feature assumes that the the Doppler shift changes slowly in time; if the flow velocity changes too rapidly, the system will no longer be able to track the Doppler shift. This same assumption is inherent in the alias extension method of Jaffe[312], and those of Hoeks et al.[313] and Hartley[314], which work on signals from a zero crossing detector. The assumption should, of course, be avoided for a flow in which rapid changes in velocity are expected to occur, but it should be reasonable for a wide variety of biological flows.

Alias extension techniques have also been applied to frequency domain processing of Doppler ultrasound signals. Again, assumptions of continuity in the Doppler shift[315, 316], the Doppler spectrum[315], or the velocity profile[317] are used. Bias caused by noise can also be reduced through frequency-domain processing if a suitable model for the underlying noise spectrum is obtained and this is subtracted from the spectral estimates.

The above section demonstrates that the specific signal analysis method used strongly affects the quality of the velocity estimation waveform. However, it has not been shown that any general approach to Doppler analysis is inherently superior to others. Modern spectral analysis methods can reduce the variance in noisy signals, but can also increase it for narrow band signals with high signal to noise. Furthermore, a reduction in variance might also be achieved by appropriate post-processing of the Fourier spectrum. Time domain methods have advantages in ease of implementation, but the noise subtraction and alias extension capabilities of some of these methods are achieved through the imposition of assumptions on the velocity being measured or the character of the background noise. These assumptions can also be applied to frequency domain processing with equivalent effects. Care must be taken to assure that these assumptions are valid before they are used in a given measurement application.

VI. SUMMARY

The examination of recent developments in Doppler ultrasound repeatedly emphasizes that the ability to accurately measure flow velocity depends on *a priori* knowledge of the flow field and the instrumentation. Only after this knowledge has been carefully evaluated can the optimal Doppler method and associated signal processing technique be identified. Some information, such as the location and orientation of the artery and the shape of the additive noise spectrum can be acquired prior to the measurement. Other information, such as a rough estimate of the velocity must be assumed from a reasonable knowledge of physiology.

Some of the recent work in Doppler ultrasound has the potential to reduce the number of required assumptions through the use of information that is not considered in conventional Doppler ultrasound. For example, time domain correlation and other wide-band methods use more of the information in the returned signal and can eliminate the alias-

ing problems associated with low sample rates. Also, multi-dimensional Doppler uses two or more measurements from different angles to directly provide the Doppler angle, which is critical to accurate measurement. These techniques show potential for fundamental improvement in the accuracy and resolution of ultrasound measurements.

References

1. Satomura, S., "Study of the flow patterns in peripheral arteries by ultrasonics," *J Acoust Soc Jpn,* 15, 151, 1959.
2. Franklin, D.L., Schlegel, W., Rushmer, R.F. "Blood flow measured by Doppler frequency shift of back-scattered Ultrasound," *Science,* **134,** 564, 1961.
3. Franklin, D.L., Schlegel, W., Watson, N.W., "Ultrasonic Doppler shift blood flowmeter: Circuitry and practical applications," *Proc ISA Biomed Sci Instrum Symp,* **1,** 309, 1963.
4. Baker, D.W., "Pulsed ultrasonic Doppler blood-flow sensing," *IEEE Trans Sonics Ultrason,* **17,** 170, 1970.
5. Fish, P.J., "A method of transcutaneous blood flow measurement -- accuracy considerations," in *Recent Advances in Ultrasound Diagnosis,* Excerpta Medical, A. Kurjak and A. Kratochwil, Eds., Amsterdam, **3,** 1981.
6. Gill, R.W., "Pulsed Doppler with B-mode imaging for quantitative blood flow measurement.," *Ultrasound Med Biol,* **5,** 223, 1979.
7. McMillan, S.T., Woo, Y.-R., Jones, M., Eidbo, E.E., Yoganathan, A.P., Foster, K.R., " In vitro/in vivo velocity and turbulence characterization of a number of mitral heart valve prostheses," *Proc Thirteenth Ann Northeast Bioeng Conf,* **1,** 261, 1987.
8. Clemente, F., Cesarelli, M., Bracale, M., Bracale, G.C., Selvetella, L. Cappellini, V., "A different approach to processing Doppler US signal: the estimate of pseudo velocity profile from spectral data," *Time-Varying Image Processing Moving Object Recognition 2 Proc 3rd Internat Workshop,* 189, 1990.
9. Cheung, J.Y., Ashrafzadeh, A.R., Dormer, K.J., "Determining stenosis in turbulent blood flow using a dual-transducer pulsed Doppler ultrasound system," *IEEE 1986 Ultrason Symp Proc,* **2,** 851, 1986.
10. Brandestini, M., "Topoflow -- A digital full range Doppler velocity meter," *IEEE Trans Sonics Ultrason,* **25,** 287, 1978.
11. D'Luna, L.J., Newhouse, V.L., "Vortex characterization and identification by ultrasound Doppler," *Ultrasonic Imaging,* **3,** 271, 1981.
12. Ahmed, S.A., Giddens, D.P., "Flow disturbance measurements through a constricted tube at moderate Reynolds numbers," *J Biomech,* **16,** 955, 1983.
13. Kitney, R.I., Giddens, D.P., "Linear estimation of blood flow waveforms measured by Doppler ultrasound," in *Medinfo 86,* R. Salamon, B.Blum, M. Jorgensen, Eds., Elsevier Science Publishers, North-Holland, 1986.
14. Lieber, B.B., Giddens, D.P., Kitney, R.I., Talhami, H., "On the Discrimination Between Band-Limited Coherent and Random Apparent Stresses in Transitional Pulsatile Flow," *J Biomech Eng,* **111,** 42, 1989.
15. Garbini, J.L., Forster, F.K., Jorgensen, J.E., "Measurement of fluid turbulence based on pulsed ultrasound techniques. Part 1. Analysis," *J Fluid Mech,* **118,** 445, 1982.

16. Garbini, J.L., Forster, F.K., Jorgensen, J.E., "Measurement of fluid turbulence based on pulsed ultrasound techniques. Part 2. Experimental Investigation," *J Fluid Mech,* **118,** 471, 1982.
17. Mann, K.A., Deutsch, S., Tarbell, J.M., Geselowitz, D.B., Rosenberg, G., Pierce, W.S., "An experimental study of Newtonian and non-Newtonian flow dynamics in a ventricular assist device," *Trans ASME J Biomech Eng,* **109,** 139, 1987.
18. Pohl, M., Wendt, M.-O., Lerche, D., "Hydrodynamic *in vivo* comparison of a new artificial heart valve with the Bjork-Shiley valve (standard)," *Biomedizinische Technik,* **36,** 134, 1991.
19. Ashrafzadeh, A.R., Cheung, J.Y., Dormer, K.J., Botros, N., " *In vivo* and *in vivo* measurements of turbulent blood flow characteristics using a multi-dimensional ultrasonic probe," *Acoust Imaging, Proc 16th Internat Symp,* **19,** 209, 1988.
20. Campbell, J.D., Hutchinson, K.J., Karpinski, E., "Variation of Doppler ultrasound spectral width in the post-stenotic velocity field," *Ultrasound Med Biol,* **15,** 611, 1989.
21. Markou, C.P., Ku, D.N., "Accuracy of velocity and shear rate measurements using pulsed Doppler ultrasound: a comparison of signal analysis techniques," *Ultrasound Med Biol,* **17,** 803, 1991.
22. Ashrafzadeh, A.R., Dormer, K.J., Cheung, J.Y., "A two-dimensional Doppler ultrasonic probe for flow measurement," *Biomed Instrumen Technol,* **23,** 301, 1989.
23. Tamura, T., Fronek, A., "Shear-layer detection in poststenotic flow by spectrum analysis of Doppler signals," *J Biomech Eng,* **110,** 320, 1988.
24. Sloerdahl, S.A., Skjaerpe, T., Piene, H., "Aortic regurgitation evaluated by pressure half-time in a cardiovascular hydromechanical simulator," *Heart Vessels,* **suppl. 3,** 9, 1987.
25. Gardiner, W.M., Fox, M.D., LaCourse, J.R., "Pressure gradient determination by three dimensional Doppler ultrasound (medical haemodynamics)," *Proc Fourteenth Ann Northeast Bioeng Conf,* 266, 1988.
26. Loyd, D., Ask, P., Wranne, B., "Mitral valve flow and its relation to pressure gradient halftime," *Proc Ninth Ann Conf IEEE Eng Med Biol Soc,* 867, **2,** 1987.
27. Holen, J., Waag, R.C., Gramiak, R., "Doppler ultrasound in aortic stenosis: *in vivo* studies of pressure gradient determination," *Ultrasound Med Biol,* **13,** 321, 1987.
28. Sillesen, H., Schroeder, T., "Changes in Doppler waveforms can predict pressure reduction across internal carotid artery stenoses," *Ultrasound Med Biol,* **14,** 649, 1988.
29. Kitabatake, A., Ito, H., Inoue, M., "Current development in Doppler echocardiography. The real-time two-dimensional Doppler flow imaging system," *Med Prog Technol,* **12,** 87, 1987.
30. De Knecht, S., Hopman, J.C.W, Alsters, J.L.C.M, Daniels, O., Hoeks, A.P.G., Reneman, R.S., "Automated calculation of stenosis diameters from the width of the velocity jet with the use of a multi-gate pulsed Doppler system," *Ultrasound Med Biol,* **14,** 575, 1988.
31. Evans, J.M., Skidmore, R., Baker, J.D., Wells, P.N.T., "A new approach to the non-invasive measurement of cardiac output using an annular array Doppler technique -- II. Practical implementation and results," *Ultrasound Med Biol,* **15,** 179, 1989.
32. Rijsterborgh, H., Roelandt, J., "Doppler assessment of aortic stenosis: Bernoulli revisited," *Ultrasound Med Biol,* **13,** 241, 1987.

33. Hatle, L., Brubakk, A., Tromsdal, A., Angelsen, B., "Noninvasive assessment of pressure drop in mitral stenosis by Doppler ultrasound," *Br Heart J,* **40,** 131, 1978.
34. Spencer, M.P., Denison, A.B. Jr., "Pulsatile blood flow in the vascular system," in *Handbook of Physiology,* W.F. Hamilton, Eds., American Physiological Society, Bethesda, MD, **2, Circulation II,** 839-864, 1963.
35. Gosling, R.G., Dunbar, G., King, D.H., Newman, D.L., Side, C.D., Woodcock, J.P., Fitzgerald, D.E., Keates, J.S., MacMillan, D., "The quantitative analysis of peripheral arterial disease by a non-intrusive ultrasonic technique," *Angiol,* **22,** 52, 1971.
36. Kassam, M.S., Cobbold, R.S.C., Johnston, K.W., Graham, C.M., "Methods for estimating the Doppler mean velocity waveform," *Ultrasound Med Biol,* **8,** 537, 1982.
37. David, T., Clamp, J., Fisher, J., "Analysis of regurgitant jets in natural and bioprosthetic heart valves," *J Biomech,* **25,** 457, 1992.
38. Angelsen, B.A.J., Slordahl, S.A., Solbakken, J.E., Samstad, S.O., Linker, D.T., Torp, H., Piene, H., "Estimation of regurgitant volume and orifice in aortic regurgitation combining c.w. Doppler and parameter estimation in a Windkessel-like model," *Modeling Identification Control,* **12,** 3, 1991.
39. Angelsen, B.A.J., Slordahl, S.A., Solbakken, J.E., Samstad, S.O., Linker, D.T., Torp, H., Piene, H., "Estimation of regurgitant volume and orifice in aortic regurgitation combining CW Doppler and parameter estimation in a Windkessel-like model," *IEEE Trans Biomed Eng,* **37,** 930, 1990.
40. Cape, E.G., Yoganathan, A.P., Levine, R.A., "A new theoretical model for noninvasive quantification of mitral regurgitation," *J Biomech,* **23,** 27, 1990.
41. Ask, P., Loyd, D., Wranne, B., "Regurgitant flow through heart valves: a hydraulic model applicable to ultrasound Doppler measurements," *Med Biol Eng Comput,* **24,** 643, 1986.
42. Mauyama, T., Kodama, K., Kitabatake, A., "Noninvasive evaluation of aortic regurgitation by continuous-wave Doppler echocardiography," *Circulation,* **3,** 460, 1986.
43. Teague, S.M., Heinsimer, J.A., Anderson, J.L., "Quantification of aortic regurgitation utilizing continuous wave Doppler ultrasound," *J Am Coll Cardiol,* **8,** 1341, 1986.
44. Pearlman, A.S., Otto, C.M., "The use of Doppler techniques for quantitative evaluation of valvular regurgitation," *Eur Heart J,* **8,** 35, 1987.
45. Miller, F.A., "Aortic stenosis: Most cases no longer require invasive hemodynamic study," *J Am College Cardiol,* **13,** 551, 1989.
46. Hoskins, P.R., "Quantitative techniques in arterial Doppler ultrasound," *Clin Phys Physiol Meas,* **11, suppl.A,** 75, 1990.
47. Mayo, A., Rawles, J., "Comparison of four different Doppler instruments used to measure linear and volumetric cardiac output: a study of reproducibility and agreement," *Ultrasound Med Biol,* **17,** 347, 1991.
48. Eriksen, M., Walloe, L., "Improved method for cardiac output determination in man using ultrasound Doppler technique," *Med Biol Eng Comput,* **28,** 555, 1990.
49. Weber, R.E. Kim, Y., Spelman, F.A., "Transtracheal Doppler: a new method of cardiac output measurement," *Images Twenty-First Century Proc Ann Internat Conf IEEE Eng Med Biol Soc,* 1571, **5,** 1989.
50. Haude, M., Gerber, T., Brennecke, R., Erbel, R., Meyer, J., "Non-invasive determination of cardiac output by transesophageal Doppler ultrasound--clinical application and validation," *Proc Comput Cardiol 1988,* 485, 1989.

51. Evans, J.M., Skidmore, R., Luckman, N.P., Wells, P.N.T., "A new approach to the noninvasive measurement of cardiac output using an annular array Doppler technique. I. Theoretical considerations and ultrasonic fields," *Ultrasound Med Biol,* **15,** 169, 1989.
52. Lydon, M., Franks, C.I., Freeston, I.L., "Online measurement of cardiac indices from frequency transformed TAV Doppler ultrasound signals," *Med Biol Eng Comput,* **24,** 625, 1986.
53. McLennan, F.M., Haites, N.E., Mackenzie, J.D., Daniel, M.K., Rawles, J.M., "Reproducibility of linear cardiac output measurement by Doppler ultrasound alone," *Br Heart J,* **55,** 25, 1986.
54. Bernstein, D.P., "Noninvasive cardiac output, Doppler flowmetry, and gold-plated assumptions," *Crit Care Med,* **15,** 886, 1987.
55. Drayton, M.R., Skidmore, R., "Doppler ultrasound in the neonate," *Ultrasound Med Biol,* **12,** 761, 1986.
56. Soul, F.J., Hames, T.K., Thomas, V.L., Bacon, R.J., "Estimation of aortic and pulmonary blood flow in a paediatric population using Doppler ultrasound: an *in vivo* study," *Ultrasound Med Biol,* **16,** 659, 1990.
57. Serruys, P.W., Julliere, Y., Zijlstra, F., Beatt, K.J., De Feyter, P.J., Suryapranata, H., Van Den Brand, M., Roelandt, J., "Coronary blood flow velocity during percutaneous transluminal coronary angioplasty as a guide for assessment of the functional result," *Am J Cardiol,* **61,** 253, 1988.
58. Johnson, E.L., Yock, P.G., Hargrave, V.K., Srebro, J.P., Manubens, S.M., Seitz, W., Ports, T.A., "Assessment of severity of coronary stenoses using a Doppler catheter. Validation of a method based on the continuity equation," *Circulation,* **80,** 625, 1989.
59. Kajiya, F., Ogasawara, Y., Tsujioka, K., Fujiwara, T., "Multigated 20 MHz dual mode (zero-cross + Fourier transform) ultrasound pulsed Doppler velocimeter and its application to the measurement of human coronary artery blood flow," *Automedica,* **12,** 63, 1989.
60. Dole, W.P., Richards, K.L., Hartley, C.J., Alexander, G.M., Campbell, A.B, Bishop, V.S., "Diastolic coronary artery pressure-flow velocity relationships in conscious man," *Cardiovasc Res,* **18,** 584, 1984.
61. Hartley, C.J., Millar, H.D., "Ultrasonic Sensors for Measuring Coronary Blood Flow," *Soc Photo-Optical Instrumen Engineers Symp Med Applications Lasers, Fiber Optics Electro Optics,* 1, 1988.
62. Cole, J.S., Hartley, C.J., "The pulsed Doppler coronary artery catheter. Preliminary report of a new technique for measuring rapid changes in coronary artery flow velocity in man," *Circulation,* **56,** 18, 1977.
63. Matsuo, S., Tsuruta, M., Hayano, M., Imamura, Y., Eguchi, Y., Tokushima, T., Tsuji, S., "Phasic coronary artery flow velocity determined by Doppler flowmeter catheter in aortic stenosis and aortic regurgitation," *Am J Cardiol,* **62,** 917, 1988.
64. Voyles, W.F., Greene, E.R., Altobelli, S.A., Hartley, C.J., " In vitro and in vivo studies using a 4F pulsed Doppler velocimeter catheter system," *Biomed Sci Instr,* **20,** 17, 1984.
65. Sibley, D.H., Millar, H.D., Hartley, C.J., Whitlow, P.L., "Subselective measurement of coronary blood flow velocity using a steerable Doppler catheter," *J Am Coll Cardiol,* **8,** 1332, 1986.

66. Martin, R.W., Watkins, D.W., "An ultrasonic catheter for intravascular measurement of blood flow: technical details," *IEEE Trans Sonics Ultrason,* **27,** 277, 1980.
67. Hartley, C.J., "Review of intracoronary Doppler catheters," *Internat J Cardiac Imaging,* **4,** 159, 1989.
68. Wilson, R.F., Johnson, M.R., Marcus, M.L., Aylward, P.E.G., Skorton, D.J., Collins, S., White, C.W., "The effect of coronary angioplasty on coronary flow reserve," *Circulation,* **77,** 873, 1988.
69. Wilson, R.F., Marcus, M.L., White, C.W., "Prediction of the physiologic significance of coronary arterial lesions by quantitative lesion geometry in patients with limited coronary artery disease," *Circulation,* **75,** 723, 1987.
70. McGinn, A.L., White, C.W., Wilson, R.F., "Interstudy variability of coronary flow reserve. Influence of heart rate, arterial pressure and ventricular preload," *Circulation,* **81,** 1319, 1990.
71. Serwer, G.A., Armstrong, B.E., Anderson, P.A.W., "Continuous wave Doppler ultrasonographic quantitation of patent ductus arteriosus flow," *J Pediatrics,* **100,** 297, 1982.
72. Wilcox, W.D., Carrigan, T.A., Dooley, K.J., Giddens, D.P., Dykes, F.D., Lazzara, A., Ray, J.L., Ahmann, P.A., "Range-gated pulsed Doppler ultrasonographic evaluation of carotid arterial blood flow in small preterm infants with patent ductus arteriosus," *J Pediatrics,* **102,** 294, 1983.
73. Hanretty, K.P., Rubin, P.C., "The use of Doppler ultrasound in the study of fetal cardiovascular physiology," *J Neurosci Meth,* **34,** 159, 1990.
74. Griffin, D., Teague, M., "Blood flow in obstetrics using Doppler ultrasound," *J Med Eng Technol,* **12,** 97, 1988.
75. Kurjak, A., Alfirevic, Z., Miljan, M., "Conventional and color Doppler in the assessment of fetal and maternal circulation," *Ultrasound Med Biol,* **14,** 337, 1988.
76. Thompson, R.S., Trudinger, B.J., Cook, C.M., "A comparison of Doppler ultrasound waveform indices in the umbilical artery. I. Indices derived from the maximum velocity waveform," *Ultrasound Med Biol,* **12,** 835, 1986.
77. Thompson, R.S., Trudinger, B.J., Cook, C.M., "A comparison of Doppler ultrasound waveform indices in the umbilical artery. II. Indices derived from the mean velocity and first moment waveforms," *Ultrasound Med Biol,* **12,** 845, 1986.
78. Malcus, P., Andersson, J., Marsal, K., Olofsson, P.A., "Waveform pattern recognition--a new semiquantitative method for analysis of fetal aortic and umbilical artery blood flow velocity recorded by Doppler ultrasound," *Ultrasound Med Biol,* **17,** 453, 1991.
79. Adamson, S.L., Morrow, R.J., Langille, B.L., Bull, S.B., Ritchie, J.W.K., "Site-dependent effects of increases in placental vascular resistance on the umbilical arterial velocity waveform in fetal sheep," *Ultrasound Med Biol,* **16,** 19, 1990.
80. Thompson, R.S., Trudinger, B.J., "Doppler waveform pulsatility index and resistance, pressure and flow in the umbilical placental circulation: an investigation using a mathematical model," *Ultrasound Med Biol,* **16,** 449, 1990.
81. Stale, H., Marsal, K., Gennser, G., Benthin, M., Dahl, P., Lindstrom, K., "Aortic diameter pulse waves and blood flow velocity in the small, for gestational age, fetus," *Ultrasound Med Biol,* **17,** 471, 1991.

82. Chen, H.Y., Chang, F.M., Huang, H.C., Hsieh, F.J., Lu, C.C., "Antenatal fetal blood flow in the descending aorta and in the umbilical vein and their ratio in normal pregnancy," *Ultrasound Med Biol,* **14,** 263, 1988.
83. Arbeille, P., Roncin, A., Berson, M., Patat, F., Pourcelot, L., "Exploration of the fetal cerebral blood flow by duplex Doppler-linear array system in normal and pathological pregnancies," *Ultrasound Med Biol,* **13,** 329, 1987.
84. Brown, J.S., Gee, H., Olah, K.S., Docker, M.F., Taylor, E.W., "A new technique for the identification of respiratory sinus arrhythmia in utero," *J Biomed Eng,* **14,** 263, 1992.
85. Van Woerden, E.E., Van Geijn, H.P., Caron, F.J.M., Mantel, R., "Spectral analysis of fetal heart rhythm in relation to fetal regular mouthing," *Internat J Bio-Med Comput,* **25,** 253, 1990.
86. Patel, M.C., Taylor, M.G., Kontis, S., Padayachee, T.S., Gosling, R.G., "An online technique for estimating cerebral carbon dioxide reactivity," *J Biomed Eng,* **12,** 316, 1990.
87. Vaitkus, P.J., Johnston, K.W., Bondar, R.L., Stein, F., Bascom, P.A.J., Mo, L.Y.L., Kassam, N.M., Chadwick, L.C., Mehi, J., Cobbold, R.S.C., "Development of methods to analyse transcranial Doppler ultrasound signals recorded in microgravity," *Med Biol Eng Comput,* **28,** 306, 1990.
88. Grolimund, P., Seiler, R.W., "Age dependence of the flow velocity in the basal cerebral arteries--a transcranial Doppler ultrasound study," *Ultrasound Med Biol,* **14,** 191, 1988.
89. Hennerici, M., Rautenberg, W., Sitzer, G., Schwartz, A., "Transcranial Doppler ultrasound for the assessment of intracranial arterial flow velocity -- Part 1: Examination technique and normal values," *Surg Neurol,* **27,** 439, 1987.
90. Hennerici, M., Rautenberg, W., Sitzer, G., Schwartz, A., "Transcranial Doppler ultrasound for the assessment of intracranial arterial flow velocity -- Part 1: Evaluation of intracranial arterial disease," *Surg Neurol,* **27,** 523, 1987.
91. Ringelstein, E.B., Kahlscheuer, B., Niggemeyer, E., Otis, S.M., "Transcranial Doppler sonography: Anatomical landmarks and normal velocity values," *Ultrasound Med Biol,* **16,** 745, 1990.
92. Fujioka, K.A., Douville, C.M., "Anatomy and Freehand Examination Techniques," in *Transcranial Doppler,* D.W. Newell and R. Aaslid, Eds., Raven Press, Ltd., New York, 1992.
93. Hoskins, P.R., "Measurement of arterial blood flow by Doppler ultrasound," *Clin Phys Physiol Meas,* **11,** 1, 1990.
94. Greene, E.R., Avasthi, P.S., Voyles, W.F., Seigel, R.S., "Noninvasive versus invasive Doppler renal blood velocity and flow measurements," *IEEE Trans Biomed Eng,* **33,** 302, 1986.
95. Hartley, C.J., Lewis, R.M., Pinsky, W.W., "Pulsed Doppler evaluation of renal flow disturbances in dogs," *Proc 31st ACEMB,* 344, 1978.
96. Brown, T.D., Blair, W.F., Gabel, R.H., Morecraft, R.J., "Effects of episodic air hammer usage on digital artery hemodynamics of foundry workers with vibration white finger disease," *J Occupational Med,* **30,** 853, 1988.
97. Lerner, R.M., Huang, S.R., Parker, K.J., "`Sonoelasticity' images derived from ultrasound signals in mechanically vibrated tissues," *Ultrasound Med Biol,* **16,** 231, 1990.

98. Parker, K.J., Huang, S.R., Musulin, R.A., Lerner, R.M., "Tissue response to mechanical vibrations for `sonoelasticity imaging'," *Ultrasound Med Biol,* **16,** 241, 1990.
99. Adler, D.D., Carson, P.L., Rubin, J.M., Quinn-Reid, D., "Doppler ultrasound color flow imaging in the study of breast cancer: preliminary findings," *Ultrasound Med Biol,* **16,** 553, 1990.
100. Vaupel, P., Okunieff, P., Kluge, M., "Response of tumour red blood cell flux to hyperthermia and/or hyperglycaemia," *Internat J Hyperthermia,* **5,** 199, 1989.
101. Ramos, I., Fernandez, L.A., Morse, S.S., Fortune, K.L., Taylor, K.J.W., "Detection of neovascular signals in a 3 day Walker 256 rat carcinoma by CW Doppler ultrasound," *Ultrasound Med Biol,* **14,** 123, 1988.
102. Shimamoto, K., Sakuma, S., Ishigaki, T., Makino, N., "Intratumoral blood flow: evaluation with color Doppler echography," *Radiol,* **165,** 683, 1987.
103. Pedersen, P.C., Abraham, V.P., West, F.W., Reid, J.M., "Breast tumor detection with Doppler ultrasound under reduced ambient pressure," *Proc Ninth Ann Conf IEEE Eng Med Biol Soc,* **3,** 1687, 1987.
104. Dymling, S.O., Persson, H.W., Hertz, C.H., "Measurement of blood perfusion in tissue using Doppler ultrasound," *Ultrasound Med Biol,* **17,** 433, 1991.
105. Eriksson, R., Persson, H.W., Dymling, S.O., Lindstrom, K., "Evaluation of Doppler ultrasound for blood perfusion measurements," *Ultrasound Med Biol,* **17,** 445, 1991.
106. Berson, M., Patat, F., Wang, Z.Q., Besse, D., Pourcelot, L., "Very high frequency pulsed Doppler apparatus," *Ultrasound Med Biol,* **15,** 121, 1989.
107. Cooperberg, E., "Ultrasound Doppler spectral analysis in the diagnosis of occlusive lesions of the carotid arteries," *Ultrasound Med Biol,* **18,** 421, 1992.
108. Shortland, A.P., Cochrane, T., "Doppler spectral waveform generation in vitro: an aid to diagnosis of vascular disease," *Ultrasound Med Biol,* **15,** 737, 1989.
109. Mo, L.Y.L., Yun, L.C.M., Cobbold, R.S.C., "Comparison of four digital maximum frequency estimators for Doppler ultrasound," *Ultrasound Med Biol,* **14,** 355, 1988.
110. Sigel, B, Gibson, R.J., Amatneek, K.V., Felix, W.R. Jr., Edelstein, A.L., Popky, G.L., "A Doppler ultrasound method for distinguishing laminar from turbulent flow," *J Surg Res,* **10,** 221, 1970.
111. Kikkawa, S., Yamaguchi, T., Tanishita, K., Sugawara, M., "Spectral broadening in ultrasonic Doppler flowmeters due to unsteady flow," *IEEE Trans Biomed Eng,* **34,** 388, 1987.
112. Thompson, R.S., Trudinger, B.J., "Doppler ultrasound velocity waveform analysis," *Australasian Phys Eng Sci Med,* **10,** 183, 1987.
113. Wijn, P.F., Van der Sar, P., Gootzen, T.H.J.M., Tilmans, M.H.J., Skotnicki, S.H., "Value of the spectral broadening index in continuous wave Doppler measurements," *Med Biol Eng Comput,* **25,** 377, 1987.
114. Sillesen, H., Bitsch, K., Steenberg, H.J., Schroeder, T., Hansen, L., Hansen, H.J.B., "The clinical use of objective quantification of flow disturbance in carotid artery disease: correlation between spectral broadening index and arteriography," *Ultrasound Med Biol,* **13,** 519, 1987.
115. Kasai, C., Namekawa, K., "Real-time two-dimensional blood flow imaging using ultrasound Doppler," *Jpn J Appl Phys Suppl,* **26,** 9, 1987.
116. Reid, J.M., "Doppler Ultrasound," *IEEE Eng Med Biol Mag,* 14, 1987.

117. Hutchison, K.J., Karpinski, E., "Stability of flow patterns in the In vivo post-stenotic velocity field," *Ultrasound Med Biol,* **14,** 269, 1988.
118. Sheldon, C.D., Murie, J.A., Quin, R.O., "Ultrasonic Doppler spectral broadening in the diagnosis of internal carotid artery stenosis," *Ultrasound Med Biol,* **9,** 575, 1983.
119. Talukder, N., Fulenwider, J.T., Mabon, R.F., Giddens, D.P., "Poststenotic flow disturbance in the dog aorta as measured with pulsed Doppler ultrasound," *Trans ASME J Biomech Eng,* **108,** 259, 1986.
120. Khalifa, A.M.A, Giddens, D.P., "Analysis of disorder in pulsatile flows with application to poststenotic blood velocity measurement in dogs," *J Biomech,* **11,** 129, 1978.
121. Jones, S.A., Fronek, A., "Analysis of Break Frequencies Downstream of a Constriction in a Cylindrical Tube," *J Biomech,* **20,** 319, 1987.
122. Brody, W.R., Meindl, J.D., "Theoretical analysis of the CW Doppler ultrasonic flowmeter," *IEEE Trans Biomed Eng,* **21,** 183, 1974.
123. Ahmed S.A., Giddens, D.P., "Pulsatile poststenotic flow studies with laser Doppler anemometry," *J Biomech,* **17,** 695, 1984.
124. Lieber, B.B., Giddens, D.P., "Post-stenotic core flow behavior in pulsatile flow and its effect on wall shear stress," *J Biomech,* **23,** 597, 1990.
125. Jones, S.A., Fronek, A., "Effects of vibration on steady flow downstream of a stenosis," *J Biomech,* **21,** 903, 1988.
126. Kitney, R.I., Talhami, H., Giddens, D.P., "The analysis of blood velocity measurements by autoregressive modelling," *J Theoretical Biol,* **120,** 419, 1986.
127. Papoulis, A., "Probability, Random Variables, and Stochastic Processes," McGraw-Hill, New York, 1965.
128. Morita, I., Fujiwara, T., Katsumura, T., Kajiya, F., Tsujioka, K., Ogasawara, Y., Jones, S.A., "Analysis of blood flow microstructure as the origin of intimal thickening at end-to-side anastomosis of vascular grafting to femoral artery," *J Jpnese College Angiol,* **32,** 1992.
129. Rinaldi, J.E., Smith, S.W. Harris, G., Walker, C., " *In vivo* ultrasonic imaging of flow patterns in a left ventricular assist device," *Proc Ann Internat Conf IEEE Eng Med Biol Soc,* 556, 1988.
130. Atkinson, P., Woodcock, J.P., "Doppler Ultrasound and its Clinical Uses," Academic, New York, 1982.
131. Hatle, L., Angelsen, B., "Doppler Ultrasound in Cardiology: Physical Principles and Clinical Applications," Lea and Febiger, Philadelphia, PA, 1982.
132. Wells, P.N.T., "Physical Principles of Ultrasonic Diagnosis," Academic Press, New York, 1969.
133. Goldberg, B.B., Kotler,M.N., Ziskin, M.C., Waxham, B.A., "Diagnostic Uses of Ultrasound," Grune and Stratton, New York, 1975.
134. Hussey, M., "Basic Physics and Technology of Medical Diagnostic Ultrasound," Elsevier Science Publishing Co., Inc., New York, 1985.
135. Hussey, M., "Diagnostic Ultrasound," Blackie and Son, Limited, London, 1975.
136. Evans, D.H., McDicken, W.N., Skidmore, R., Woodcock, J.P., "Doppler Ultrasound," Wiley, New York, 1989.
137. Doppler, C.J., "Über das farbige Licht der Doppelsterne und einiger anderer Gestirne des Himmels (On the colored light of the double stars and certain other stars of the heavens)," *Abh. Königlich Böhmischen Ges. Wiss.,* **2,** 467-482, 1842.

138. White, D.N., "Johann Christian Doppler and his effect -- A brief history," *Ultrasound Med Biol,* **8,** 583, 1982.
139. Jonkman, E.J., "An historical note: Doppler research in the nineteenth century," *Ultrasound Med Biol,* **6,** 1, 1980.
140. Pasquale, M., Paulshock, B.Z., "Christian Doppler (1803-1853): An ingenious theory, an important effect," *J Lab Clin Med,* **118,** 384, 1991.
141. Halliday, D., Resnik, R., "Fundamentals of Physics," John Wiley & Sons, New York, 1981.
142. Newhouse, V.L., Amir, I., "Time dilation and inversion properties and the output spectrum of pulsed Doppler flowmeters," *IEEE Trans Sonics Ultrason,* **30,** 174, 1983.
143. Forsberg, F., Jorgensen, M.O., "Sampling technique for an ultrasound Doppler system," *Med Biol Eng Comput,* **27,** 207, 1989.

144. Jones, S.A., Giddens, D.P., "A simulation of transit time effects in Doppler ultrasound signals," *Ultrasound Med Biol,* **16,** 607, 1990.
145. Wendling, F., Jones, S.A., Giddens, D.P., "Simulation of Doppler ultrasound signals for a laminar, pulsatile, nonuniform flow," *Ultrasound Med Biol,* **18,** 179, 1992.
146. V.L. Newhouse, Ed., "Progress in Medical Imaging," Springer, New York, 1988.
147. Phillips, D.J., Beach, K.W., Primozich, J., Strandness, D.E., Jr., "Should results of ultrasound Doppler studies be reported in units of frequency or velocity?," *Ultrasound Med Biol,* **15,** 205, 1989.
148. D.N. Ku, D.P. Giddens, D.J. Phillips , D.E. Strandness, Jr., "Hemodynamics of the normal human carotid bifurcation: In vitro and in vivo studies," *Ultrasound Med Biol,* **11,** 13, 1985.
149. Barber, F.E., Baker, D.W., Strandness, D.E. Jr., Mahler, G.D., "Duplex Scanner II," *ULTSYM Proc,* 1974.
150. Newhouse, V.L., Furgason, E.S., Johnson, G.F., Wolf, D.A., "The dependence of ultrasound Doppler bandwidth on beam geometry," *IEEE Trans Sonics Ultrason,* **27,** 50, 1980.
151. Kinsler, L.E., Frey, A.R., Coppens, A.B., Sanders,, J.V., "Fundamentals of Acoustics," Wiley & Sons, Inc., New York, 1982.
152. Wells, P.N.T., "Ultrasonic Doppler equipment," in *Medical Physics of CT and Ultrasound: Tissue Imaging and Characterization,* Gary D. Fullerton and James A. Zagzebski, Eds., American Institute of Physics, New York, 1980.
153. Hoeks, A.P.G., Hennerici, M., Reneman, R.S., "Spectral composition of Doppler signals," *Ultrasound Med Biol,* **17,** 751-760, 1991.
154. Fish, P.J., "Nonstationarity broadening in pulsed Doppler spectrum measurements," *Ultrasound Med Biol,* **17,** 147-155, 1991.
155. Brown, T.D., Bell, L.D., Pedersen, D.R., Blair, W.F., "A three-dimensional computational simulation of some sources of measurement artifact in microvascular pulsed ultrasound Doppler velocimetry," *Trans ASME, J Biomech Eng,* **107,** 274, 1985.
156. Cobbold, R.S.C., Veltink, P.H., Johnston, K.W., "Influence of beam profile and degree of insonation on the CW Doppler ultrasound spectrum and mean velocity," *IEEE Trans Sonics Ultrasonics,* **30,** 364, 1983.

157. Law, Y.F., Bascom, K.W., Johnston, K.W., Vaitkus, P., Cobbold, R.S.C., "Experimental study of the effects of pulsed Doppler sample volume size and position on the Doppler spectrum," *Ultrasonics,* **29,** 404, 1991.
158. Jorgensen, J.E., Garbini, J.L., "An analytical procedure of calibration for the pulsed ultrasonic Doppler flow meter," *Trans ASME, J Fluids Eng,* 158, 1974.
159. Bascom, P.A.J., Cobbold, R.S.C., "Effects of transducer beam geometry and flow velocity profiles on the Doppler power spectrum: A theoretical study," *Ultrasound Med Biol,* **16,** 279, 1990.
160. Evans, J.M., Beard, J.D., Skidmore, R., Horrocks, M., "An analogue mean frequency estimator for the quantitative measurement of blood flow by Doppler ultrasound," *Clin Phys Physiol Meas,* **8,** 309, 1987.
161. Angelsen, B.A.J., "A theoretical study of the scattering of ultrasound from blood," *IEEE Transacations Biomed Eng,* **27,** 61, 1980.
162. Shung, K.K., Sigelmann, R.A., Reid, J.M., "Scattering of ultrasound by blood," *IEEE Trans Biomed Eng,* **23,** 460, 1976.
163. Borders, S.E., Fronek, A., Kemper, W.S., Franklin, D., "Ultrasonic energy backscattered from blood, An experimental determination of the variation of sound energy with hematocrit," *Annals Biomed Eng,* **6,** 83, 1978.
164. Shung, K.K., Yuan, Y.W., Fei, D.Y., Tarbell, J.M., "Effect of flow disturbance on ultrasonic backscatter from blood," *J Acoust Soc Am,* **75,** 1265, 1984.
165. Shung, K.K., "On the ultrasound scattering from blood as a function of hematocrit," *IEEE Trans Sonics Ultrason,* **29,** 327, 1982.
166. Routh, H.F., Gough, W., Williams, R.P., "One-dimensional computer simulation of a wave incident on randomly distributed inhomogeneities withy reference to the scattering of ultrasound by blood," *Med Biol Eng Comput,* **25,** 667, 1987.
167. Mo, L.Y.L, Cobbold, R.S.C., "A stochastic model of the backscattered Doppler ultrasound from blood," *IEEE Trans Biomed Eng,* **33,** 20, 1980.
168. Mo, L.Y.L., Cobbold, R.S.C., "A unified approach to modeling the backscattered Doppler ultrasound from blood," *IEEE Trans Biomed Eng,* **39,** 450, 1992.
169. Sigel, B., Machi, J., Beitler, J., Justin, J.R., "Red cell aggregation as a cause of blood-flow echogenicity," *Radiology,* **148,** 799, 1983.
170. Kadaba, M.P., Bhagat, P.K., Wu, V.C., "Attenuation and backscattering of ultrasound in freshly excised animal tissues," *IEEE Trans Biomed Eng,* **27,** 76, 1980.
171. Round, W.H., Bates, R.T.H.., "Modification of spectra of pulses from ultrasonic transducers by scatterers in non-attenuating and in attenuating media," *Ultrasonic Imaging,* **9,** 18, 1987.
172. Newhouse, V.L., Ehrenwald, A.R., Johnson, G.F., "The effect of Rayleigh scattering and frequency dependent absorption on the output spectrum of Doppler blood flowmeters," *Ultrasound Med Biol/San Francisco Meeting Am Inst for Ultrason Medicine,* **3B,** 1181, 1977.
173. Holland, S.K., Orphanoudakis, S.C., Jaffe, C.C., "Frequency dependent attenuation effects in pulsed Doppler ultrasound: Experimental results," *IEEE Trans Biomed Eng,* **31,** 626, 1984.
174. Gilson, W.H., Schultheiss, P., Tuteur, F., Holland, S.K., "Error bounds on Doppler ultrasound blood flow measurements," *Proc Twelfth Ann Northeast Bioeng Conf,* 253, 1986.

175. Embree, P.M., O'Brien, W.D., Jr., "Pulsed Doppler accuracy assessment due to frequency-dependent attenuation and Rayleigh scattering error sources," *IEEE Trans Biomed Eng,* **37,** 322, 1990.
176. O'Donnell, M., Jaynes, E.T., Miller, J.G., "Kramers-Kronig relationship between ultrasonic attenuation and phase velocity," *J Acoust Soc Am,* **69,** 696, 1981.
177. Fish, P.J., Cope, J.A., "Effect of frequency dependent processes on pulsed Doppler sample volume," *Ultrasonics,* **29,** 275, 1991.
178. Kak, A.C., Dines, K.A., "Signal processing of broadband pulsed ultrasound: Measurement of attenuation of soft biological tissues," *IEEE Trans Biomed Eng,* **25,** 321, 1978.
179. Oates, C.P., "Towards an ideal blood analogue for Doppler ultrasound phantoms," *Phys Med Biol,* **36,** 1433, 1991.
180. Thompson, R.S., Aldis, G.K., Linnett, I.W., "Doppler ultrasound spectral power density distribution: measurement artifacts in steady flow," *Med Biol Eng Comput,* **28,** 60, 1990.
181. Kremkau, F.W., Taylor, K.J.W, "Artifacts in ultrasound imaging," *J Ultrasound Med,* **5,** 227, 1986.
182. Jones, S.A., Leclerc, H., Scott, N.A., "Influence of Acoustic Impedance Mismatch on Intracoronary Doppler Flow Velocity Spectra," *ASME/AICHE/ASCE Summer Bioeng Conf,* Breckenridge, Colorado, June, 25-29, 1993..
183. Poots, J.K., Johnston, K.W., Cobbold, R.S.C., Kassam, M., "Comparison of CW Doppler ultrasound spectra with the spectra derived from a flow visualization model," *Ultrasound Med Biol,* **12,** 125, 1986.
184. Wilson, L.S., "Description of broad-band pulsed Doppler ultrasound processing using the two-dimensional Fourier transform," *Ultrasonic Imaging,* **13,** 301, 1991.
185. Kim, Y.M., Park, S.B., "Modeling of Doppler signal considering sample volume and field distribution," *Ultrasonic Imaging,* **11,** 175, 1989.
186. Newhouse, V.L., Bendick, P.J., Varner, L.W., "Analysis of transit time effects on Doppler flow measurement," *IEEE Trans Biomed Eng,* **23,** 381, 1976.
187. Censor, D., Newhouse, V.L., Vontz, T., Ortega, H.V., "Theory of ultrasound Doppler-spectra velocimetry for arbitrary beam and flow configurations," *IEEE Trans Biomed Eng,* **35,** 740, 1988.
188. Newhouse, V.L., Censor, D., Vontz, T., Cisneros, J.A., Goldberg, B.B., "Ultrasound Doppler probing of flows transverse with respect to beam axis," *IEEE Trans Biomed Eng,* **34,** 779, 1987.
189. Newhouse, V.L., Varner, W., Bendick, P.J., "Geometrical spectrum broadening in ultrasonic Doppler systems," *IEEE Trans Biomed Eng,* **24,** 478, 1977.
190. George, W.K., Lumley, J.L., "The laser-Doppler velocimeter and its application to the measurement of turbulence," *J Fluid Mech,* **60,** 321, 1973.
191. Newhouse, V.L., Furgason, E.S., Ho, C.T., "A technique for increasing the range-velocity product of pulsed Doppler systems," in *Ultrasound Med,* **4,** Plenum, New York, 355, 1978.
192. Altes, R.A., "Suppression of radar clutter and multipath effects for wide-band signals," *IEEE Trans Information Theory,* **17,** 344, 1971.
193. Helstrom, C., "An introduction to signal and system analysis," Holden-Day, Inc., San Francisco, 1978.

194. Green, P.S., "Spectral broadening of acoustic reverberation in Doppler-shift fluid flowmeters," *J Acoust Soc Am,* **36,** 1383, 1964.
195. Edwards, R.V., Angus, J.C., French, M.J., Dunning, J.W. Jr., "Spectral analysis of the signal from the laser Doppler flowmeter: time-independent systems," *J Appl Phys,* **42,** 837, 1971.
196. Ata, O.W., Fish, P.J., "Effect of deviation from plane wave conditions on the Doppler spectrum from an ultrasonic blood flow detector," *Ultrasonics,* **29,** 395, 1991.
197. Censor, D., Newhouse, V.L., "Theory of ultrasound Doppler-spectra velocimetry for arbitrary beam and flow configurations," *IEEE 1986 Ultrason Symp Proc,* 923, **2,** 1986.
198. Censor, D., Newhouse, V.L., "Generalized Doppler effect: coherent and incoherent spectra," *J Acoust Soc Am,* **83,** 2012, 1988.
199. Newhouse, V.L., Reid, J.M., "Invariance of Doppler bandwidth with flow axis displacement," *IEEE 1990 Ultrason Symp Proc,* 1533, **3,** 1990.
200. Tortoli, P., Guidi, G., Mariotti, V., Newhouse, V.L., "Experimental proof of Doppler bandwidth invariance," *IEEE Trans Ultrason, Ferroelect, Freq Control,* **39,** 196,
201. Morse, Ingard, "Theoretical Acoustics," McGraw-Hill, New York, 381, 1968.
202. Censor, D., Le Vine, D.M., "The Doppler effect: Now you see it, now you don't," *J Math Phys,* **25,** 309, 1984.
203. Adrian, R.J., "Laser velocimetry," in *Fluid Mechanical Measurements,* R.J. Goldstein, Eds., Hemisphere Publishing Corp, 155, 1983.
204. Sigelmann, R.A., Reid, J.M., "Analysis and measurement of ultrasound backscattering from an ensemble of scatterers excited by sine-wave bursts," *J Acoust Soc Am,* **53,** 1351, 1973.
205. Atkinson, P., Berry, M.V., "Random noise in ultrasonic echoes diffracted by blood," *J Phys A: Math Nucl Gen,* **7,** 1293, 1974.
206. Kristoffersen, K., Angelsen, B.A.J., "A time-shared ultrasound Doppler measurement and 2-D imaging system," *IEEE Trans Biomed Eng,* **35,** 285, 1988.
207. Sheldon, C.D., Duggen, T.C., "Low-cost Doppler signal simulator," *Med Biol Eng Comput,* **25,** 226, 1987.
208. Sirmans, D., Bumgarner, W., "Numerical comparison of five mean frequency estimators," *J Appl Meteorol,* **14,** 991, 1975.
209. Mo, L.Y.L., Cobbold, R.S.C., ""Speckle" in continuous wave Doppler ultrasound spectra: a simulation study," *IEEE Trans Ultrason, Ferroelectr, Freq Control,* **UFFC-33,** 747, 1986.
210. VanLeeuwen, G.H., Hoeks, A.P.G., Reneman, R.S., "Simulation of real-time frequency estimators for pulsed Doppler systems," *Ultrasonic Imaging,* **8,** 252, 1986.
211. Mo, L.Y.L., Cobbold, R.S.C., "A nonstationary signal simulation model for continuous wave and pulsed Doppler ultrasound," *IEEE Trans Ultrasound, Ferroelec Freq Control,* **36,** 522, 1989.
212. Talhami, H.E., Kitney, R.I., "Maximum likelihood frequency tracking of the audio pulsed Doppler ultrasound signal using a Kalman filter," *Ultrasound Med Biol,* **14,** 599, 1988.
213. Olinger, M., Siegel, M., "A simulation study and theoretical comparison of various processing techniques used in ultrasonic bloodflow measurement," *Ultrasonic Imaging,* **3,** 294, 1981.

214. Bonnefous, O., Pesquè, P., "Time domain formulation of pulse-Doppler ultrasound and blood velocity estimation by cross correlation," *Ultrason Imaging,* **8,** 73, 1986.
215. Azimi, M., Kak, A.C., "An analytical study of Doppler ultrasound systems," *Ultrasonic Imaging,* **7,** 1, 1985.
216. Kerr, A.T., Hunt, J.W., "A method for computer simulation of ultrasound Doppler color flow images -- I. Theory and numerical method," *Ultrasound Med Biol,* **18,** 861, 1992.
217. Kerr, A.T., Hunt, J.W., "A method for computer simulation of ultrasound Doppler color flow images -- II. Simulation results," *Ultrasound Med Biol,* **18,** 873, 1992.
218. McGillem, C.D., Cooper, G.R., Waltman, W.B., "Use of wide-band stochastic signals for measuring range and velocity," *EASCON Conf Record,* 305, 1969.
219. Bendick, P.J., Newhouse, V.L., "Ultrasonic random-signal flow measurement system," *J Acoust Soc Am,* **56,** 860, 1974.
220. Jewtha, C.P., Kaveh, M., Cooper, G.R., Saggio, F., "Blood flow measurements using ultrasonic pulsed random signal Doppler System," *IEEE Trans Sonics Ultrason,* **22,** 1, 1975.
221. Newhouse, V.L., Cathignol, D., Chapelon, J.Y., "Introduction to ultrasonic pseudorandom code systems," in *Progress in Medical Imaging,* V.L. Newhouse, Eds., Springer, New York, 215-226, 1988.
222. Shiozaki, A., Senda, S., Kitabatake, A., Inoue, M., Matsuo, H., "A new modulation method with range resolution for ultrasonic Doppler flow sensing," *Ultrasonics,* **17,** 269, 1979.
223. Cathignol, D.J., Fourcade, C., Chapelon, J., "Transcutaneous blood flow measurements using a pseudorandom noise Doppler system," *IEEE Trans Biomed Eng,* **27,** 30, 1980.
224. Chen, J., Wan, M., "On increasing signal-to-clutter ratio of pseudorandom ultrasound Doppler system," *Proc Ann Internat Conf IEEE Eng Med Biol Soc,* 464, **1,** 1988.
225. Cathignol, D.J., "Signal-to-clutter ratio in pseudo random Doppler flowmeter," *Ultrasonic Imaging,* **8,** 272, 1986.
226. Wilhjelm, J.E., Pedersen, P.C., "Coherent FM Doppler system," *Proc IEEE 1986 Ultrason Symp,* 903, 1986.
227. Wilhjelm, J.E., Pedersen, P.C., "FM Doppler systems -- Experimental results," *Proc IEEE 1990 Ultrason Symp,* 1553, 1990.
228. Pedersen, P.C., Wilhjelm, J.E., Fox, M.D., Epstein, M.A.F., Davis, R.B., Alward, T.M., "Ultrasound Doppler system with swept frequency excitation," *Proc 1991 IEEE Seventeenth Ann Northeast Bioeng Conf,* 237, 1991.
229. Holland, S.K., Orphanoudakis, S.C., "Estimation of blood flow parameters using pulse Doppler ultrasound with corrections for spectral broadening," *Proc Twelfth Ann Northeast Bioeng Conf,* 249, 1986.
230. Zrinc, D.S., "Spectral moment estimates from correlated pulse pairs," *IEEE Trans Aerospace Electron Syst,* **13,** 344, 1977.
231. Gilson, W., Orphanoudakis, S., "Error bounds for wide-band high resolution Doppler ultrasound blood flow measurement," *Proc Ann Internat Conf IEEE Eng Med Biol Soc,* 473, 1988.

232. McLeod, F.D., "Multichannel pulse Doppler techniques," in *Cardiovascular Applications of Ultrasound,* Renemann, R.S., Eds., North-Holland/American Elsevier, Amsterdam, 85, 1974.
233. McLeod, F.D., Anliker, M., "A multiple gate pulsed directional Doppler flowmeter," *Proc IEEE Ultrason Symp,* Miami, Florida, December, 1971.
234. Casty, M., Giddens, D.P., "25 + 1 Channel pulsed ultrasound Doppler velocity meter for quantitative flow measurements and turbulence analysis," *Ultrasound Med Biol,* **10,** 161, 1984.
235. Kim, Y.K., "A study on a multichannel (128) ultrasound pulsed Doppler system with serial data processing for sensing the blood flow," *J Korea Inst Electron Eng,* **23,** 389, 1986.
236. Reneman, R.S., Van Merode, T., Hick, P., Hoeks, A.P.G., "Cardiovascular applications of multi-gate pulsed Doppler systems," *Ultrasound Med Biol,* **12,** 357, 1986.
237. Greenleaf, J.F., Sehgal, C.M., "Biologic system evaluation with ultrasound," Springer-Verlag, New York, 88-92, 1992.
238. Mitchell, D.G., "Color Doppler imaging: principles, limitations, and artifacts," *Radiol,* **177,** 1, 1990.
239. Barber, W.D., Eberhard, J.W., Karr, S.G., "A new time domain technique for velocity measurements using Doppler ultrasound," *IEEE Trans Biomed Eng,* **32,** 213, 1985.
240. Tortoli, P., Andreuccetti, F., Manes, G., Atzeni, C., "Blood flow images by a SAW-based multigate Doppler system," *IEEE Trans Ultrason, Ferroelec Freq Control,* **35,** 545, 1988.
241. Goldman, M.E., "Real-time two-dimensional Doppler flow imaging: A word of caution," *J Am Coll Cardiol,* **7,** 89, 1986.
242. Cormack, A.M., "Representation of a function by its line integrals, with some radiological applications," *J Appl Phys,* **34,** 2722, 1963.
243. Beylkin, G., "Discrete radon transform," *IEEE Trans Acoust, Speech, Signal Processing,* **35,** 162, 1987.
244. Greenleaf, J.F., Ylitalo, "Doppler Tomography," *Proc IEEE 1986 Ultrason Symp,* 837, 1986.
245. Schmolke, J.K., Ermert, H., "Ultrasound pulse Doppler tomography," *IEEE 1988 Ultrason Symp Proc,* 785, **2,** 1988.
246. Schmolke, J, Ermert, H, "Tomographic two-dimensional pulsed Doppler imaging," *Ultrasonic Imaging,* **9,** 46, 1987.
247. Guler, I., "A method determining the Doppler angle in pulsed Doppler flowmeters," *IEEE Eng Med Biol 10th Ann Internat Conf,* 227, 1988.
248. Newhouse, V.L., Cathignol, D., Chapelon, J.Y., "Vector flow estimation with transverse Doppler," *IEEE Ultrasound Symp, Orlando, FL,* 1991.
249. Daigle, R.E., Miller, C.W., Histand, M.B., McLeod, F.D., Hokanson, D.E., "Nontraumatic aortic blood flow sensing by use of an ultrasonic esophageal probe," *J Appl Physiol,* **38,** 1153, 1975.
250. Fox, M.D., Gardiner, W.M., "Three-dimensional Doppler velocimetry of flow jets," *IEEE Trans Biomed Eng,* **35,** 834, 1988.
251. Fox, M.D., "Solution to the three dimensional Doppler equation: experimental verification," *Proc Ninth Ann Conf IEEE Eng Med Biol Soc,* 408, **1,** 1987.

252. Fox, M.D., Foster, K.R., "True volume flow measurement with multiple beam ultrasound Doppler," *Proc Thirteenth Ann Northeast Bioeng Conf,* 357, **2,** 1987.
253. Ashrafzadeh, A., Cheung, J.Y., Dormer, K.J., "Analysis of velocity estimation error for a multidimensional Doppler ultrasound system," *IEEE Trans Ultrason, Ferroelec Freq Control,* **35,** 536, 1988.
254. Tamura, T., Cobbold, R.S.C., Johnston, K.W., "Determination of 2-D velocity vectors using color Doppler ultrasound," *IEEE 1990 Ultrason Symp Proc,* 1537, **3,** 1990.
255. Furuhata, H, Kanno, R, Kodaira, K, Fujishiro, K, Hayashi, J, Matsumoto, H, Yoshimura, S, "An ultrasonic quantitative blood flow measuring system to measure the absolute volume flow rate," *Proc 12th Internat Conf Med Biol Eng,* 9, 1979.
256. Overbeck, J.R., Beach, K.W., Strandness, D.E., Jr., "Vector Doppler: accurate measurement of blood velocity in two dimensions," *Ultrasound Med Biol,* **18,** 19, 1992.
257. Dotti, D., Lombardi, R., Piazzi, P., "Vectorial measurement of blood velocity by means of ultrasound," *Med Biol Eng Comput,* **30,** 219-225, 1992.
258. Hottinger, CF, Meindl, JD, "Blood flow measurement using the attenuation-compensated volume flowmeter," *Ultrasonic Imaging,* **1,** 1, 1979.
259. Dotti, D, Gatti, E, Svelto, V, Ugge, A, Vidali, P, "Blood flow measurement by ultrasound correlation techniques," *Energia Nucleare,* **23,** 571, 1976.
260. Bassini, M, Dotti, D, Gatti, E, Pizolati, P, Svelto, V, "An ultrasonic non-invasive blood flowmeter based on cross-correlation techniques," *Ultrason Int Proc,* 1979.
261. Bassini, M, Gatti, E, Longo, T, Martinis, G, Pignoli, P, Pizzolati, P, " In vivo recording of blood velocity profiles and studies in vitro of profile alterations induced by known stenoses," *Texas Heart Inst J,* **9,** 185, 1982.
262. Bonnefous, O, Pesquè, P, Bernard, X, "A new velocity estimator for color flow mapping," *IEEE Ultrason Symp,* 1986.
263. Foster, S.G., Embree, P.M., O'Brien, W.D., "Flow velocity profile via time-domain correlation: Error analysis and computer simulation," *IEEE Trans Ultrason, Ferroelec, Freq Control,* **37,** 164, 1990.
264. Embree, P.M., O'Brien, W.D., "Volumetric blood flow via time-domain correlation: Experimental verification," *IEEE Trans Ultrason, Ferroelec, Freq Control,* **37,** 176, 1990.
265. Trahey, G.E., Hubbard, S.M., von Ramm, O.T., "Angle independent ultrasonic blood flow detection by frame-to-frame correlation of B-mode images," *Ultrasonics,* **26,** 271, 1988.
266. Mayo, W.T., Embree, P.M., "Two dimensional processing of pulsed Doppler signals," U.S. Patent no. 4,930,513.
267. Ferrara, K.W., Algazi, V.R., "A new wideband spread target maximum likelihood estimator for blood velocity estimation - Part I: Theory," *IEEE Trans Sonics Ultrason,* **38,** 1, 1991.
268. Ferrara, K.W., Algazi, V.R., "A new wideband spread target maximum likelihood estimator for blood velocity estimation - Part II: Evaluation," *IEEE Trans Sonics Ultrason,* **38,** 17, 1991.
269. Lee, F., Jr., Bronson, J.P., Lerner, R.M., Parker, K.J., Sung-Rung Huang, Roach, D.J., "Sonoelasticity imaging: results in in vitro tissue specimens," *Radiol,* **181,** 237, 1991.

270. Tristam, M., Barbosa, D.C., Cosgrove, D.O., Nassiri,, "Soft tissue movement information in ultrasonic M-mode images," *Acoust Imaging Proc 14th Internat Symp,* 771, 1985.
271. Flax, S.W., Webster, J.G., Updike, S.J., "Statistical evaluation of the Doppler ultrasonic blood flowmeter," *Biomed Sci Instrumen,* **7,** 201, 1970.
272. Jorgensen, J.E., Campau, D.N., Baker, D.W., "Physical characteristics and mathematical modelling of the pulsed ultrasonic flowmeter," *Med Biol Eng,* 404, 1973.
273. Reneman, R.S., Hoeks, A.P.G., "Doppler ultrasound -- principle, advantages and limitations," in *Doppler Ultrasound in the Diagnosis of Cerebrovascular Disease,* R.S. Reneman and A.P.G. Hoeks, Eds., Research Studies Press, Chichester, New York, Brisbane, Toronto, Singapore, 1982.
274. Baker, D.W., Lorch, G., Rubenstein, S., "Pulsed Doppler echochardiography," in *Echocardiology,* N. Bom, Eds., Martinus Nijhoff, The Hague, Netherlands, 1977.207,
275. Burkhardt, C.B., "Comparison between spectrum and time interval histogram of ultrasound Doppler signals," *Ultrasound Med Biol,* **7,** 79, 1981.
276. Gill, R.W., "Performance of the mean frequency Doppler modulator," *Ultrasound Med Biol,* **5,** 237, 1979.
277. Johnston,K.W., Maruzzo, B.C., Cobbold,R.S.C., "Inaccuracies of a zero-crossing detector for recording Doppler signals," *Surg Forum,* **28,** 201, 1977.
278. Blackshear, W.M., Phillips, D.J., Thiele, B.L., Hirsch, J.H., Chikos, P.M., Marinelli, M.R., Ward, K.J., Strandness, D.E., "Detection of carotid occlusive disease by ultrasonic imaging and pulsed Doppler spectrum analysis," *Surgery,* **86,** 698, 1979.
279. Rittgers, S.E., Putne, W.W., Barnes, R.W., "Real-time spectrum analysis and display of directional Doppler ultrasound blood velocity signals," *IEEE Trans Biomed Eng,* **27,** 723, 1980.
280. Goldberg, S.J., Sahn, D.J., Allen, H.D., Valdes-Cruz, L.M., Hoenecke, H., Carnahan, Y., "Evaluation of pulmonary and systemic blood flow by 2-dimensional Doppler echocardiology using fast Fourier transform spectral analysis," *Am J Cardiol,* **50,** 1394, 1982.
281. Voyles, W.F., Altobelli, S.A., Fisher, D.C., Greene, E.R., "A comparison of digital and analog methods of Doppler spectral analysis for quantifying flow," *Ultrasound Med Biol,* **11,** 727, 1985.
282. Cote, G.L., Fox, M.D., "Comparison of zero crossing counter to FFT spectrum of ultrasound Doppler," *IEEE Trans Biomed Eng,* **35,** 498, 1988.
283. Kay, S.M., Marple, S.L. Jr., "Spectrum analysis - A modern perspective," *Proc IEEE,* **69,** 1380, 1981.
284. Vaitkus, P.J., Cobbold, R.S.C., "A comparative study and assessment of Doppler ultrasound spectral estimation techniques. I. Estimation methods," *Ultrasound Med Biol,* **14,** 661, 1988.
285. Burg, J.P., "Maximum entropy spectral analysis," *PhD Dissertation, Stanford University,* Stanford, California, 1975.
286. Marple, L., "A new autoregressive spectrum analysis algorithm," *IEEE Trans Acoust, Speech, Sig Proc,* **28,** 441, 1980.
287. Barrodale, I., Delves, L.M., Erickson, R.E., Zala, C.A., "Computational experience with Marple's algorithm for autoregressive spectrum analysis," *Geophysics,* **48,** 1274, 1983.

288. Hsu, F.M., Giordano, A.A., "Line tracking using autoregressive spectral estimates," *IEEE Trans Acoust Speech Signal Processing,* **25,** 510, 1977.
289. Kay, S.M., "Comments on `Line tracking using autoregressive spectral estimates'," *IEEE Trans Acoust, Speech Sig Proc,* **28,** 475, 1980.
290. Thorvaldsen, T., "A comparison of the least squares method and the Burg method for autoregressive spectral analysis," *IEEE Trans Antennas Propagation,* **29,** 675, 1981.
291. Shon, S., Mehrotra, K., "Performance comparison of autoregressive estimation methods," *IEEE Internat Conf Acoust, Speech, Sig Proc,* **1,** 14.3/1, 1984.
292. Kaluzynski, K., "Analysis of application possibilities of autoregressive modelling to Doppler blood flow signal spectral analysis," *Med Biol Eng Comput,* **25,** 373, 1987.
293. Vaitkus, P.J., Cobbold, R.S.C., Johnston, K.W., "A comparative study and assessment of Doppler ultrasound spectral estimation techniques. II. Methods and results," *Ultrasound Med Biol,* **14,** 673, 1988.
294. David, J.-Y., Jones, S.A., Giddens, D.P., "Modern spectral analysis techniques for blood flow velocity and spectral measurements with pulsed Doppler ultrasound," *IEEE Trans Biomed Eng,* **38,** 589, 1991.
295. Musicus, B.R., "Fast MLM power spectrum estimation from uniformly spaced correlations," *IEEE Trans Acoust, Speech Sig Proc,* **33,** 1333, 1985.
296. Jones, S.A., Giddens, D.P., "Effects of Doppler ultrasound device parameters on the behavior of spectral analysis models," *Proc 1991 Biomech Symp, ASME Summer Appl Mech Biomechanics Meeting,* Columbus, Ohio, June 16-19, 1991.
297. Schlindwein, F.S., Evans, D.H., "A real-time autoregressive spectrum analyzer for Doppler ultrasound signals," *Ultrasound Med Biol,* **15,** 263, 1989.
298. Schlindwein, F.S., Evans, D.H., "Selection of the order of autoregressive models for spectral analysis of Doppler ultrasound signals," *Ultrasound Med Biol,* **16,** 81, 1990.
299. Kaluzynski, K., "Order selection in Doppler blood flow signal spectral analysis using autoregressive modelling," *Med Biol Eng and Comput,* **27,** 89, 1989.
300. Forsberg, F., "On the usefulness of singular value decomposition-ARMA models in Doppler ultrasound," *IEEE Trans Ultrason, Ferroelec, Freq Control,* **38,** 418, 1991.
301. Hoeks, A.P.G., "On the development of a multigated pulsed Doppler system with serial data processing," *PhD Thesis, Rijksuniv Lumberg te Maastricth,* The Netherlands, 1982.
302. Bharath, A.A., Kitney, R.I., "Advanced spectral estimators for detailed blood flow studies," *Trans ASME J Biomech Eng,* **114,** 34, 1992.
303. Mohamed, A.S.A., "Doppler ultrasound spectral estimation and classification for clinical diagnosis," *Automedica,* **12,** 289, 1990.
304. DeStefano, J., *PhD Dissertation, Department Mathematics Computer Science, Dartmouth College,* 1993.
305. Angelsen, B.J., "Instantaneous frequency, mean frequency, and variance of mean frequency estimators for ultrasonic blood velocity Doppler signals," *IEEE Trans Biomed Eng,* **28,** 733, 1981.
306. Kristoffersen, K., Angelsen, B.A.J., "A comparison between mean frequency estimators for multigated Doppler systems with serial signal processing," *IEEE Trans Biomed Eng,* **32,** 645, 1985.
307. Brody, W.R., "Theoretical analysis of the ultrasonic blood flowmeter," *PhD Dissertation, Stanford University,* **Technical Report 4958-1,** Stanford, CA, 1971.

308. Arts, M.,J., Roevros, M.J.G., "On the instantaneous measurement of bloodflow by ultrasonic means," *Med Biol Eng,* **10,** 23, 1972.
309. Gerzberg, L., Meindl, J.D., "Power-spectrum centroid detection for Doppler systems applications," *Ultrasonic Imaging,* **2,** 232, 1980.
310. Angelsen, B.A.J., Kristoffersen, K., "Discrete time estimation of the mean Doppler frequency in ultrasonic blood velocity measurements," *IEEE Trans Biomed Eng,* **30,** 207, 1983.
311. Kristoffersen, K., "Time-domain estimation of the center frequency and spread of Doppler spectra in diagnostic ultrasound," *IEEE Trans Ultrason, Ferroelec, Freq Control,* **35,** 484, 1988.
312. Jaffe, R.S., "Extended-range pulsed Doppler mean-frequency estimation based on mean-frequency prediction," *Technical Report,* **G556-3,** Stanford Electronics Lab., Stanford University, Stanford, California, 1983.
313. Hoeks, A.P.G., Peeters, H., Ruissen, C., Reneman, R., "A novel frequency estimator for sampled Doppler signals," *IEEE Trans Biomech Eng,* **31,** 212, 1984.
314. Hartley, C.J., "Resolution of frequency aliases in ultrasonic pulsed Doppler velocimeters," *IEEE Trans Sonics Ultrason,* **28,** 69, 1981.
315. Tortoli, P., "A tracking FFT processor for pulsed Doppler analysis beyond the Nyquist limit (medical ultrasound)," *IEEE Trans Biomed Eng,* **36,** 232, 1989.
316. Lucas, C.L., Keagy, B.A., Hsiao, H.S., Wilcox, B.R., "Software analysis of 20 MHz pulsed Doppler quadrature data," *Ultrasound Med Biol,* **9,** 641, 1983.
317. Baek, K.R., Bae, M.H., Park, S.B., "A new aliasing extension method for ultrasonic 2-dimensional pulsed Doppler systems," *Ultrasonic Imaging,* **11,** 233, 1989.

Figure 9: Theoretical spectra for several flow configurations with a uniform beam pattern. Couette and Poiseuille flow have identically shaped spectra. With a blunter entry flow, more power is concentrated near $f_{\max}$.

Figure 10: Theoretical spectrum for flow downstream of a stenosis when the beam pattern is uniform. The reverse flow causes the peak at negative frequency and the forward part of the recirculation region causes the high power at low positive frequencies. The reduction in power near zero frequency is caused by the high pass filter.

Figure 11: Theoretical spectrum for flow downstream of a stenosis when the beam pattern is Gaussian. The reverse flow and forward recirculation parts of the spectrum have been greatly reduced in power over the uniform beam case of Figure 10.

Figure 12: a) An illustration of a particle that crosses through the sound field of a simple source. b) The in-phase signal generated by a Doppler instrument signal which uses the simple sources as a transducer. The instantaneous frequency of this signal is high at first and then becomes lower as the angle between the particle velocity vector and the propagation direction of the wavefronts approaches 90°. c) The power spectrum of the signal in b). Broadening is caused by changes in both amplitude and instantaneous frequency.

Figure 13 Signals and spectra generated by particles that traverse the sample volume. Two 2 mm long sample volumes are shown (dashed lines). One of these is centered 9 mm from the probe and the other is centered 19 mm from the probe. The beam pattern used is that for the far field of a circular piston in an infinite rigid wall. Particle path 1 crosses the near sample volume along the axial direction. Particle path 2 crosses the near sample volume at a flow-to-beam angle of 60°. Particle path 3 crosses perpendicularly through the near sample volume at a distance of 9.075 mm from the probe. Particle path 4 crosses perpendicularly thorugh the far sample volume at a distance of 19.075 mm. The spectrum for particle 4 is generally narrower than that for particle 3 as a result of a longer transit time. However, as shown in the inset, energy in the spectrum for particle 4 extends to higher frequencies. The absoulute bandwidth for particle 4 is thus as wide as that for particle 3, as predicted by Newhouse and Reid[38].

Figure 14: Effect of multiple scatterers on the estimated Doppler spectrum. The signal from a single particle (a) has a smooth spectrum (b) from which the Doppler shift (f_d) can be readily estimated. However, when signals from multiple particles (c) are summed (d), the result has a spectrum with sharp peaks, and the Doppler shift is difficult to locate (e).

Figure 15: A summary of transmitted signals that have been commonly used in Doppler ultrasound.

Figure 16: Illustration of the time-domain correlation technique. **a** and **b** show the cross-correlation functions between the two A-lines at times surrounded by the boxes. The two A-lines represent the return from two consecutive transmitted pulses scattered from Poiseuille flow with a beam-to-flow angle of 30°. The second return (lower A-line) is shifted to the left with respect to the first return (upper A-line). The shift is more noticable near the center of the A-line since this represents signal returned from the centerline of the flow, where the velocity is higher. This is reflected in the value of τ at which the cross-correlations are maximal.

Figure 17: Two dimensional Fourier transform method for Doppler ultrasound signal processing. a) Consecutive A-lines are arranged such that the coordinate along the A-line represents (approximately) depth, and the coordinate from one A-line to the other represents time. b) The two-dimensional spectrum has components along the line $g = h/v$, where g represents the spatial part of the transform and h represents the temporal part. c) If aliasing occurs, some spectral components lie on lines which does not pass through the origin.